THE EVOLUTION OF OCEANIC CRUST IN THE SOUTH ATLANTIC

A Dissertation

by

JUSTIN DAVID ESTEP

Submitted to the Office of Graduate and Professional Studies of
Texas A&M University
in partial fulfillment of the requirements for the degree of

DOCTOR OF PHILOSOPHY

Chair of Committee,	Robert S. Reece
Committee Members,	Richard L. Carlson
	Katerina Petronotis
	David W. Sparks
Head of Department,	Julie Newman

May 2020

Major Subject: Geophysics

ABSTRACT

Oceanic crust comprises two thirds of the crust on Earth and is the surface manifestation of mantle convection, the driving force behind plate tectonics. The age-progressive nature of oceanic crust away from its origin at mid-ocean ridges inherently works as a time series of changes in the style of accretion and of aging-related effects. The very nature of oceanic crust forming ocean basins and, therefore, residing under hundreds to thousands of meters of water has reduced our ability to broadly sample and measure in situ oceanic crust. Studies of large-scale temporal and spatial processes have thus far relied on scattered data collected in various ocean basins and of crust created at multiple spreading centers. This dissertation takes advantage of a multichannel seismic dataset that surveyed oceanic crust continuously from 0-70 Myrs old created at one spreading segment in the South Atlantic Ocean at spreading half-rates of 12-31 mm/yr. Using this dataset, we find that layer 2A, the uppermost igneous crust, continues to evolve for at least ~48 Myrs and layer 2A thickness is not dependent on crustal age or spreading rate. Furthermore, we find that the accommodation of spreading, the rate of spreading, and the roughness of the crust are all interrelated. We also find differences in subsidence rate between normal crust and thickened crust causes deformation across the transition from normal to thickened crust. Our findings imply that the hydrothermal circulation system in the South Atlantic oceanic crust is active into older crustal ages, that primarily magmatic accommodation of spreading exists in the South Atlantic, and that deformation can occur in areas where no tectonic forcing is expected.

ACKNOWLEDGEMENTS

I would like to thank my committee chair and faculty advisor, Dr. Bobby Reece, for the opportunity to participate in this study and for all his help throughout this dissertation process. Thanks also to the remainder of my committee for the invaluable help and discussion. Thank you to both Dr. Gail Christeson and Dominik Kardell at the University of Texas at Austin for their collaboration.

Thanks to all my friends, colleagues, and fellow students in the Department of Geology & Geophysics and at Texas A&M as a whole.

Special thanks to my parents for the encouragement throughout this process.

CONTRIBUTORS AND FUNDING SOURCES

Contributors

This work was supervised by a dissertation committee of Professors Dr. Bobby Reece (advisor), Dr. Richard L. Carlson, and Dr. Dave Sparks of the Department of Geology & Geophysics and Associate Research Scientist Dr. Katerina Petronotis from the International Ocean Discovery Program.

The velocity values used in Chapter II and the gravity model used in Chapter IV were provided by Dominik Kardell at the University of Texas at Austin. The crustal thickness values used in Chapter III were provided by Dr. Gail Christeson at the University of Texas at Austin. The structural interpretation in Chapter IV was significantly aided by Dr. Nick Perez.

Funding Sources

Graduate study was supported in part by fellowships, teaching assistantships, and research assistantships from the Department of Geology & Geophysics at Texas A&M University. Additional graduate support was provided by the Berg-Hughes Center. Data collection and research was supported by National Science Foundation (NSF) grant OCE-1537108 to Texas A&M University and OCE-1537169 to the University of Texas.

TABLE OF CONTENTS

Page

ABSTRACT ii

ACKNOWLEDGEMENTS iii

CONTRIBUTORS AND FUNDING SOURCES iv

TABLE OF CONTENTS v

LIST OF FIGURES vii

LIST OF TABLES ix

CHAPTER I INTRODUCTION 1

CHAPTER II THE THICKNESS AND EVOLUTION OF LAYER 2A 3
- Introduction 3
- Background 4
- Study Area 8
- Data and Methods 10
- Results 19
- Discussion 29
- Conclusions 40

CHAPTER III THE BALANCE BETWEEN SPREADING AND MAGMATISM 42
- Introduction 42
- Background 43
- Study Area 47
- Methods 51
- Results 60
- Discussion 66
- Conclusions 74

CHAPTER IV RECENT DEFORMATION IN OLD OCEANIC CRUST 77
- Introduction 77
- Background 78
- Study Area 81
- Results and Interpretation 83
- Discussion 90
- Conclusions and Implications 95

Page

CHAPTER V SUMMARY 98

REFERENCES 100

LIST OF FIGURES

FIGURE		Page
1	Chapter II survey area	9
2	Triplication and NMO flattening	13
3	Migration of layer 2A comparison	14
4	Upper crust velocities	17
5	Line 1F layer 2A MCS and CMP	18
6	Line 1D layer 2A MCS and CMP	20
7	Line 1B layer 2A MCS and CMP	21
8	Layer 2A thickness across age	22
9	Source of heterogeneity in layer 2A	23
10	Line 1F migrated MCS	25
11	Line 1B migrated MCS	26
12	Line 1D MCS	27
13	Layer 2A thickness vs. spreading rate	29
14	Basement, spreading rate, and layer 2A vs. age	32
15	Chapter III survey area annotated	47
16	Basement filtered and unfiltered comparison	51
17	Basement power spectra and filter selection	52
18	Roughness window length effect	55
19	M cartoon	56
20	Fault prediction examples	57

Page

21 Age comparison of crust and derived parameters 59

22 Linear regression correlations of M, RMS, and spreading rate 62

23 Roughness spikes and propagator wakes multibeam bathymetry 64

24 Propagator wakes MCS 65

25 Roughness spikes MCS 68

26 Smooth crust at 25 Ma 72

27 Proportional variance from mean for M and crustal thickness 73

28 Chapter IV survey area annotated 80

29 MCS Line 1A with faulting 82

30 Crustal thickness gravity model 83

31 Faulting in western Line 1A 86

32 Unconformity 87

33 Fault type zoom 89

34 Seafloor faults in multibeam bathymetry 90

LIST OF TABLES

TABLE		Page
1	CREST MCS ridge-normal profile list	10
2	Layer 2A thickness for ridge-normal profiles	23
3	Layer 2A thickness published comparison	34
4	M and roughness linear regression results and coefficients	60

CHAPTER I

INTRODUCTION

In aggregate, my dissertation investigates the evolution of oceanic crust using multichannel seismic data. The research that produced this dissertation is part of a larger collaboration of scientists. The intent is to provide a comprehensive understanding of what changes can be detected in the physical properties of oceanic crust using multichannel seismic data, and what is the cause and implication of those changes. My specific contributions to this collaboration are documented in this dissertation and include the following products: 1) an investigation of the evolution and thickness of layer 2A in the South Atlantic Ocean; 2) an assessment of the deformation that results from differential subsidence between 'normal' oceanic crust and hotspot-affected oceanic crust; and, 3) a quantification of tectonic versus magmatic accommodation of spreading for the past 70 million years at 30°S in the South Atlantic.

Oceanic crust is the surface expression of mantle convection (Stein & Stein, 1992) and comprises two thirds of Earth's crust (Henstock et al., 1993). The nature of how oceanic crust is generated and subsequently transported away from the mid-ocean ridge enables it to act as a time series record of changes that have occurred during its evolution (White et al., 1992). As melt that is sourced from the mantle cools and forms ocean crust at spreading centers, a record of Earth's magnetic field polarity (Gee & Kent, 2007; Heirtzler et al., 1968; Vine & Matthews, 1963) and melt composition (Langmuir et al., 1993) is recorded. As crust is then transported away from the spreading center, rock-water interaction and changes associated with crustal cooling are recorded (Stein & Stein, 1994).

The record provided by the crust is instrumental in understanding Earth history, but in situ studies are difficult due to the inaccessibility of ocean crust. Only a small number of drilling expeditions (e.g., Ocean Drilling Program Hole 504B and Hole 1256D (Anderson et al., 1982; Wilson et al., 2006)) and submersible dives (e.g., Hess Deep, Blanco Transform (Francheteau et al., 1990; Juteau et al., 1995; Stewart et al., 2003)) have been conducted that provide data for the study of in situ oceanic crust. Ophiolites, obducted sections of oceanic crust accessible on land in outcrop, have provided significant constraint for the prevailing model of the lithology and structure of oceanic crust (Salisbury & Christensen, 1978). The classic ophiolite model for the oceanic crustal sequence consists of, from top to bottom, an upper ~1 km of extrusive basalt, ~1 km of intrusive basaltic diabase sheeted dikes, and ~5 km of gabbroic rocks (Nicolas, 1989). Drilling and submersible expeditions have found similar structure at the crustal depths that have been reached (Donnelly et al., 1980; Wilson et al., 2006), which provides support for the ophiolite model being relatively representative of in situ oceanic crust. However, ophiolites are not in situ crust; ophiolites have been influenced by the processes of obduction and subaerial alteration, and offer only a narrow time window of crustal evolution. Furthermore, it is predominantly thought now that the majority of known ophiolites were produced at suprasubduction zones rather than mid-ocean ridge spreading centers (Pearce et al., 1984). Given the limitations of ophiolite sequences and because of the inaccessibility of in situ oceanic crust, geophysical measurements provide some of the best methods to study oceanic crust beyond the borehole. My dissertation uses a multichannel seismic dataset collected in a transect-style expedition that images oceanic crust in the South Atlantic Ocean across an age range of 0-70 Ma for the purpose of investigating the evolution of oceanic crust at a single spreading segment.

CHAPTER II

THE THICKNESS AND EVOLUTION OF LAYER 2A*

Introduction

Oceanic crust divided into layers based on characteristic seismic velocities (i.e. layer 2, layer 3) is the common nomenclature for segregating depth regions of distinct properties (Raitt, 1963). Layer 2A is the term given to the uppermost igneous portion of oceanic crust with relatively low P-wave velocities that increases with crustal age (Houtz & Ewing, 1976). Layer 2A properties have a direct impact on interactions at the rock-water interface. The upper crust is a porous medium that facilitates circulation of seawater within the rock (Alt et al., 1986). Chemical exchange and thermal dissipation are intricately tied to the circulation system within the upper crust (Johnson & Pruis, 2003; Stein & Stein, 1994), and the thickness of layer 2A can be viewed as a proxy for the permeable and porous interval within the crust in which significant circulation of seawater can take place (Carlson, 2011).

The evolution of layer 2A thickness across a large crustal age range and its persistence in older crustal ages has yet to be fully described, primarily due to a lack of data from which thickness can be determined away from the ridge crest. This data paucity has limited the evaluation of the water/crust circulation system magnitude and persistence as crust ages (Fisher & Becker, 2000). Additionally, because layer 2A studies have primarily focused on young crust, potential controls on the thickness of layer 2A, such as mineral precipitation as crust ages and

---

* Reprinted with permission from Estep, J., Reece, R., Kardell, D. A., Christeson, G. L., & Carlson, R. L. (2019a). Seismic Layer 2A: Evolution and Thickness From 0-to 70-Ma Crust in the Slow-Intermediate Spreading South Atlantic. *Journal of Geophysical Research-Solid Earth, 124*(8), 7633-7651. doi:10.1029/2019jb017302

crustal topography manifested by spreading rate, and their influence on changes in layer 2A thickness remains poorly constrained.

We use seismic reflection data from the Crustal Reflectivity Experiment Southern Transect (CREST) to estimate the layer 2A extent and thickness using the pseudoreflection method of Harding et al. (1993) and Vera and Diebold (1994). CREST continuously imaged 0-70 Ma ocean crust created at one spreading segment in the slow-intermediate spreading South Atlantic. We use the thickness and persistence of layer 2A with age as a proxy for the depth and extent at which water can circulate within the crust. We also compare thickness and its variability with crustal age, spreading rate, basement rugosity, and sediment cover across the transect in order to evaluate the possible controlling factors.

Background

Layer 2A Velocity vs. Age

The layered nomenclature differentiates oceanic crust based on the seismic velocity structure rather than lithology (Raitt, 1963). Layer 2A is an interval at the top of the igneous oceanic crust that is characterized by relatively low seismic velocities, 2.5 – 5 km/s depending on crustal age, bounded above by water or accumulated sediment and below by a rapid increase in velocities to those typical of layer 2B (~5-6 km/s). Houtz and Ewing (1976) made important and early observations regarding layer 2A; using a global dataset of airgun/sonobuoy data they found that layer 2A velocities increase with crustal age, from an average ~3.3 km/s in very young crust to >5 km/s in older crust and that layer 2A was thinning with age, eventually disappearing at 25 Myr in the Pacific and 40 Myr in the Atlantic. Later reanalysis of the layer-2A-thinning-with-age phenomenon strongly indicates that thinning is an artifact of assumptions made in the original study and that no evidence exists for layer 2A thinning with age (Carlson & Jacobson, 1994).

Whether or not layer 2A does thin and disappear with age has not been conclusively shown, but the increase in velocities has been observed in subsequent studies. Carlson (1998) and Grevemeyer and Weigel (1996) showed that upper crust velocities increase in crust <10 Ma and remain relatively unchanged in older crust. The increase in layer 2A velocities with age has been well documented by other studies with all reporting a relatively young age (<15 Ma) for reaching a mature velocity (Grevemeyer et al., 1999; Grevemeyer & Weigel, 1996, 1997; Nedimović et al., 2008; Purdy, 1987; Rohr, 1994). The cause of the velocity-increase-with-age phenomenon has most commonly been attributed to be the reduction of porosity within upper crust (Houtz & Ewing, 1976; Jacobson, 1992; Rohr, 1994; Swift et al., 2008; Wilkens et al., 1991). However, Carlson (2014b), using in situ measurements, contends that, while porosity accounts for ~90% of the velocity variation within the upper crust (Carlson, 2010), porosity remains effectively unchanged in crust older than 0.2 Ma and the observed layer 2A velocity increase is caused by changing crack morphology (see also Wilkens et al. (1991)).

Layer 2A Velocity vs. Depth

The high vertical velocity gradient increase at the base of layer 2A produces retrograde arrivals of refracted waves turned within the region of rapidly increasing velocity (Vera & Diebold, 1994). Normal moveout (NMO) correction to stack these retrograde arrivals as a reflection produces a reflection-like, or pseudoreflection, event in MCS reflection images. Previous studies predominantly either correlate the base of layer 2A to the extrusive-to-sheeted dike transition (Christeson et al., 1992; Harding et al., 1993; Toomey et al., 1990) or to a porosity boundary within the upper crust (Carlson & Herrick, 1990; Christeson et al., 2007; McClain et al., 1985). The exploration of in situ crust has yielded results inconsistent with the correlation of the 2A/2B boundary to the extrusive-to-sheeted dike transition; at tectonic

windows where oceanic crust is exposed in cross-section, the extrusive-to-sheeted dike transition is not always at the depth of the layer 2A/2B boundary observed in seismic data (Christeson et al., 2010; Christeson et al., 2007). Recent work with downhole measurements taken at ODP Hole 504B yielded the most conclusive evidence that the transition from velocities representative of layer 2A to those of layer 2B and the associated velocity gradient change is from a porosity change at depth (Carlson, 2010, 2011, 2014b).

Upper Crustal Porosity and Fluid Interaction

Laboratory-measured seismic velocities of fresh basalt collected from drill holes or dredged from the seafloor are ~6 km/s (Hyndman & Drury, 1976; Schreiber & Fox, 1976), while in situ seismic investigations of the upper oceanic crust reveal velocities of ~2-5 km/s (Carlson, 1998, 2014a). The velocity difference between laboratory measurements and in situ seismic investigations can be attributed predominantly to porosity within the upper crust at scales not sampled by dredging or coring. Pore space in the form of hollow pillows, contraction joints, and fault-related fractures all contribute to the porosity within the upper crust (Karson, 2002). The porosity and permeability of layer 2A allows for hydrologic circulation within the upper crust, which impacts the chemical and thermal exchange between the geosphere and the hydrosphere. Johnson and Pruis (2003) estimated from global porosity values that roughly 2% of ocean water resides within the upper crust and that flux between the water in the crust and the ocean is near 20% of that from riverine input, which provides for a significant amount of chemical and heat exchange. High-temperature alteration near the heat source of the spreading center and later low-temperature alteration lead to the precipitation of secondary minerals in the pore space, which reduces the porosity and produces the layer 2A velocity increase with age (Houtz & Ewing, 1976; Rohr, 1994; Stein & Stein, 1994). Global heat flow studies indicate that circulation may

continue in the upper crust for ~65±10 million years (Stein & Stein, 1994). However, previous studies of seismic velocities have not shown the change expected if circulation is taking place in older crust, whether due to a limited age range of the study or limited data (Carlson, 1998; Grevemeyer et al., 1999; Nedimović et al., 2008). Grevemeyer et al. (1999) suggest that the fluid circulation system in the upper crust becomes a closed system at 6-7 Ma, which may slow the alteration and evolution process in layer 2A. More recently, Kardell et al. (2019) found that seismic velocities continue to slowly increase for ~ 58 Myr in the South Atlantic, which seems to agree with the global heat flow studies. While the discrepancy between global heat flow values and upper crustal seismic velocity values remains, Fisher and Becker (2000) proposed that the circulation system becomes channelized in the upper crust. Their work suggests that the sparse constraint on velocities in older crust would not reflect its heterogeneity, and that the channelized flow could still remove significant amounts of heat, which would agree with the global heat flow measurements.

Layer 2A Thickness Variations

Layer 2A has been imaged at spreading centers of varying spreading rates and morphologic expressions (Arnulf et al., 2011; Baran et al., 2010; Blacic et al., 2004; Hussenoeder et al., 2002; Nedimović et al., 2008; Vera & Diebold, 1994). The thickness of layer 2A ranges from 200-1000 m (Christeson et al., 2010; Hooft et al., 1996). Layer 2A thickness varies both parallel to the spreading axis (Baran et al., 2010; Hussenoeder et al., 2002) and normal to the spreading axis (Kent et al., 1994; Vera & Diebold, 1994), but no clear correlation of thickness with spreading rate, which is often used as an indicator of crustal morphology, has been found (Christeson et al., 2010). Layer 2A thickness at the fast spreading East Pacific Rise doubles within 1-3 km from the ridge crest (Hooft et al., 1996), which is attributed to off-axis

volcanism (Vera & Diebold, 1994) and to large lava flows moving down the ridge flank (Hooft et al., 1996). At the slow spreading North Mid-Atlantic Ridge, layer 2A does not exhibit significant off-axis thickening, and Hussenoeder et al. (2002) concluded that its thickness is predominantly established within the axial valley where crust is created before being transported away. At intermediate spreading ridges like Juan de Fuca and the Southeast Indian Ridge, layer 2A thickness variation with crustal age is more ambiguous; Nedimović et al. (2008) observed no systematic change in thickness at the Juan de Fuca Ridge, while Baran et al. (2010) observed both increasing thickness and static thickness at differing locations along the Southeast Indian Ridge. However, no study since Houtz and Ewing (1976) has examined layer 2A thickness into crustal ages beyond ~10 Ma, and the eventual course of layer 2A evolution remains ambiguous.

Study Area

The survey area lies at ~30° S, roughly 450 km south of the Rio Grande Fracture Zone along a relatively uninterrupted, 300 km wide (from fracture zone to fracture zone) spreading segment of the Mid-Atlantic Ridge in the South Atlantic (Figure 1). Apart from two propagator wakes crossing the spreading segment, the study area is otherwise relatively devoid of the crustal and bathymetric complexity present in much of the Atlantic Ocean. The large distance between fracture zones and the long uninterrupted flow line makes this segment of crust ideal for investigating oceanic crustal evolution in the South Atlantic. Additionally, Kardell et al. (2019) examined velocity trends across the CREST transect with tomographic modeling using downward-continued, hydrophone streamer data. They show that velocities increase rapidly in 0-6 Ma crust (2.4 km/s to 4.2 km/s) and continue to gradually increase out to crust of age 58 Ma, which they concluded indicates a continuing evolution of the upper crust beyond the expected mature age of 10-15 Ma. At the western end of the crustal flow line, ~1500 km from the ridge

axis, the Rio Grande Rise interrupts the "normal" oceanic crust. The CREST transect just reaches the eastern margin of the Eastern Rio Grande Rise (as defined by Camboa & Rabinowitz, 1984) at 69.22 Ma according to the age grid of Pérez-Díaz and Eagles (2017), which is coeval to when the Rio Grande Rise construction ceased (O'Connor & Duncan, 1990). The transect lies near the DSDP Leg 3 drilling transect, which predicts a sediment composition of calcareous ooze (Maxwell et al., 1970). Spreading half-rates of the crust imaged along the transect vary between a minimum of 12 mm/yr and a maximum of 31 mm/yr (Pérez-Díaz & Eagles, 2017).

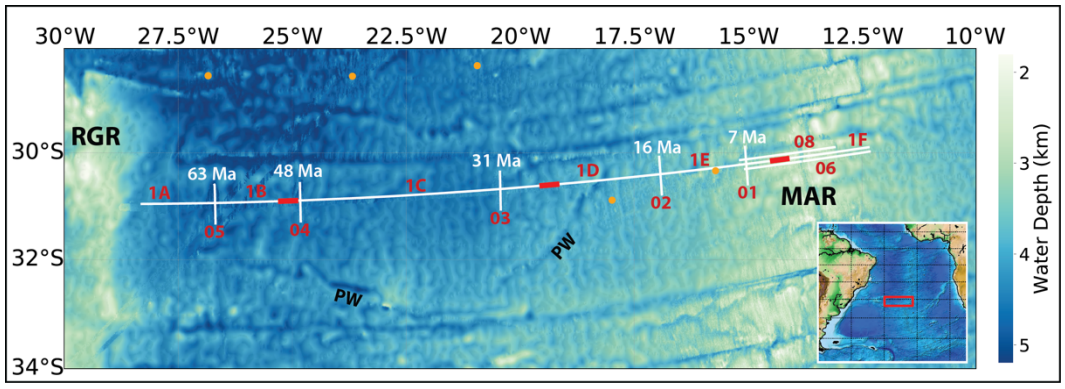

Figure 1: CREST MCS survey area. Background image is global bathymetry from the Global Multi-Resolution Topography Synthesis (Ryan et al., 2009). MCS profile names are adjacent to the respective line in red. Red highlights indicate location of selected seismic images. The crustal age at ridge-parallel lines in white are from Pérez-Díaz and Eagles (2017). Orange circles are locations of DSDP Leg 3 holes. Inset shows regional setting, with red box marking the location of the study area. RGR = Rio Grande Rise, MAR = Mid-Atlantic Ridge, PW = Propagator Wakes.

Line Name	Length (km)	Age West (Ma)	Age East (Ma)	1/2 Spreading Rate (mm/yr)
1F	250	7.4	7.9	14 - 27
1E	183	15.9	7.4	14 - 29
1D	331	29.9	15.9	20 - 29
1C	421	47.3	29.9	16 - 31
1B	180	59.5	47.3	12 - 19
1A	141	69.2	59.5	12 - 21

Table 1: Name, length, age, and spreading rate of CREST MCS ridge-normal profiles used. ***Note: line 1F crosses 0 Myr crust at the Mid-Atlantic Ridge and samples crust from both the South American and African plates.***

Data and Methods

We use seismic reflection data collected between January and March 2016 during the CREST expedition, MGL1601, aboard the *R/V Marcus G. Langseth.* In total, ~ 2,700 km of 2D MCS data were collected over oceanic crust ranging in age from 0-70 Ma (Figure 1). This study focuses on the ~1500 km continuous, ridge-normal transect extending from the Mid-Atlantic Ridge to the eastern margin of the Rio Grande Rise. The MCS data collection was conducted in a west to east order. The transect is subdivided into five profiles for practical purposes; line names, lengths, and ages are presented in *Table 1*. Data were collected using a 12,587.5 m hydrophone streamer, towed at 8-12 m water depth depending on conditions, containing 1008 channel groups at 12.5 m spacing and a shot spacing of 37.5 m. The acoustic source was a tuned array of 36-active air guns with a total volume of 108.2 L (6600 in^3) towed at a depth of 6 m. For each shot, 15 s of data were recorded at a sample rate of 2 ms and later resampled to 4 ms. When binned into common midpoint (CMP) gathers, maximum fold is 168 traces at 6.25 m spacing. To assign ages and spreading rates to the crust imaged in the CREST transect, we extracted the locations of each shotpoint from the age and spreading rate grids of Pérez-Díaz and Eagles (2017). To estimate the thickness of layer 2A along the CREST transect, we convert the travel time between

the top of the igneous crust and the base of layer 2A to thickness using velocities of Kardell et al. (2019) derived from the CREST data.

To image the base of layer 2A, we use the method first pioneered by Harding et al. (1993) and Vera and Diebold (1994) of flattening and stacking the retrograde arrivals in MCS data, which result from waves turned within the high velocity gradient at the transition from layer 2A to layer 2B. The method takes advantage of the rapid velocity increase at the base of layer 2A to produce a pseudoreflection from the retrograde arrivals, commonly referred to as the Layer 2A Event, in a seismic reflection section. Unlike detailed velocity modeling of upper crustal structure (e.g., Nedimović et al., 2008), this method does not differentiate between the upper layer 2A velocity gradient and the high velocity gradient transition to layer 2B (layer 2A upper and lower, respectively). Instead, pseudoreflections arising from the retrograde arrivals are taken to mark the base of layer 2A and we interpret our associated thickness measurements to represent the whole layer 2A interval. The presence of the Layer 2A Event in reflection sections allows for the lateral mapping of the transition. While the Layer 2A Event (once converted from two-way time to depth) may not provide a direct measurement of the depth to the layer 2A/2B transition, several studies (Arnulf et al., 2011; Baran et al., 2010; Christeson et al., 2010; Christeson et al., 2007) have shown that the Layer 2A Event does serve as a good estimate for the base of layer 2A. A source of uncertainty is that we can manipulate the arrival time of the pseudoreflection slightly (up to ~30 ms total or ~75 m of layer 2A thickness at 5 km/s velocity) in the stacked section by modifying the NMO-correction velocity used for flattening the retrograde arrivals in the CMP gathers (e.g., Baran et al., 2010; Baran et al., 2005). This uncertainty may result in the pseudoreflection not truly representing the depth of the high velocity gradient at very small scales. We believe our procedure of NMO velocity estimation and

stacking does not introduce any systematic bias affecting the zero-offset two-way travel time of the Layer 2A Event on stacked sections.

To define the top of layer 2A, we mapped the top of the igneous crust in prestack time migrated sections created using a standard reflection processing workflow in Paradigm seismic software applications, Echos and Geodepth. Our processing began by importing the raw SEGD data into Paradigm where we applied a 3, 7, 100, 120 Hz bandpass filter, a 3-10 Hz noise-suppression filter, a spherical divergence correction, and multichannel gap-deconvolution. We then sorted shot gathers into CMP gathers, and performed interactive velocity picking every 50th CMP (312.5 m) in order to select normal moveout (NMO) correction velocities that best flatten coherent reflections within the sediment and the reflection at the igneous basement interface. Within the crust, where reflections are weak, sparse, and/or absent, we used a velocity model derived from CREST line 03 wide-angle ocean bottom seismometer (OBS) data (Christeson et al., 2018) for the time migration beneath the basement interface velocity pick. We interactively drew mutes on NMO-corrected CMP gathers to remove unwanted energy in the water layer, refracted arrivals, and stretched portions of the gathers. We used a Kirchhoff prestack time migration algorithm to collapse diffractions and assign dipping reflections correctly in time. Once an initial migrated stack was available, we used it as a guide to repick velocities and mutes on the original gathers at areas with rapid changes in bathymetric or structural complexity and then applied a final Kirchhoff prestack time migration with a mute above the seafloor to remove any artifacts.

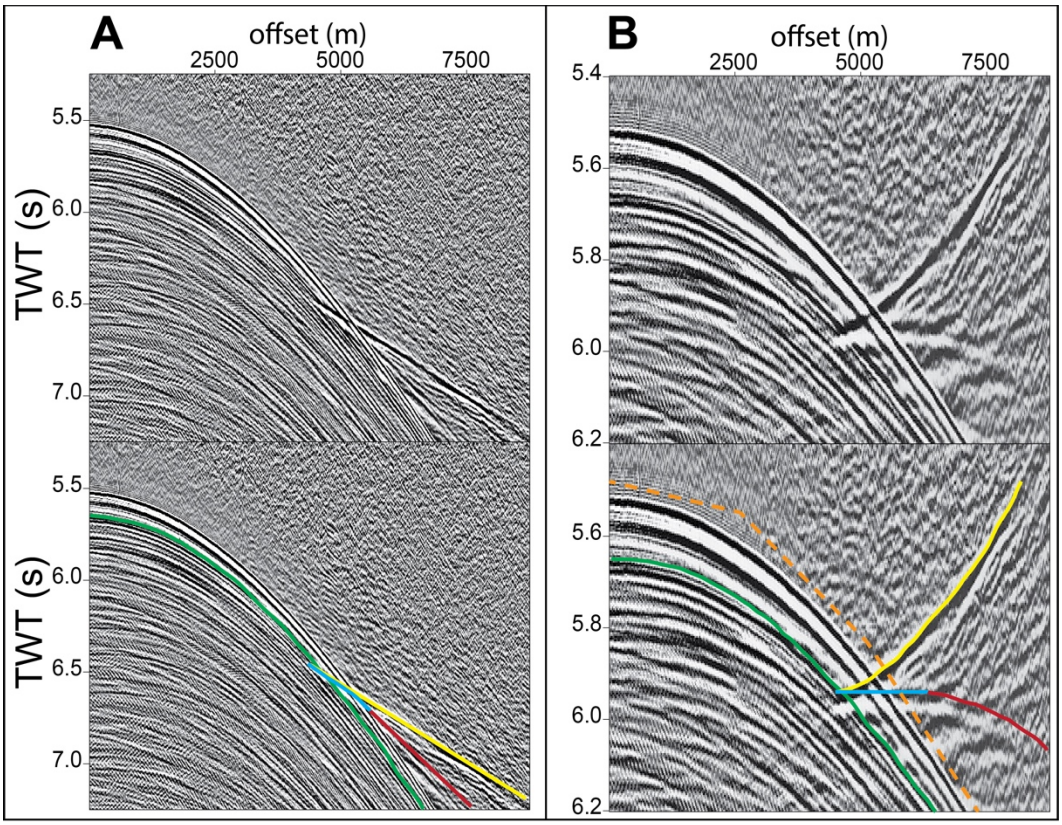

Figure 2: Zoom of CREST line 1D CMP 15600 supergather of 11 adjacent CMP gathers. Top: uninterpreted; Bottom: interpreted. A: Supergather shown with no velocity correction applied. B: Supergather shown with a constant NMO-correction of 1720 m/s to flatten the retrograde arrivals for stacking. Orange dashed line is the outer trace mute applied after NMO correction. Constituent branches of the triplication were visually interpreted and are indicated with: green – top of the basement reflection, red – layer 2A prograde refraction, blue – layer 2A retrograde refraction, yellow – layer 2B prograde refraction. TWT: two-way travel time. Note: A and B are at different scales.

For imaging of the Layer 2A Event, we used similar processing steps, with the exception of the velocity analysis and migration steps. During the velocity analysis, we interactively picked

a single NMO correction velocity every 50 CMPs that best flattened the retrograde branch of the triplication arrivals (Figure 2). As noted by earlier studies (e.g., Vera & Diebold, 1994), the addition of velocity picks to flatten true reflections along with the retrograde-flattening pick causes severe stretching of the gather.

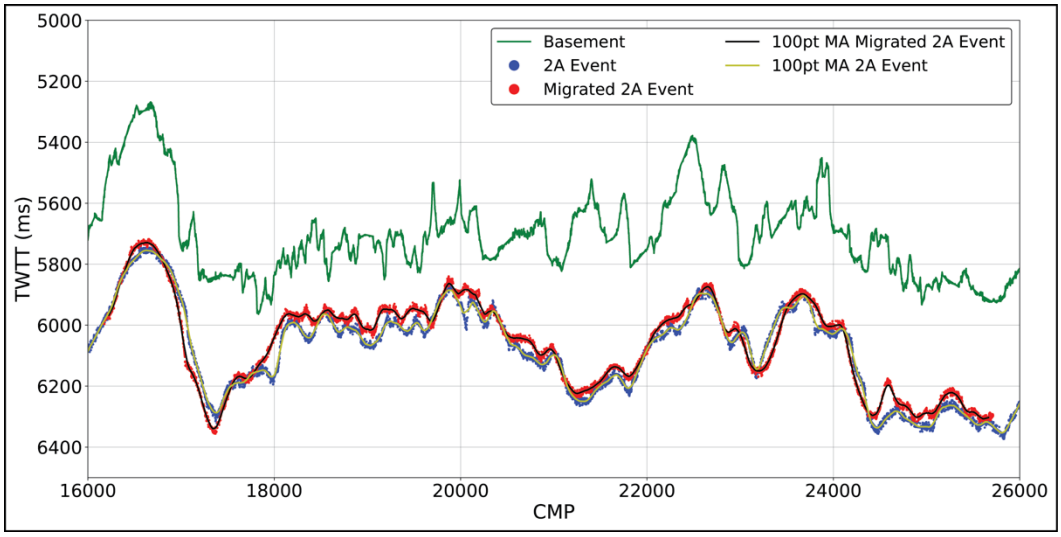

Figure 3: Comparison of Layer 2A Event arrival time when migrated vs. when unmigrated. Green line = basement arrival time, blue circles = unmigrated Layer 2A Event, yellow line = 100-point moving average of unmigrated Layer 2A Event, red circles = migrated Layer 2A Event, black line = 100-point moving average of migrated Layer 2A Event.

Therefore, to mitigate the stretch effect, we prepared a Layer 2A Event stacked section through stacking each CMP gather with one unique velocity value that best flattened the retrograde arrival on that CMP gather. Post-stack migration of these stacked sections was attempted, but the incorrect velocity model for true reflections caused severe distortion and

image degradation, especially where the basement topography is not smooth. This problem has been addressed in other studies by muting above and below the Layer 2A Event to remove the incorrectly migrated data and then extracting and merging the migrated Layer 2A Event with the standard reflection section to form a composite section (Nedimović et al., 2008).

We tested the effect of migration on the arrival time of the Layer 2A Event over a 60 km portion of Line 1D where the basement topography is the smoothest. Interpretation of the arrival time of the migrated event was more difficult due to the introduction of migration noise from the true reflections even on the smoothest basement of the transect. We found the mean absolute value of the difference in arrival time between a migrated and an umigrated Layer 2A Event is 34 ms with a standard deviation of 26 ms, which equates to a possible 85±65 m of difference at 5 km/s (less at lower velocities). The mean value of the difference is -17 ms with a standard deviation of 40 ms, which suggests that the difference remains around zero and no systematic increase or decrease in arrival time of the Layer 2A Event is introduced by migration. It should be noted that we cannot rule out that some (or even all) of the difference between the migrated and unmigrated Layer 2A Event arrival time is due to interpretation; the arrival time of the Layer 2A Event is not always unambiguous where basement complexity exists. Additionally, we cannot confidently state that some (or all) of the difference between the migrated and unmigrated Layer 2A Event is not due to differences in the interpreted arrival time due to migration noise. Because we found no systematic influence of migration and image quality suffered significantly, especially where the basement topography is roughest, we did not apply migration to the Layer 2A Event sections. After all processing was completed, each MCS line had two processed versions: a prestack time migrated section for accurate seafloor and basement interfaces and a constant velocity stack for the Layer 2A Event.

We used Paradigm 3D Canvas for seismic reflection data interpretation and mapping. We interpreted and laterally mapped the top of the igneous basement and the seafloor from our prestack time migrated sections. The seafloor horizon only differs from the top of the igneous basement where there is a sedimentary cover; the basement horizon is the seafloor where no overlying sediment is imaged. In the constant velocity stacks, we interpreted and mapped the Layer 2A Event horizon, where present, at the peak of the first amplitude deflection associated with the interpreted event (as illustrated in Figure 2 for pre-stack data).

To convert seismic reflection two-way travel time values to thickness and depth in meters, we used velocities extracted from the streamer tomography models of Kardell et al. (2019), which are derived from the same CREST MCS profiles used in this study. We converted the arrival time of our Layer 2A Event to depth then extracted the mean vertical velocity between the top of the igneous basement and the Layer 2A Event at every CMP where the event was present in the velocity model. To reduce scatter and to extend velocities across the length of the transect, we fit a 6^{th} order polynomial curve to the equally-weighted velocity values of Kardell et al. (2019), which provided an estimated mean layer 2A velocity at every shotpoint along the transect (Figure 4).

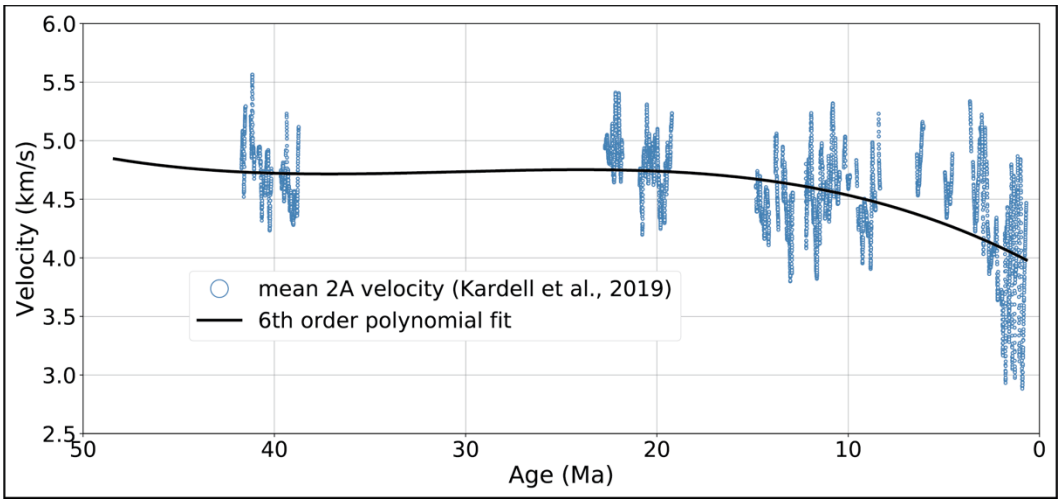

Figure 4: Upper crustal velocities from CREST transect and the polynomial curve calculated for the time-to-thickness conversion. Blue circles are the mean layer 2A velocities from the coincident streamer tomography models of Kardell et al. (2019) obtained for portions of the CREST transect. The 6th order polynomial curve in black is used to calculate layer 2A thickness at every CMP containing an interpreted Layer 2A Event.

A result of using the polynomial curve is that the detailed along-transect variations in mean layer 2A velocity will not be captured in our thickness estimates, which is a source of error. This is especially evident at young ages in *Figure 4.* In an effort to quantify this, we calculate, at each shot point position, the absolute value of the difference between the mean layer 2A velocity and that provided by the polynomial curve. We find a mean of 0.26 km/s and a standard deviation of 0.22 km/s, which, from our average layer 2A time thickness of 0.325 sec, results in an associated mean error of 42 m with a standard deviation of 36 m.

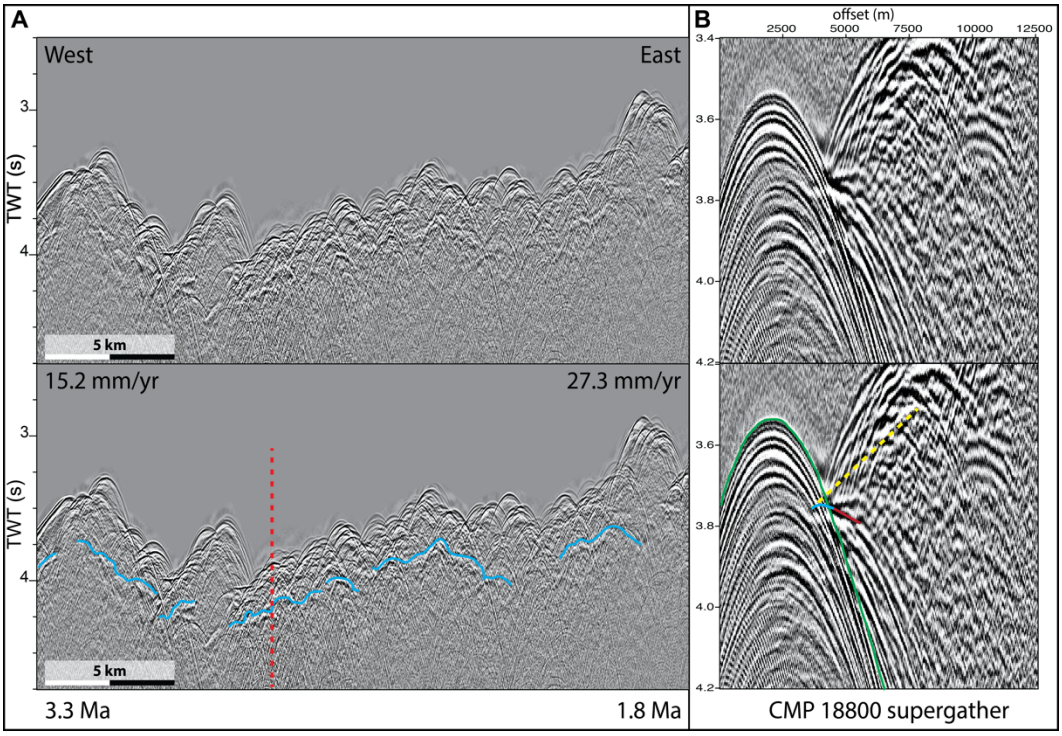

Figure 5: A: Constant velocity stack of seismic reflection profile 1F showing layer 2A in ~2 Ma crust with a rough basement interface. Blue line is the interpreted Layer 2A Event. Vertical dashed red line is the location of CMP supergather. B: CMP supergather of 11 adjacent CMP gathers from seismic profile 1F with 4 km/s reduction velocity showing interpreted branches of the triplication. Constituent branches of the triplication are visually interpreted with: green – top of the basement reflection, red – layer 2A prograde refraction, blue – layer 2A retrograde refraction, yellow – layer 2B prograde refraction (dashed when unclear). Top: uninterpreted; Bottom: interpreted. Seismic profile location shown in Figure 1.

Results

Layer 2A Thickness vs. Crustal Age

We observe the Layer 2A Event in the stacked sections (Figures 5-7, Panel A) and a layer 2A-2B triplication in CMP gathers (Figures 5-7, Panel B) intermittently, but consistently, at crustal ages from 0 to 48 Ma. The percentage of an observable Layer 2A Event in each section is the ratio of interpreted Layer 2A Event to top basement lengths. At the youngest crust (Figure 5), 0-15 Ma, we observe the triplication in the CMP gathers and the Layer 2A Event is present in 55% of the stacked section, but it is rarely laterally continuous for more than 20 km. In crustal ages from 15-48 Ma (Figure 6), we still observe the triplication in CMP gathers and the Layer 2A Event becomes much more laterally continuous and easily observable (80% of the section). Beyond 48 Ma, the Layer 2A Event is absent completely (Figure 7A) and we do not observe the retrograde arrival in the CMP gathers (Figure 7B). We limit our thickness measurements to 0-48 Ma crust, the age range that contains the observable 2A-2B triplication. When we compare thickness values vs. crustal age we observe significant scatter at even small scales (<1 Myr) (Figure 8). Thickness ranges from 0 to ~2 km, with an overall mean thickness of 760 m, and a standard deviation of 290 m. Mean thickness and standard deviation by individual CREST profile are reported in Table 2. To better evaluate the large-scale trend, we apply a 100-point moving average (625 m lateral distance) and a 6^{th} order polynomial-fit curve to the thickness trend. While the moving average still contains significant variability, the poly-fit curve works to express a large-scale sinusoidal trend in thickness with age, with no systematic thinning observable. A 4 Myr zoom (Figure 9) reveals how small-scale trends can deviate significantly from the large-scale trend. Figure 9 also reveals how small scale variations in the basement

interface (red arrows) that are not present in the Layer 2A Event can significantly affect the calculated depth of the Layer 2A Event and, therefore, the calculated thickness of layer 2A.

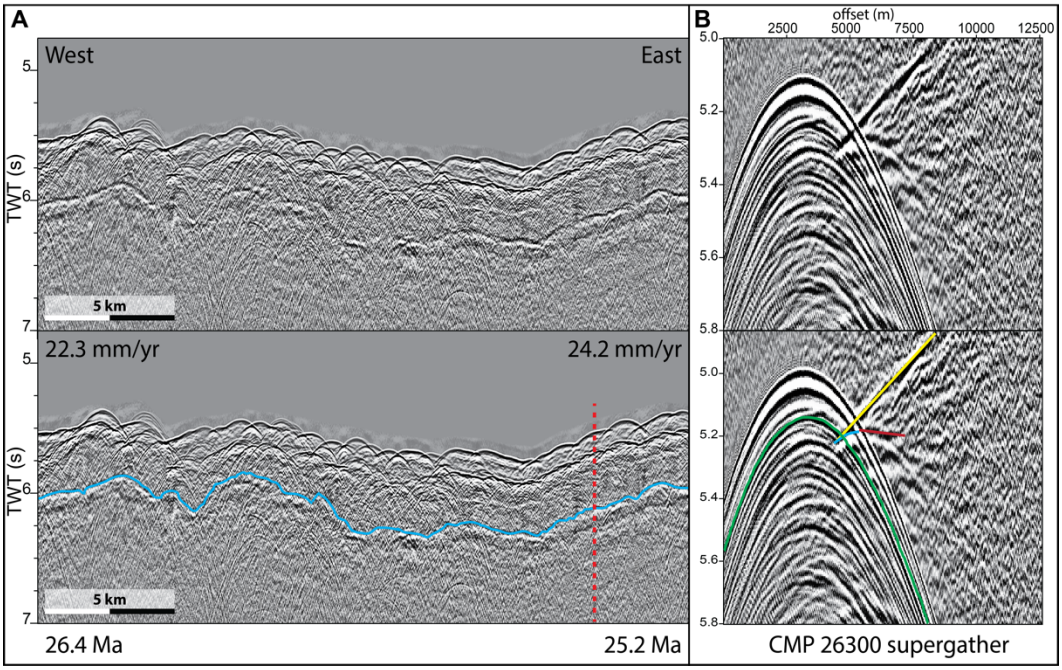

Figure 6: As in Figure 5, except reflection profile 1D.

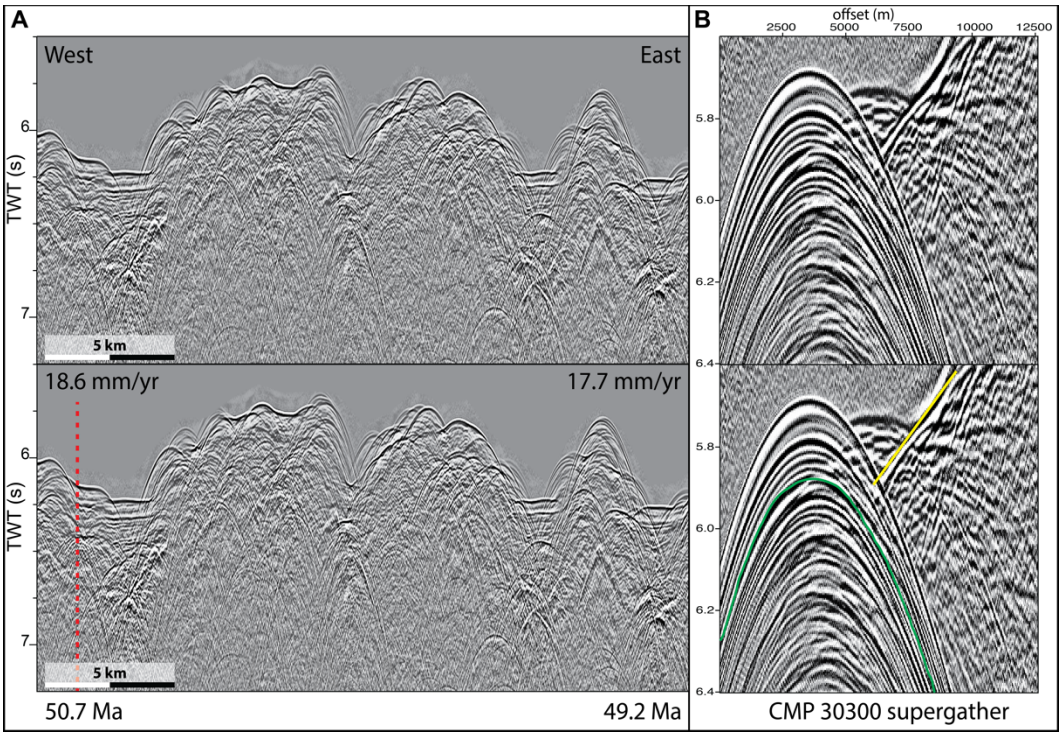

Figure 7: As in Figure 5, except reflection profile 1B and stacking velocity is 1700 m/s (a velocity chosen due to similarity to that which produced a pseudoreflection in other lines).

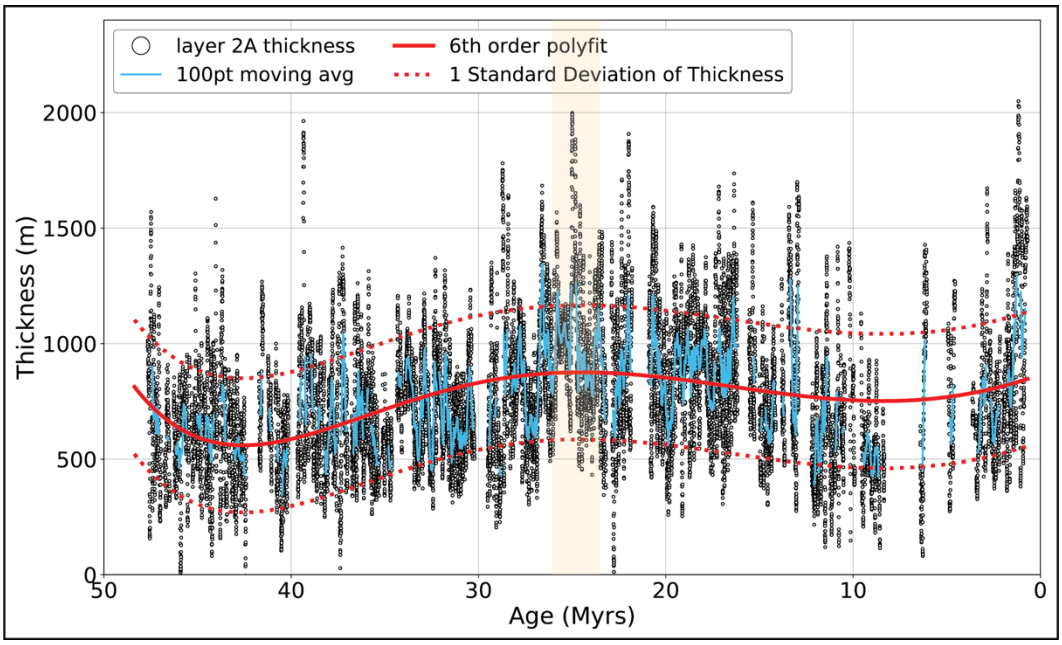

Figure 8: Thickness values of layer 2A from seismic profiles 1F-1C, displayed by individual common midpoint (black, open circles), 100-point moving average (cyan), 6th order polynomial curve (solid red), and 1 standard deviation of thickness from the polynomial curve (dashed red). Tan shading indicates zoom area of Figure 9.

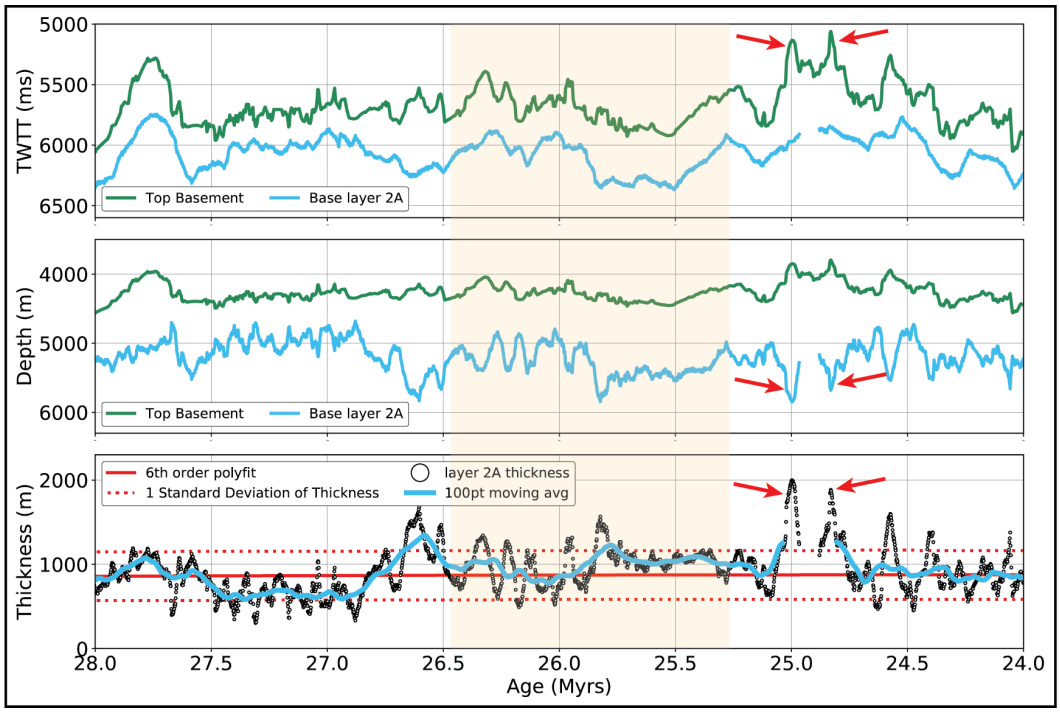

Figure 9: Zoom in of thickness values from 24-28 Ma crust. Top: Arrival time of basement interface (green) from prestack time-migrated section and Layer 2A Event (blue) from constant velocity section. Middle: Depth of basement interface and Layer 2A Event. Colors same as top. Bottom: Zoom from Figure 8 showing thickness of layer 2A with data colors same as in Figure 8. Tan shading indicates the extent shown in Figures 6, 12. Red arrows indicate small scale variations in the basement interface not present in the Layer 2A Event and how they affect layer 2A thickness.

Line Name	Mean 2A thickness (m)	Layer 2A Thickness Standard Deviation (m)	Percentage of 2A Event Occurrence	Mean Sediment Thickness (m)
1F	759	326	55	34
1E	690	285	56	72
1D	898	282	84	85
1C	669	230	75	131
1B			0	132
1A			0	223

Table 2: Layer 2A and sediment thickness values for CREST ridge normal MCS lines.

Layer 2A Thickness vs. Spreading Rate

Approximately 63% of our measured thickness values are taken from crust generated at intermediate spreading rates (half rates of 20-31 mm/yr), with the remaining ~37% taken from crust generated at slow-spreading rates (12-20 mm/yr half rates). Along the CREST ridge-normal transect, the youngest, <7 Ma, and oldest, >45 Ma, crustal sections contain the majority of slow-spread crust, while the crust between 7 Ma and 45 Ma is predominantly intermediate-spread crust (Figure 1, Table 1). The slower spread crust contains either a lack of lateral continuity of the Layer 2A Event (Figure 5A) or a complete absence of the Layer 2A Event (Figure 7A). The intermediate-spread crust generally contains a greater occurrence of the Layer 2A Event (Figure 6A) with a lateral continuity greater than that observed in slow-spreading crust. The roughness of the basement interface is greatest in the youngest (Figure 10) and oldest crust (Figure 11), which corresponds with the slow spreading rates at which these portions of crust were generated. Crust of ages 16-48 Ma, where the Layer 2A Event is most extensively observed, exhibits the smoothest basement topography of the CREST transect (Figure 12). *Figure 9* also reveals how the layer 2A thickness variability is reduced when the top of basement interface is very smooth. Cross-plotting spreading rate and thickness data from the CREST transect (Figure 13) reveals no obvious trend, and linear regression returns an R^2 of $1x10^{-3}$. The thickness measurements from crust created in the intermediate-spreading regime have a mean thickness of 780 m and standard deviation of 290 m, and thickness measurements from slow-spreading crust have a mean thickness of 690 m and standard deviation of 290 m.

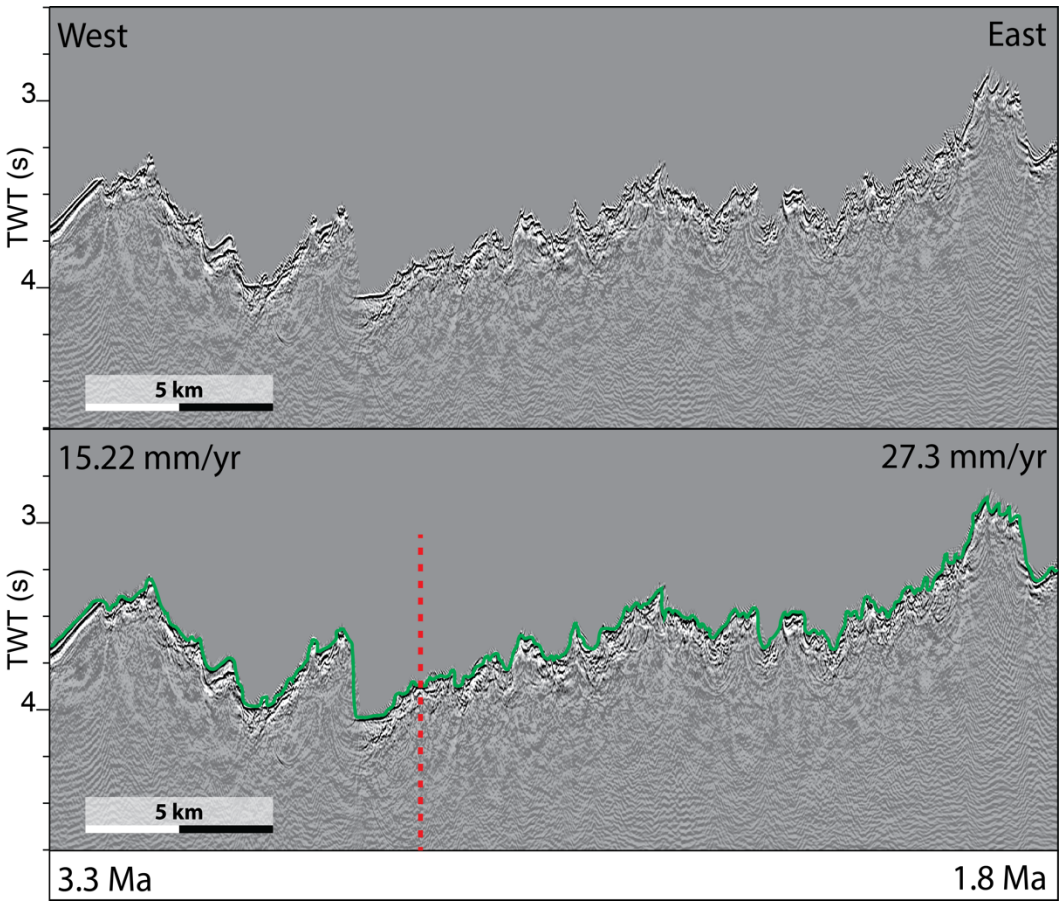

Figure 10: Top: Prestack time migrated section of seismic reflection profile 1F shown as constant velocity stack in Figure 5A. Bottom: Same section interpreted with: green – top of the basement reflection, vertical dashed red line is location of CMP supergather in *Figure 5B*. Seismic profile location shown in Figure 1.

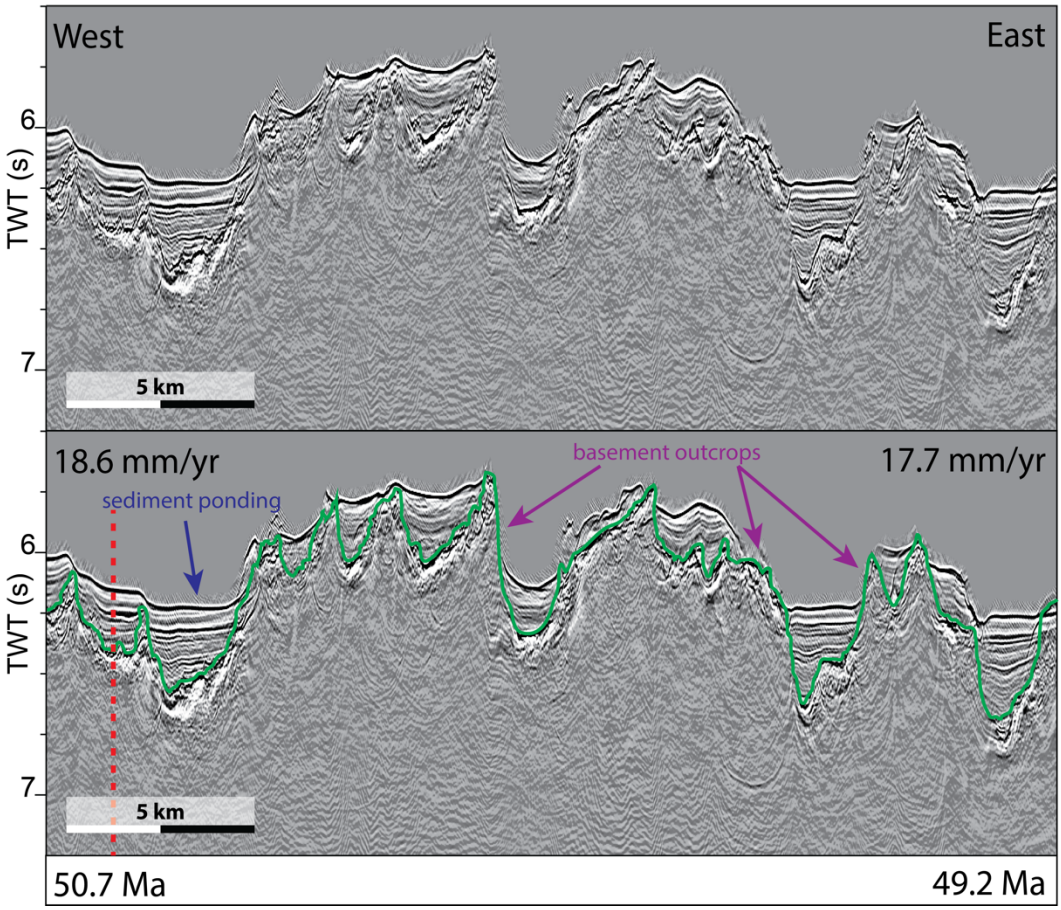

Figure 11: Top: Prestack time migrated section of seismic reflection profile 1B shown as constant velocity stack in Figure 7A. Bottom: Same section interpreted with: green – top of the basement reflection, vertical dashed red line is location of CMP supergather shown in Figure 7B. Seismic profile location shown in Figure 1.

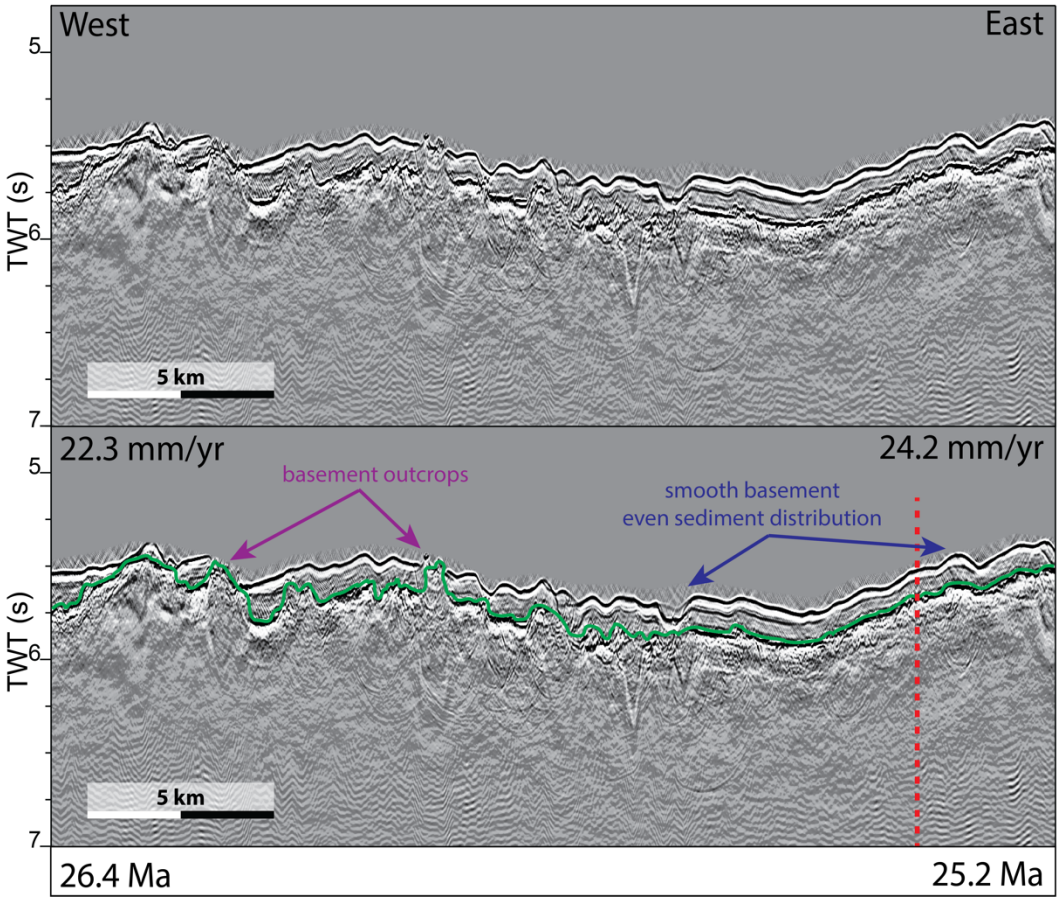

Figure 12: Top: Prestack time migrated section of seismic reflection profile 1D shown as constant velocity stack in Figure 6A. Bottom: Same section interpreted with: green – top of the basement reflection, vertical dashed red line is location of CMP supergather shown in Figure 6B. Seismic profile location shown in Figure 1.

Layer 2A Thickness vs. Sediment Cover

Oceanic crust in the CREST study area contains a progressive increase in sediment cover with increasing crustal age, which is to be expected in the open ocean away from any significant continental sediment source. Accumulation of sedimentary deposits focuses within valleys

between bathymetric highs where basement topography is rough (Figure 11) and covers areas of relatively smooth basement topography in a more even distribution (Figure 12). 0-15 Ma crust contains the least amount of sediment (Figure 10) and exhibits an intermittently discontinuous or absent Layer 2A Event (Figure 5). 16-48 Ma crust contains increased amounts of sediment, which is often more evenly distributed due to the relative smoothness of the basement interface (Figure 12). The Layer 2A Event is more readily observed at these crustal ages than anywhere else on the transect (Figure 6). In 48-70 Ma crust, the sediment is the thickest (up to ~400 m), but the significant rugosity of the basement interface causes the sediment to pond between basement highs (Figure 11). The presence and thickness of sediment is visually correlated with the observable appearance of the Layer 2A Event or its thickness anywhere along the transect. Because we only interpreted a sediment layer when visible in the seismic reflection sections and the top of the basement is interpreted across the entire transect, the ratio of their respective lengths in each seismic profile provides a percentage of sediment cover. Approximately 74 percent of the transect between 0 and 48 Ma has sediment cover visible in the seismic reflection sections; 0-16 Ma crust is 57 percent covered and 16-48 Ma crust is 84 percent covered.

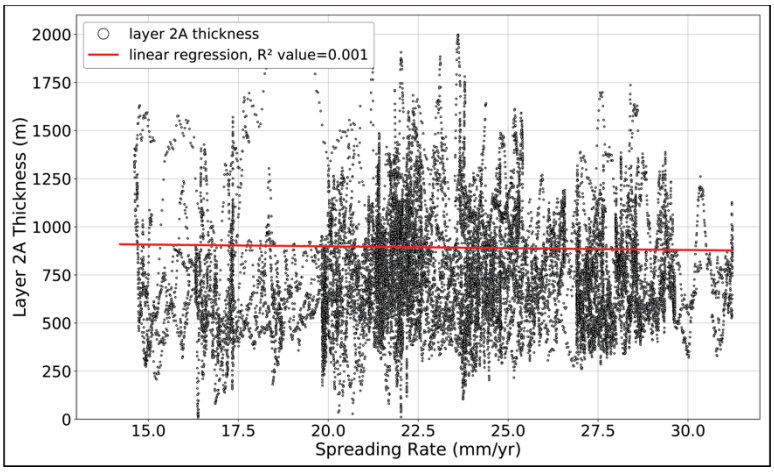

Figure 13: Plot of layer 2A thickness vs. spreading rate for 0-48 Ma crust.

Discussion

Upper Crustal Evolution

The recent upper crust tomographic velocity models using the CREST data (Kardell et al., 2019) indicate that velocities continue to increase slowly out to ~58 Ma, significantly older than the expected mature age of ~10-15 Ma (e.g., Carlson (1998); Nedimović et al. (2008)). Kardell et al. (2019) concluded that circulation of seawater in the upper crust continues to occur in older crustal ages, which results in precipitation of minerals within the pore space. The disappearance the Layer 2A Event after 48 Ma in our results also suggests that crust is continuing to evolve to ages of at least ~48 Ma, which agrees with the findings of Kardell et al. (2019). The difference in the age of continued evolution may be a result of the different methodologies used. In our study, the presence of both a triplication from the layer 2A/2B velocity transition in CMP gathers and the Layer 2A Event pseudoreflection in seismic reflection sections out to at least 48 Ma crust serves as evidence that the velocity gradient separating layer

2A from 2B persists into these crustal ages. If the velocity gradient that marks the transition does persist to 48 Ma, then a porosity change significant enough to produce the velocity disparity between layers 2A and 2B (Carlson, 2011) must persist as well.

An increase in velocity of layer 2A that reduces the velocity disparity between layers 2A and 2B implies that precipitation of minerals within the pore space of the upper crust is occurring. Wilkens et al. (1991) showed that just a small decrease in porosity in low aspect ratio pore space can result in a significant change in velocity. Moreover, Carlson (2014b) uses gravity and borehole data to show that upper crustal porosity is essentially unchanging in crust older than 0.2 Ma and that velocity increases can be attributed to a change in crack morphology as opposed to bulk porosity. The precipitation of secondary minerals in low aspect ratio pores (i.e., very thin cracks, Wilkens et al., 1991) could serve to increase velocity at the magnitudes shown by Kardell et al. (2019) between 6 Ma and 58 Ma (4.2 – 4.9 km/s) by changing the crack morphology without significantly changing the porosity. Additionally, the drill holes into ocean crust that do exist are, in effect, finite points from a very heterogeneous upper crust (Karson, 2002) and do not sample crust collected at the same spreading center (Carlson, 2014b), which may limit their ability to accurately characterize the porosity evolution of the upper oceanic crust.

Possibly contributing to the loss of our ability to image the Layer 2A Event in crust older than 48 Ma is that a gradient change producing a pseudoreflection that can be exploited by the seismic reflection method may only exist when the extent of precipitation of secondary minerals in thin fractures and low aspect ratio pores is below a certain threshold. Additionally, our ability to resolve a Layer 2A Event in 48 Ma crust and beyond is probably strongly affected by the topography of the basement interface. The crust between 48 Ma and 67 Ma displays a very rough

topography (Figure 7) and was generated at some of the slowest spreading rates of the transect, 13-19 mm/yr (Figure 14). A rough or jagged basement interface, where the top of the presumed igneous crust is imaged, will scatter seismic energy (Peirce et al., 2007), which could influence the appearance of the Layer 2A Event. Other portions of the CREST transect nearer to the spreading axis are of crust generated at similarly slow spreading rates, contain a rough basement interface (Figure 10), and the Layer 2A Event is less continuously imaged there (Figure 5), even with a strong gradient expected due to the young age of the crust. Given that Kardell et al. (2019) show continuing velocity evolution out to 58 Ma, 10 Myr older than our study, we suggest that the lack of a seismically imageable Layer 2A Event in crust older than 48 Ma may arise from both a fading of the gradient change caused by precipitation of secondary minerals over time, and the roughness of the basement interface caused by tectonic extension processes dominating during the slow spreading intervals. *Figure 14* shows the spreading rate and basement roughness at a large-scale across the transition at 48 Ma crust. Even at the large scale shown in *Figure 14*, the correlation between the basement roughness and slow spreading rate in crust older than 48 Ma is apparent. Additionally, the increase in basement roughness and decrease in spreading rate in older crust appears to correspond with loss of and imageable Layer 2A Event.

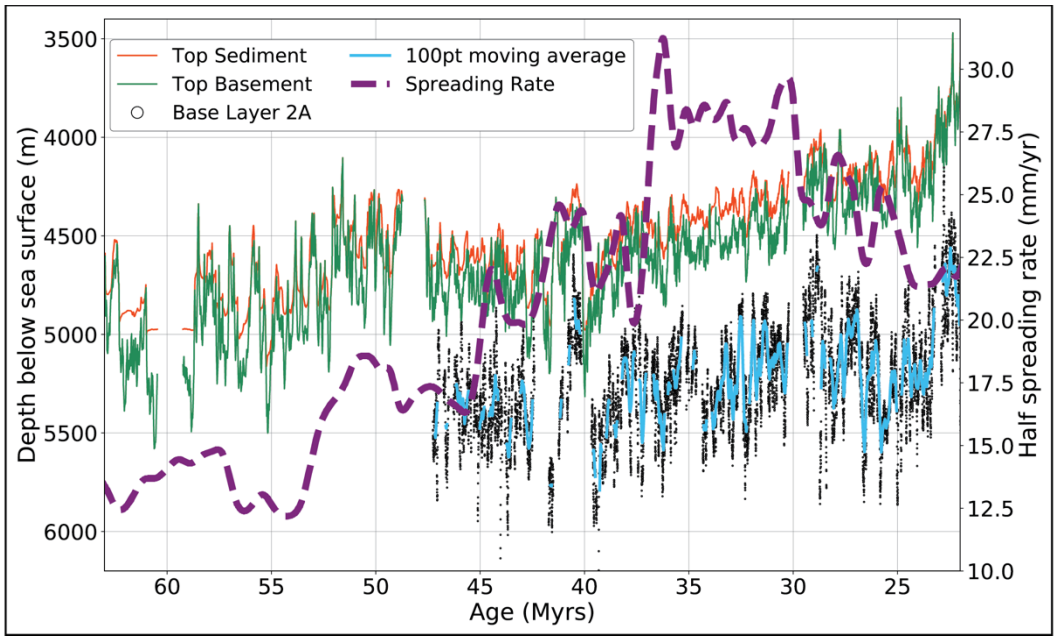

Figure 14: Depth and spreading rate vs. age plot showing the top of the sediment (orange), the top of the basement (green), the base of layer 2A as estimated by the Layer 2A Event (black circles), a 100-point moving average of the base of layer 2A (blue), and spreading rate from Pérez-Díaz and Eagles (2017) (purple).

The lack of continuity of the layer 2A Event we observe, which results in the gaps in our thickness data (Figure 8), is possibly a result of the roughness of the basement interface at the slower spreading rates. Also possible is that the sharp gradient change necessary to produce the triplication may not be present everywhere, even when the absolute magnitude of velocities seen in the streamer tomography models of Kardell et al. (2019) is indicative of layer 2A. Kardell et al. (2019) report that their models cannot resolve the rapid gradient change needed to produce the triplication we use to estimate the base of Layer 2A, so further determination of whether or not the gradient change exists where we do not image the Layer 2A Event will require higher-

resolution velocity modeling. Based on our results of imaging more and a more continuous Layer 2A Event where the basement interface is smoothest (Figure 6), we interpret much of the gaps in our thickness calculations (Figure 8) to be caused by rough basement topography scattering refraction paths.

Layer 2A Thickness with Crustal Age and Spreading Rate

Table 3 is a comparison of one standard deviation of layer 2A thicknesses from our overall mean in the South Atlantic with thickness ranges reported by previous studies at slow and intermediate spreading ridge systems (Arnulf et al., 2014; Arnulf et al., 2011; Baran et al., 2010; Blacic et al., 2004; Christeson et al., 2010; Hussenoeder et al., 2002; Nedimović et al., 2008). While our range is larger than those of other studies, we suggest that this is an expected result given our larger age range. Furthermore, our thickness range roughly brackets those of previous studies, indicating our values are reasonable. Kardell et al. (2019) found slightly different layer 2A thickness values along the CREST transect where they obtained velocity models. We believe the difference is a product of both data and methods. Our thickness estimates in *Table 2* are for entire CREST MCS lines where we imaged a Layer 2A Event, whereas theirs are only for subsections where they have velocity models. Also, the tomographic models they used significantly smoothed the basement interface, which removes some of the variation we observe. While the results may differ based on methodology, the thickness estimates of Kardell et al. (2019) are similar in magnitude; therefore, we contend that the large layer 2A mean thickness in the South Atlantic is not only a product of the methodology. Many of the studies we compare our layer 2A thickness to in *Table 3* used the same method as ours to determine layer 2A thickness. While *Figure 8* indicates that our mean thickness would not be lower if we excluded older

crustal ages to match the ages of previous surveys, *Figure 8* also shows that the mean could be smaller or larger if taken from a subsample of our total age range.

Spreading Center	Layer 2A Thickness (m)	Author
South MAR	470-1050**	This Study
North MAR	600	Arnulf et al. (2011)
North MAR	700-850	Arnulf et al. (2014)
North MAR	350-600**	Hussenoeder et al (2002)
JDF	485	Christeson et al. (2010)
JDF	320-460	Nedimović et al. (2008)
SEIR	570-990**	Baran et al. (2010)
GSC	380-670**	Blacic et al. (2004)

Table 3: Comparison of layer 2A thickness from this and previous studies of slow and intermediate spread crust. Colors indicate spreading rate; teal: this study (slow and intermediate spreading), one standard deviation from the overall mean of thickness shown, violet: slow spreading, green: intermediate spreading. Values are reported as given in study. ** = off-axis values, MAR = Mid-Atlantic Ridge, JDF = Juan da Fuca Ridge, SEIR = Southeast Indian Ridge, GSC = Galapagos Spreading Center.

Layer 2A thickness does not systematically decrease with crustal age along the CREST transect (Figure 8), which would be expected if layer 2A was thinning from the bottom up. Our results instead suggest that the location of the gradient increase remains in place at a constant depth, and, as velocities in layer 2A increase, the magnitude of the velocity disparity between 2A and 2B is slowly reduced. We do not observe any rapid off-axis thickening of layer 2A (e.g.,

Blacic et al., 2004; Hooft et al., 1996; Vera & Diebold, 1994), which agrees with the conclusion of Hussenoeder et al. (2002) that the thickness of layer 2A is established within the axial valley at the MAR.

Spreading rate has been proposed as a predictor of crustal morphology (Morgan & Chen, 1993), but global studies have not shown a relationship between spreading rate and crustal thickness, except possibly at ultraslow spreading rates (Brown & White, 1994; Chen, 1992). We find no correlation when comparing the thickness of layer 2A to spreading rate across the transect (Figure 13); this interpretation matches a similar comparison of published layer 2A thickness values (Christeson et al., 2010).

While spreading rate alone may not be a determining factor of layer 2A thickness, the ratio of tectonic extension to magmatic supply (i.e., Buck et al., 2005; Ito & Behn, 2008) may control how much porous upper crust is emplaced and how rough or smooth the topography is before that crust is transported away from the on-axis eruptive zone. The thickness of the porous upper layer that results in the lower velocities of layer 2A could be inherited from the parameters of crustal genesis at the ridge such as magmatic budget, ratio of tectonic extension to magmatic eruption, melt source and supply, and melt fractionation/evolution determining eruptive volume and style. Buck et al. (2005) showed that the ratio of tectonic to magmatic spreading at the ridge controls the development and longevity of normal faulting in the crust as it is transported away from the ridge. Ito and Behn (2008) later refined this to show that the time a spreading center spends in a magmatically or tectonically dominant spreading regime will determine the axial morphology and topographic expression of the top of the crust (i.e., the more magmatically dominant a spreading regime is and the longer amount of time the spreading center spends in that regime, the smoother the top of the crust will be). We observe the most laterally continuous and

homogenous layer 2A thicknesses (Figures 6, 9) where the top of the basement is smoothest (Figure 12).

Because the base of layer 2A has been observed occurring within the extrusives (Christeson et al., 2010; Christeson et al., 2007), within the transition zone from extrusive to intrusive (Carlson, 2011; Christeson et al., 2010; Christeson et al., 2007), and within the intrusive dikes of the upper crust (Carlson, 2011), lithology must be secondary to porosity for the interval of layer 2A. This implies that our thickness results are not specifically indicative of any particular lithologic thicknesses, but rather the thickness of porous upper crust. With increasing upper crustal velocities with age (Kardell et al., 2019) and the gradient separating layers 2A and 2B marking a porosity and permeability change (Carlson, 2011), our results provide an estimate of the thickness and the lateral extent of the region where fluid can circulate within the upper crust. Our imaging of the Layer 2A Event in crust up to 48 Ma implies that circulation of sea water within the crust, and, therefore, chemical and thermal exchange between the ocean and the crust, can occur at these older ages. The continued evolution of upper oceanic crust through the process of low-temperature alteration agrees with global heat flow and fluid flux studies (Johnson & Pruis, 2003; Stein & Stein, 1994).

Layer 2A Heterogeneity

Our layer 2A thickness estimates contain significant variability, which introduces a broad distribution and substantial scatter when examining trends. The values of layer 2A thickness reported by Kardell et al. (2019) contain a similar standard deviation as ours, but their results do not include the rapid variation we observe (Figures 8, 9). We believe two primary contributing factors to be predominantly responsible for the scatter we observe in our thickness values. The first is that we use a smoothed velocity-with-age curve (Figure 4) that does not account for fine-

scale, local velocity variations. The second is that we measure time thickness between a migrated basement interface and an unmigrated Layer 2A Event. The unmigrated section used for the Layer 2A Event will have substantially reduced lateral resolution compared to the migrated section and will not capture short wavelength changes, which can result in rapid thickness variations when the basement interface topography changes rapidly (red arrows, Figure 9). This second case will be especially true where the basement interface is roughest, which can be seen in the relatively uniform thickness values in *Figure 9* that correspond to smooth basement in east half of *Figures 6, 12* and the more variable thickness values where basement is rougher in the western half of the same figures. The polynomial fit operates a very strong smoothing and eliminates any small-scale variations in thickness. By contrast, the 100-point moving average (625 m at its smallest), which is averaging over roughly the width of the Fresnel zone and is thus relatively insensitive to the un-migrated state of the data, captures much of the small-scale variation in thickness. The velocity values from Kardell et al. (2019) also contain significant variability, which supports our hypothesis that some of the scatter is real. We suggest that the myriad processes related to the melt sourcing, melt evolution, eruption style, and melt cooling coupled with the extensional forces fracturing the crust and transporting it from within the eruptive zone of the axial valley to the ridge flanks and out to the abyssal plain create the heterogeneity we observe in our thickness estimates. Perhaps, at more morphologically smooth spreading centers where magma availability is more continuous and dominates extensional forces (e.g., the East Pacific Rise) a more homogeneous layer 2A can be expected. However, our results agree with the heterogeneity observed at the Mid-Atlantic Ridge 37° N (Arnulf et al., 2011). Small-scale trends in the thickness of layer 2A along the CREST transect, when viewed in the context of the large-scale trend, lead to new inferences regarding previous investigations

of layer 2A. Previous studies that examined layer 2A variation (Arnulf et al., 2011; Baran et al., 2010; Blacic et al., 2004; Carbotte et al., 1997; Christeson et al., 1994; Harding et al., 1993; Hooft et al., 1996; Seher et al., 2010; Vera & Diebold, 1994; Vera et al., 1990) focused on relatively small age ranges and on crust very near the spreading axis; the largest crustal age range previously surveyed of crust from the same spreading center was across the Juan de Fuca ridge and flanks (Nedimović et al., 2008), which encompassed crust from 0-9 Ma. The CREST data illuminates the superimposition of small-scale trends within the longer, large-scale behavior of layer 2A over crustal ages 0-48 Ma (Figures 8, 9). Small-scale variations, often highly divergent from the large-scale trend, could promote inaccurate interpretations or extrapolations if viewed without the context of the full age range. Additionally, this implies that borehole measurements of the thickness of the porous upper crust cannot be extrapolated to regions even moderate distances away.

Sediment Cover and the Fate of Layer 2A

Sediment cover has been shown to affect the rate of velocity increase in upper crust by sealing of the circulation system on the flanks of the Juan de Fuca Ridge (Nedimović et al., 2008; Rohr, 1994). Once low-permeability sediment has blanketed the porous upper crust, zones of fluid circulation recharge and discharge in the forms of unsedimented fault scarps and igneous outcrops still allow for substantial lateral flow to continue the circulation of fluid within the upper crust (Fisher & Becker, 2000). Given the relatively slow sedimentation rate in the South Atlantic and the abundance of unsedimented basement outcrops (Figure 12), we infer that the circulation system never becomes a fully ‘closed’ system as may be present on the eastern flank of the Juan de Fuca ridge (Rohr, 1994) where terrigeneous sediment from North America thickly buries the ocean crust.

Houtz and Ewing (1976) observed that layer 2A thinned and eventually disappeared with crustal age at around 40 Myr in the Atlantic. The compilation of published crustal velocities from Carlson (1998) indicate that the upper crust never fully reaches the velocity values of layer 2B and, therefore, that layer 2A must persist into older crust. Kardell et al. (2019) also suggest that, based on their velocity values, layer 2A does persist into older ages along the CREST transect. However, neither study was able to show that the velocity structure of the upper crust at old ages, >40 Ma, still contains distinct gradient regions that separate layers 2A from 2B. Nedimović et al. (2008) showed that no thinning of layer 2A with age occurs on the Juan de Fuca Ridge flanks, but their study only surveys crust 0-9 Ma. Our results show no thinning with age, but we can no longer resolve the pseudoreflection resulting from a distinct difference in velocity structure between layers 2A and 2B past crust ages of ~48 Ma in the South Atlantic. Although it does appear that layer 2A does not thin with age, our results raise the question of whether layer 2A persists or does, in fact, disappear. The answer may lie in the actual definition of layer 2A: whether layer 2A is defined by upper crust with velocities lower than those typical of layer 2B, 5.2 km/s, or rather as upper crust having a vertical velocity gradient distinct from that of the underlying crust. While the answer requires a comprehensive and high-resolution analysis of the velocity structure, we suggest that if layer 2A is no longer seismically discernable from underlying crust, then layers 2A and 2B have simply become layer 2 with no internal seismically differentiable sublayers. More robust velocity modeling that resolves the fine-scale evolution of the vertical gradient separating the layers of the upper crust is needed to more conclusively determine the fate of layer 2A.

Conclusions

We use MCS imaging across crust formed 0-70 Ma in the South Atlantic to elucidate the long-term character of the porous upper oceanic crust. Using the retrograde arrival that is indicative of the velocity gradient increase at the transition between layer 2A and 2B as a proxy for the base of layer 2A, we come to the following conclusions:

1. The upper oceanic crust continues to evolve for at least 48 Myr along this transect in the South Atlantic. Where we can consistently observe the triplication and produce the Layer 2A Event pseudoreflection, we infer that the vertical velocity structure necessary to produce a triplication (and therefore the pseudoreflection we use to estimate layer 2A thickness) must persist. We can no longer observe the triplication or the Layer 2A Event beyond 48 Ma, which suggests that layer 2A is no longer a distinct region resolvable with the pseudoreflection method, likely due to both basement roughness and increased velocity. Distinguishing layer 2A solely on the magnitude of velocity may fall short of differentiating layer 2A from layer 2B and identifying that there is a difference between the two.

2. Layer 2A in the South Atlantic has a mean thickness of 760 m for 0-48 Ma crust, and layer 2A does not thin with age; thickness varies significantly, but we find no systematic increase or decrease in thickness as crust ages. This implies that the rapid velocity gradient increase that results in the triplication we use to estimate the transition between layers 2A and 2B does not change depth as crust ages. Instead, we conclude that mineral precipitation in pore space of the porous and permeable upper crust results in the velocity disparity between layers 2A and 2B being reduced.

3. Layer 2A thickness is not related to the spreading rate at which the crust was created. We find no observable correlation between the thickness of layer 2A and spreading rate across spreading half-rates from ~12 mm/yr to ~31 mm/yr in the South Atlantic. However, the Layer 2A Event appears more often and more laterally continuous, and layer 2A thickness is more homogenous when the basement topography is smooth.

4. The crust in the South Atlantic is never sealed off from the ocean by sediment cover. The abundance of outcropping basement exposures allows the circulation system to remain open into older crustal ages. This implies that that the exchange of heat and dissolved species can take place as long as the upper crust remains permeable.

5. The heterogeneity of the upper crust across the scale of 0-48 Ma crust is substantial and we observe small-scale layer 2A thickness trends that oppose the overall trend. This implies that small scale surveys and discrete borehole measurements likely may not succeed in fully and accurately capturing the overall trends of the upper crust.

CHAPTER III

THE BALANCE BETWEEN SPREADING AND MAGMATISM

Introduction

Seafloor spreading is a fundamental process for plate tectonics and mantle convection (Elsasser, 1971). The genesis of crust at a spreading center proceeds through a combination of magmatism and extensional faulting (Buck et al., 2005). The balance between these processes in accommodating spreading is intricately tied to the thermal state of the spreading center and leads to the different crustal morphologies observed at Earth's various spreading centers (Behn & Ito, 2008; Buck et al., 2005).

The morphological spectrum of ocean crust affects the heatflow from the mantle through a combination of surface area and fluid pathways (Baker et al., 1996; Fisher & Becker, 1995), which is potentially a feedback mechanism of the overall thermal state that controls the morphology (Lavier & Buck, 2002). The largest aquifer on Earth, the upper oceanic crust, is also subject to the spreading and morphology of the crust, which affects the chemical exchange between the hydrosphere and the geosphere (Johnson & Pruis, 2003). Crustal fabric and morphology also plays a role in subduction zone dynamics, from the fluid budget (Nedimović et al., 2009) to the propensity of the plate interface to lock (Shillington et al., 2015). These factors make understanding the origin of crustal morphology and how it is connected to the balance between spreading rate and magmatism important. In this study, we use a continuous multichannel seismic (MCS) profile across ~70 million years of ocean crust generated at one segment of the Southern Mid-Atlantic Ridge to investigate the relationship between spreading rate, magmatism, and crustal morphology.

Background

Spreading Rate and Accommodation

Seafloor spreading and the development of ocean basins is achieved through a combination of magmatism and tectonic extension (Scotese et al., 1988). The sinking of oceanic lithosphere into the asthenosphere at subduction zones combined with the shrinking caused by cooling and densification are the primary far-field stress that pulls oceanic plates apart (i.e., spreading), which leads to the formation of new, replacement lithosphere at mid-ocean ridges (e.g., Elsasser, 1971). To describe the relative degree of spreading accommodated by magmatism or tectonism, we use the term spreading regime. In the global mid-ocean ridge system, a spectrum of spreading regimes exist (e.g., Ito & Behn, 2008), from spreading that is nearly entirely accommodated through magmatism as one end member to spreading that is nearly entirely accommodated by extensional faulting as the other (e.g., Dick et al., 2003; Sinton & Detrick, 1992).

Perfit and Chadwick (1998) define fast spreading as half-rates of 40-80 mm/yr, intermediate spreading as half-rates of 20-40 mm/yr, and slow spreading as half-rates of 5-20 mm/yr. Ultraslow spreading is defined by certain characteristics in addition to spreading rate, but typically corresponds to half-rates of <6 mm/yr (Dick et al., 2003). Within these classifications, spreading centers with fast and slow spreading rates are generally characterized by more magmatic accommodation and more tectonic accommodation, respectively (Buck et al., 2005). At the fast spreading East Pacific Rise (EPR), the axis is marked by an axial high, the innermost axial area is smooth (Carbotte et al., 1997), and faults begin developing ~2 km or more off axis (Carbotte & Macdonald, 1994). Faults that develop off axis are both inward and outward facing (Carbotte et al., 1997), which Buck et al. (2005) show can be attributed to the unbending stress

as the crust is transported off the axial high. The absence of faulting within the neovolcanic zone indicates that the majority of spreading is accommodated by magmatism in the form of dike injection and volcanic eruption (Perfit & Chadwick, 1998). At slow spreading ridges like the Mid-Atlantic Ridge (MAR), the axis is generally marked by a valley that can be >1 km deep, topography around the axis is substantially rough (Mutter & Karson, 1992), and faults are found throughout the axial area (Escartin et al., 1999). The large majority of faults that develop at slow spreading centers are inward facing (dip toward the axis) (Carbotte & Macdonald, 1990; Escartin et al., 1999), which is consistent with expectations that extensional faults develop preferentially facing the axis (Searle, 1984). At the ultraslow spreading ridges (e.g., Gakkel Ridge, Southwest Indian Ridge), the amount of extension on some faults is great enough to exhume lower crust and upper mantle (Dick et al., 2003). The prevalence of faulting at slow spreading ridges indicates that a significant portion of the plate spreading is accommodated by tectonic extension (Mutter & Karson, 1992; Schouten et al., 2010).

Except for the large detachment faults that expose lower crust and upper mantle, intermediate spreading rate ridges exhibit the full spectrum of axial morphology and fault geometry observed in slow and fast spreading ridges (Canales et al., 2005; Cochran & Sempéré, 1997; Detrick et al., 2002). The difference in spreading rate at the axial high-characterized EPR and the axial valley-characterized MAR is substantial (up to 70-80 mm/yr difference in half rates) (Müller et al., 2008). However, relatively small changes in spreading rate (<3 mm/yr difference in half rates) at intermediate spreading ridges may reflect a change from significant faulting and an axial valley to subdued faulting and an axial high (Cochran & Sempéré, 1997; Sinton et al., 2003). These apparent large variations in the spreading regime over small changes in spreading rate led to the inference that perhaps there is a threshold or tipping point between

the relative dominance of magmatism and tectonism in accommodating plate spreading, as Wilson et al. (2019) propose for the intermediate spreading Costa Rica Rift (CCR).

Roughness of the Crust

The measure of roughness of the crust is essentially the amount of topographic deviation from a trend or average over a defined length scale. Roughness has been generally calculated as either the root-mean-square (RMS) of deviation (e.g., Hayes & Kane, 1991) or the mean absolute deviation (MAD) (e.g., Small, 1998). Both measurement systems of roughness/topography produce similar results and both indicate that the roughness of the ocean crust is inversely dependent on the spreading rate at which it was generated (Hayes & Kane, 1991; Malinverno, 1991).

Abyssal hills are the most prevalent form of off-axis topography creating roughness on the seafloor (Menard, 1964) and are thought to form from different genetic processes at fast vs. slow spreading ridges. Abyssal hills formed at fast spreading rates are generally smaller and begin developing in the near off-axis region through a combination of faulting and off-axis volcanism (Goff, 1991; Macdonald et al., 1996). Abyssal hills formed at slow spreading rates are directly linked to the axial faulting that accommodated plate spreading through extension (Buck & Poliakov, 1998). Faulting is responsible for much of the seafloor topography (e.g., Carbotte et al., 1997; Mutter & Karson, 1992), and numerical models (Behn & Ito, 2008; Buck et al., 2005) show the origin of faulting is dependent on the ratio of the magmatic vs. tectonic accommodation of spreading. The inverse dependence of roughness on spreading rate and the differences in faulting and topography with changes in the spreading regime suggest a link between seafloor roughness, spreading regime, and spreading rate.

Crustal Structure

The structure of the oceanic crust may also depend on spreading rate. Global syntheses show that the average total crustal thickness is independent of spreading rate, outside of ultraslow rates where crustal thickness decreases (Chen, 1992; Christeson et al., 2019a; White et al., 1992). However, Christeson et al. (2019a) find that the standard deviation of thickness for crustal layers 2 and 3 are higher for crust formed at slow and intermediate spreading rates than for crust formed at fast spreading rates, indicating more variability in structure with slower spreading rates.

The uppermost interval of oceanic crust, layer 2A, is igneous with an effective porosity and permeability that allows for a substantial circulation of water (Carlson & Herrick, 1990; Fisher & Becker, 2000). That high porosity results in the lower P wave velocities, ~2-5 km/s, that characterize layer 2A (Carlson, 2010). Vera and Diebold (1994) show that at the fast spreading EPR, layer 2A thickness increases as the crust is transported away from the axis, up to doubling in thickness, likely through off axis volcanism. Carbotte et al. (1997) show that the base of layer 2A at the EPR is initially smooth on axis and then matches the abyssal hill topography off axis, suggesting that the base of layer 2A is initially set by magmatic processes rather than tectonic. At slow spreading ridges, layer 2A thickness is set within the axial valley (Hussenoeder et al., 2002) where the majority of magmatism occurs. Regardless of where the thickness is set, no correlation between spreading rate and layer 2A thickness has been found (Christeson et al., 2010; Estep et al., 2019a). Layer 2A has a positional correspondence with the extrusive layer in the idealized lithologic model of oceanic crust (e.g., Boudier & Nicolas, 1995) and has occasionally been treated as synonymous with the extrusive basalts; however, the evidence from in situ oceanic crust indicates that the change in porosity responsible for the velocity change that

defines layer 2A does not always correspond to the base of the extrusives (Carlson, 2014; Christeson et al., 2010; Christeson et al., 2007). How the spreading regime, the relative accommodation of spreading through magmatism or tectonism, affects the structure of the crust and the thickness of layer 2A has not been shown.

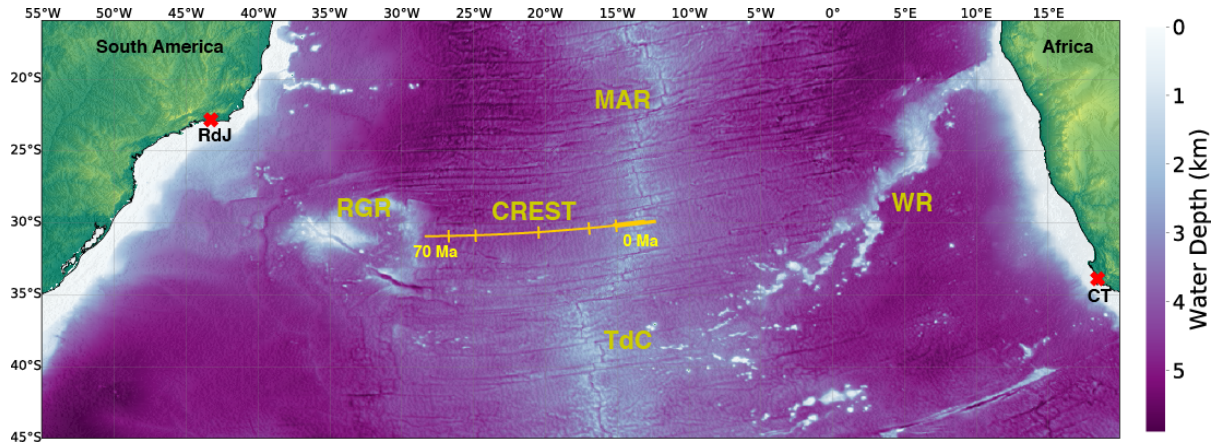

Figure 15: Study area in the South Atlantic with CREST survey in yellow lines. MAR = Mid-Atlantic Ridge; RGR = Rio Grande Rise; WR = Walvis Ridge; TdC = Tristan da Cunha; RdJ = Rio de Janeiro, Brazil; CT = Cape Town, South Africa.

Study Area

South Atlantic Spreading Segment and CREST Transect

Our examination of the relationship between magmatism, crustal roughness, spreading rate, and layer 2A leverages the data collected by the CREST (Crustal Reflectivity Experiment Southern Transect) expedition (Figure 15). The CREST expedition surveyed ~70 Myrs of crustal ages created at spreading half-rates of 12-31 mm/yr on the South American plate in the South

Atlantic Ocean. The hallmark of the dataset is a ~1500 km continuous East-West transect that follows a crustal flow line orthogonal to the axis from 0 Ma crust at the MAR in the east to 70 Ma crust at the margin of the RGR in the west. In addition to the ridge-normal transect, five 70 km, ridge-parallel, crossing North-South transects were also collected at crustal ages of 6.6, 15.2, 30.6, 49.2, and 61.2 Ma. Data acquisition was completed using the *R/V Marcus Langseth* in early 2016 and the suite of data collected includes 2D MCS, wide angle reflection and refraction ocean bottom seismometer (OBS), multibeam bathymetry, chirp sub-bottom profiler, magnetics, and gravity. OBS data was only collected at the five North-South isochron profiles (Figure 15). In this study, we primarily utilize the MCS data to investigate changes in roughness and spreading regime.

Advantageous to our study is that the oceanic crust surveyed by CREST was all created at one spreading segment at ~30° S, which avoids the bathymetric complexity related to segment boundaries or fracture zones and reduces the effects of cross-segment variations in magma supply, crustal thickness, and spreading (e.g., Baran et al., 2010; Macdonald et al., 1991). Three propagator wakes do cross the transect at ages of ~10, ~21, and ~40 Ma (Christeson et al., 2019b), which must be considered when calculating roughness and spreading regime, but the rest of the transect between the MAR and the RGR is free of large changes related to reorganization at the spreading center.

The RGR and its conjugate on the African plate, the Walvis Ridge, constitute large bathymetric features that likely influenced spreading in the past. Referred to as an aseismic ridge or oceanic plateau, the RGR formed at the MAR when the Tristan plume had captured the spreading center (Morgan, 1971; O'Connor & Duncan, 1990). The RGR formed roughly between ~84 and 70 Ma before one or a series of ridge jumps and fracture zone migrations permanently

separated the RGR on the South American plate and the Tristan plume on the African plate (Barker, 1983; O'Connor & le Roex, 1992; Thoram et al., 2019). The waning Tristan plume continued to build the remaining parts of the Walvis Ridge system and is now located beneath the islands of Tristan da Cunha (O'Connor & Duncan, 1990; O'Connor & le Roex, 1992) (Figure 15).

Layer 2A and the Upper Crust in the South Atlantic

The character and evolution of the upper crust and layer 2A in the study area has been thoroughly examined using the CREST data by Kardell et al. (2019) and Estep et al. (2019a). Kardell et al. (2019) shows that velocities in the upper crust evolve rapidly at young ages, increasing from an average of 2.4 km/s to 4.2 km/s in the first 6 Myrs of crustal ageing, and then continue to increase gradually to 58 Ma crust. Their study was able to show that alteration of the pore space from low-temperature hydrothermal circulation in layer 2A persists into older crustal ages. They also found velocity heterogeneity in the upper crust increased in the crust created at slow spreading rates compared to that created at intermediate spreading rates. The study by Estep et al. (2019a) estimated layer 2A thickness using the psuedoreflection method of Harding et al. (1993) and Vera and Diebold (1994) and finds that the thickness of layer 2A does not depend on age or spreading rate along the CREST East-West transect. However, they do conclude that layer 2A thickness is more homogenous when the crust is smooth. They also find that the roughness of the crust was enough to allow basement outcrops to persist at older crustal ages, maintaining an open circulation system in layer 2A.

Crustal Thickness, Roughness, and Structure along the CREST transect

Christeson et al. (2019b) constrained crustal thickness in the survey area at each of the five North-South transects through velocity modeling of the OBS data. Their velocity models of

the four transects closest to the ridge over crust aged 6.6, 15.2, 30.6, and 49.2 Ma exhibit relatively uniform thicknesses of 5.6, 5.6, 7.0, and 5.5 km, respectively, across the North to South length that are within the global average of Christeson et al. (2019a). Their velocity model of crust aged 61.2 Ma, at the transect farthest from the ridge, shows a more heterogenous crust with an average thickness of 3.6 km, which is ~1.5 km thinner than the range of global averages. In addition to crustal thickness from the five OBS profiles, Estep et al. (2019b) used the Moho reflection in MCS to estimate crustal thickness increasing from ~6.0 km at 66 Ma to ~9.5 km at 68.3 Ma crust.

Christeson et al. (2019b) also use the multibeam bathymetry to estimate abyssal hill RMS heights using the method of Goff et al. (1991). Their results show abyssal hill RMS heights of 57-142 m, which is lower than expected for the spreading rates surveyed by the CREST expedition. These low values agree with the prediction of low abyssal hill heights for the region by Goff (2010) who used global gravity to estimate abyssal hill RMS height. The study by Hayes and Kane (1991) that finds an inverse dependence of spreading rate on seafloor roughness used a crustal flow line transect over crust aged ~0-62 Ma at ~26° S, just north of the CREST survey area. They found RMS roughness values of 83-212 m over 5-10 Myr measurement windows.

Fox et al. (1991) used multibeam bathymetry, gravity, and magnetics collected along the MAR between 31-34.5° S, just south of the CREST survey area, to show spatial variations in the accretion of crust at the axis. Their study reported the same whole spreading rate of 35 mm/yr throughout their study area, but finds that axial morphology varies from a well-developed axial valley to a moderately rifted axial high. They attribute the changes in the axial morphology to

changes in the thermal structure of the axis and to decoupling of the processes of mantle upwelling and spreading.

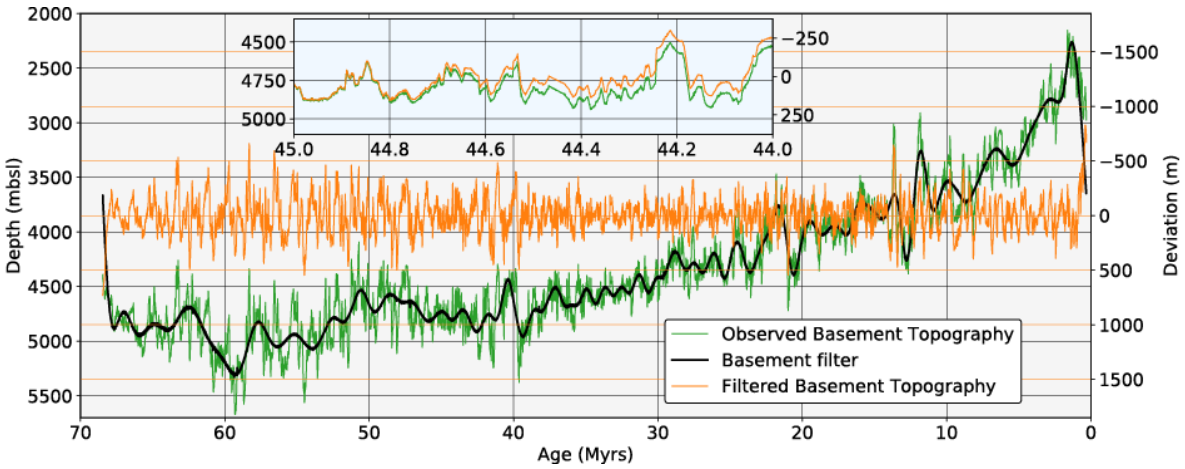

Figure 16: Comparison of the basement interface (green) with the 0.62 Myr^{-1} frequency filtered interface (orange). The deterministic component removed from the basement interface signal is shown in black. 1 Myr zoom shows small-scale topography is preserved.

Methods

Basement Interface

In order to measure the roughness of the crust and to estimate the relative magmatic and tectonic accommodation of spreading, we use the top of the interpreted igneous crust, which we reference as the basement interface, from prestack time-migrated MCS reflection images of the East-West CREST transect. The MCS data acquisition and processing workflow is described in detail in Estep et al. (2019a), where the data were processed for estimation of layer 2A thickness and evolution. The basement interface is mapped at every common midpoint gather (CMP) in

Paradigm 3D Canvas software, which allows us to estimate the depth at every 6.25 m, the CMP spacing.

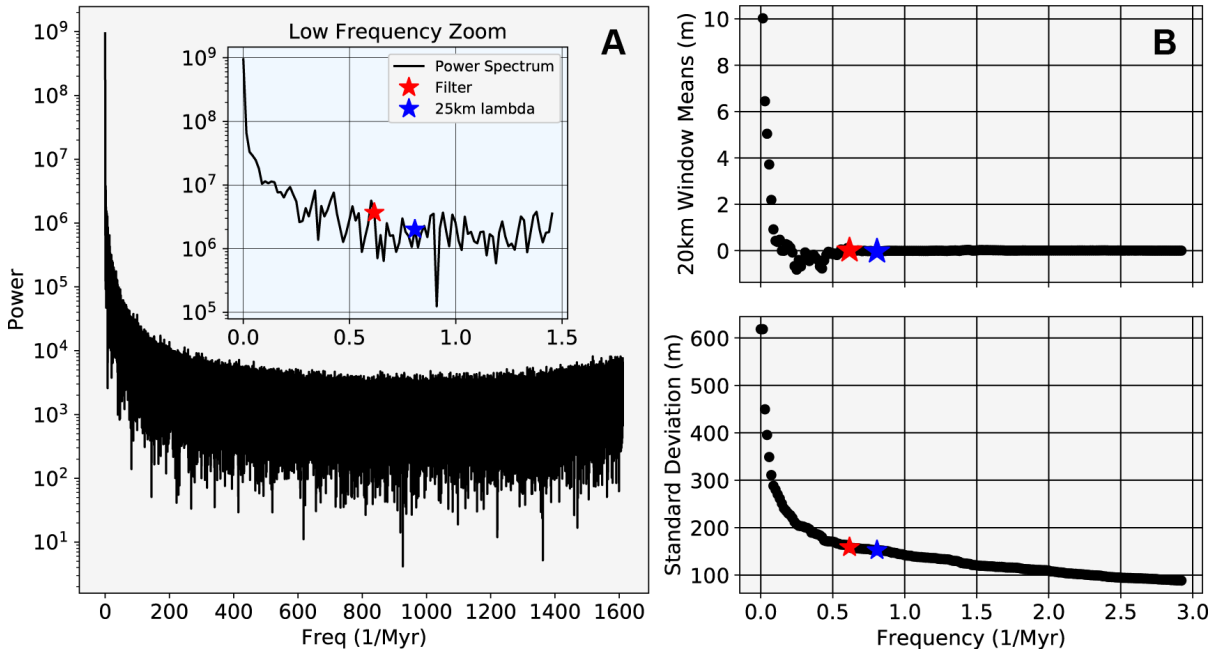

Figure 17: Basement interface filter design. A) Frequency power spectrum of unfiltered basement interface with low frequency zoom to show similarity of filter frequency (red star) and frequency of ~25 km wavelength (blue star) used by Hayes and Kane (1991). B) Top shows the mean of 20 km window means as progressively higher frequencies are filtered. Bottom shows the standard deviation of topography of the whole transect as progressively higher frequencies are filtered. Blue and red star are same as in A.

To convert the basement interface from time to depth, we use a constant water velocity of 1500 m/s and a constant sediment velocity of 1900 m/s, which is consistent with sediment

velocity found in the velocity modeling of the CREST MCS data by Kardell et al. (2019). For the comparison of layer 2A thickness to the other derived parameters, we use the layer 2A thicknesses from Estep et al. (2019a). The full flowline transect crossed the MAR, collecting data on both sides of the axis. Because only a limited age range was surveyed on the east side of the MAR, we retain only the basement interface from crust west of the MAR axis.

Filtering

In order to equitably calculate roughness and the magmatic fraction of spreading, we first removed long-wavelength signal from the basement interface. The total relief of the basement topography along the E-W transect is ~3500 m (Figure 16). We adopt the use of the terms deterministic and stochastic after Goff and Jordan (1988) and Small (1994), which distinguish between the systematic deviation of topography as direct result of lithospheric accretion processes and the random deviation of topography from stochastic processes. Normal seafloor subsidence away from the axis related to cooling is a deterministic component and abyssal hills are a stochastic component. In order to choose a filter for the deterministic components of the basement interface, we first apply a Fast-Fourier Transform to the basement topography in order to choose the frequency of the filter (Figure 17A). To best determine the frequency where deterministic components of the signal will be removed but stochastic components will be retained, we apply a series of butterworth high-pass frequency filters and measure the means of 20 km moving window means across the transect and the standard deviation of the full ~1500 m transect (Figure 17B). We find the point of decreasing returns (red star, Figure 17), where the means reach ~0 and increasing the frequency of the filter does not bring the means closer to 0. The frequency of decreasing returns is ~0.62 Myr^{-1}, which corresponds to a period of ~1.62 Myrs and a wavelength of ~34.6 km, using the mean spreading rate from the transect of ~21.3 mm/yr.

This is a slightly larger wavelength than the 25 km filter applied by Hayes and Kane (1991) (Figure 17, blue star), but we contend a well justified choice of a filter to remove deterministic components. The resulting basement interface has a mean of ~0.0, but all the small scale stochastic topography is preserved (Figure 16), and will allow us to calculate roughness, along with identify anomalies in the topography, without interference from deterministic components.

Roughness Calculation

To estimate the roughness of the crust, we used the root-mean-square of deviation (RMS) (Rice, 2006). RMS roughness has been used by several authors (e.g., Goff, 1991; Hayes & Kane, 1991; Malinverno, 1991) to estimate seafloor roughness, with which we can compare our results. Small (1998) used the median absolute deviation (MAD) to estimate seafloor roughness because of the more robust handling of outlier values compared to the RMS method. We tested the difference between MAD and RMS roughness and found statistically similar results, so we chose to use the RMS values for the ease of comparison with previous work.

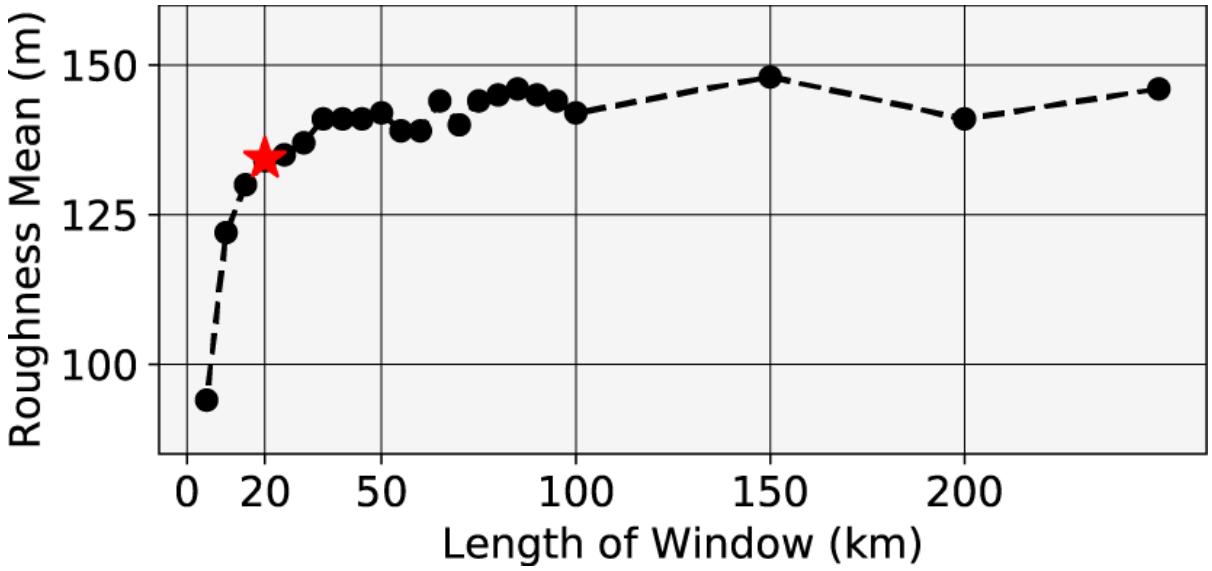

Figure 18: RMS Roughness window length selection. Red star is the mean of RMS roughness across the CREST transect using a 20 km window length.

To estimate how roughness changes along the transect, we use a 20 km sliding window that calculates the RMS roughness for each window. The window length exerts control on the calculated roughness, with the RMS roughness increasing with window length up to a certain point (Malinverno, 1991). We determined the best window length by measuring the mean of RMS deviations for the entire transect using increasing window lengths and found that roughness increases rapidly with window length up to ~20 km and then begins to asymptotically increase (Figure 18). A window of 20 km was chosen because it provided the most roughness samples for comparison across the transect and longer roughness window lengths no longer changed the result substantially.

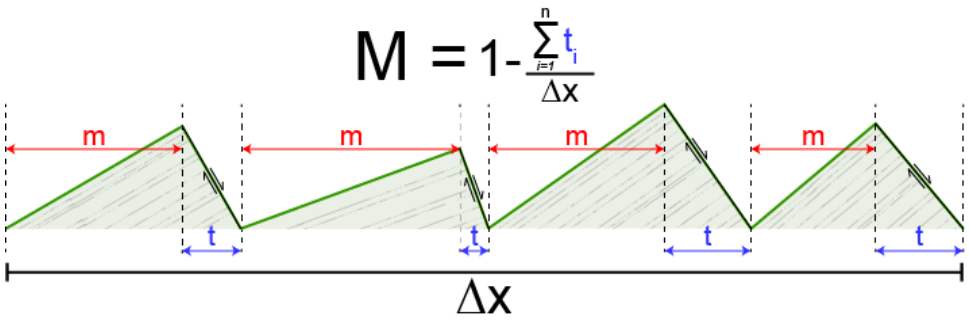

Figure 19: Cartoon illustration of the tectonic and magmatic accommodation of spreading in faulted oceanic crust. M is sum of magmatic spread crust over length Δx, m is segment of magmatic spread crust, and t is fault heave.

Fault Prediction and M Estimation

For the estimation of the magmatic and tectonic accommodation of plate spreading, we use the M factor first described by Buck et al. (2005). M is the ratio of the amount magmatic accretion of new crust to the amount of spreading. Over a length ΔX of crust that was spread from the axis, a portion of that length will be newly generated crust from cooling melt, M, and the rest of the length will be from extension along faults, T (Figure 19). Buck et al. (2005) and later Behn and Ito (2008) used numerical simulations to show how faulting and the morphology of crust being generated at a spreading center are dependent on M. We use the faulting and morphology of the CREST East-West transect to estimate M for the last 70 Myrs of spreading. To calculate M, we follow the method used by Behn and Ito (2008) and Schouten et al. (2010) (after Escartin et al., 1999), which calculates M as the sum of 1 – T, the fault heave over a distance.

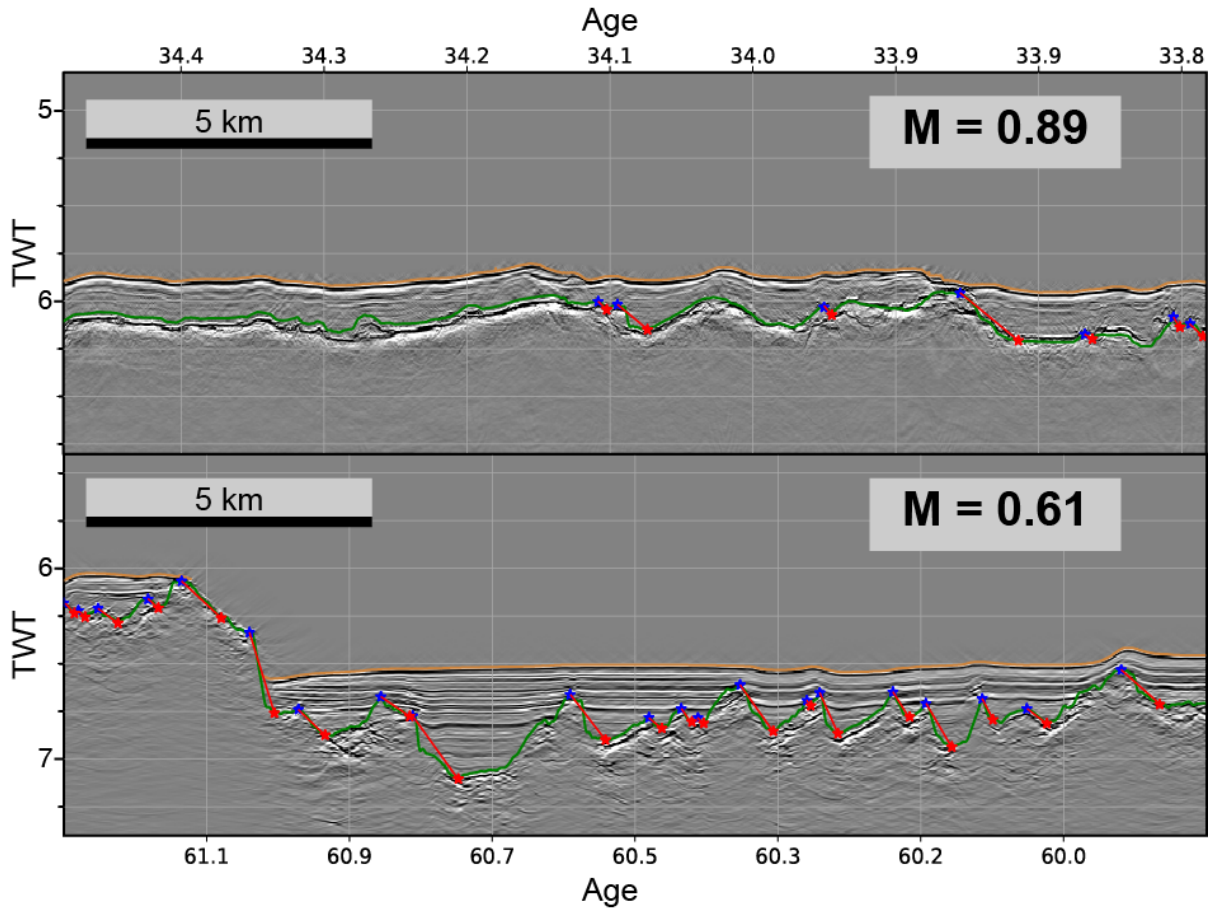

Figure 20: Predicted faults displayed on prestack time-migrated MCS reflection images from two locations of the CREST transect. The predicted top of fault is the blue star, the base of the fault is the red star, the fault plane is the red line, and basement interface is the green line. The fraction of magmatic spreading accommodation, M, for each location is indicated in the grey box.

The interpretation of faults in oceanic crust from the 2D MCS reflection images is inherently subjective, which can influence the resulting calculation of fault heave. Additionally,

the rougher the basement interface, the more energy is scattered and diffracted, and the ambiguity of the basement interface increases (Peirce et al., 2007), which is a potential source of error when interpreting faults and measuring fault heave. Furthermore, another source of error exists in the measuring of apparent fault heave by modification of the fault scarp by mass wasting, as illustrated by Escartin et al. (1999).

In order to systematically interpret faults and measure apparent fault heave, we predict faults from the basement interface across the transect based on a set of parameters determined from the data. The systematic prediction of faults reduces the subjectivity inherent in the fault interpretation across ~1500 km of faulted oceanic crust. We visually verify the integrity of predicted faults at multiple locations with different crustal roughness (Figure 20) and find good agreement with what would have been interpreted manually. Unlike roughness, which is primarily dependent on the window length over which it is measured, M is primarily dependent on fault heave prediction. Decreasing the window length increases the scatter of the results, but the mean of the scatter remains essentially the same as long as the window length is larger than fault heave, >~1 km. After faults have been predicted, we calculate M for same 20 km window used in the RMS roughness calculation. Another source of error associated with our fault predictions is that only faults dipping toward the ridge are predicted, which leads to our calculated M being a likely maximum. Even manual interpretation of faults dipping away from the ridge is highly subjective. Escartin et al. (1999) found less than 6% of the faults in their survey of the MAR at 29° N were dipping away from the ridge and Carbotte and Macdonald (1990) show that the majority of faults will dip toward the ridge in crust created at the spreading rates surveyed by the CREST expedition.

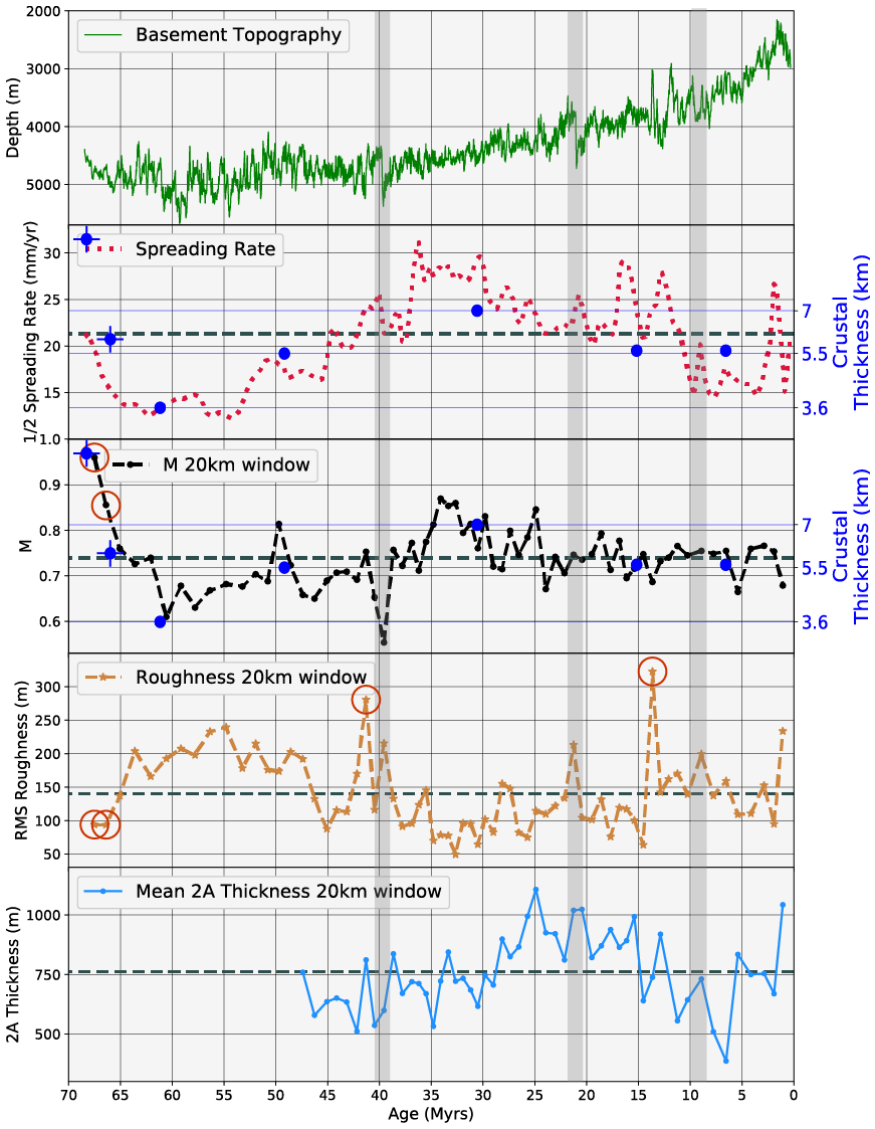

Figure 21: Age comparison of derived RMS roughness (tan) and M (black) with basement topography (green), spreading rate (red), and layer 2A thickness (light blue). Crustal thickness from Christeson et al. (2019b) shown with dark blue dots. Crustal thickness from Estep et al. (2019b) show with dark blue dots and cross. Grey bars indicate propagator wakes. Red circles indicate points from potentially atypical spreading processes. Grey horizontal dashed line is mean value for each panel.

	M	RMS roughness (m)	Spreading rate (mm/yr)	Layer 2A thickness (m)
Mean	0.74	140.3	21.33	763
Std Dev	0.067	55.63	4.9	191
Min	0.55	49.34	12.23	370
Max	0.96	322.8	31.12	1107
Without atypical points				
Mean	0.74	136.73		
Std Dev	0.056	48.65		
Min	0.61	49.39		
Max	0.87	239.6		

Table 4: Results from calculation of M, RMS roughness, and the linear regressions.

Results

We plot basement topography, spreading rate, M, RMS roughness, and layer 2A thickness against the age of the crust to show how roughness and M have varied over the past ~70 Myrs (Figure 21). *Table 4* contains the mean, standard deviation, minimum, and maximum values. We also use linear regression to test correlative relationships between RMS roughness, M, spreading rate, and layer 2A thickness (Figure 22).

Results across Crustal Ages

The RMS roughness of the basement interface across the CREST transect from 0 to 70 Ma varies from a low of 49 m to a high of 323 m with a mean of 140 m and a standard deviation of 56 m for the entire transect. RMS roughness is generally below the mean value for crustal ages of 15 to 40 Ma and generally above the mean value for crustal ages of 45 to 65 Ma. Some prominent spikes in roughness are present: one associated with the axial valley and three

associated with each of the propagator wakes. The two largest roughness spikes are in ~14 and ~41 Ma crust and correspond to anomalously large bathymetric deviations (Figure 23).

The fraction of spreading accommodated by magmatism, M, varies from 0.55 to 0.96. M has a mean of 0.74 with a standard deviation of 0.067. The lowest value of M, 0.55, occurs coincident with the 40 Ma propagator wake. The large deviations in topography associated with all three of the propagator wakes were predicted as faults (Figure 24), but only the 40 Ma wake has the lower value of M. M is generally below the mean value at crustal ages ~40-65 Ma, which is coincident with where the lowest spreading rates occur. M is generally above the mean values for crustal ages 25 to 35 Ma. The highest value of M occurs at the oldest crust, where M increases rapidly from ~60 to 68 Ma and the CREST transect is near the margin of the RGR.

We calculated the mean layer 2A thickness for each of the 20 km windows that served for roughness and M calculations. The range of values and overall trend is similar to what was reported by Estep et al. (2019a). The mean we calculate from the 20 km window means is the same 760 m, but the standard deviation we calculate is 160 m, which is smaller due to the effect of windowing. The minimum value of layer 2A thickness, 370 m, occurs at ~7 Ma and the maximum thickness, 1110 m, occurs at ~25 Ma. Estep et al. (2019a) only found definitive layer 2A in crust younger than ~48 Ma, which limits our comparison of layer 2A to those ages.

Correlations

To test for possible relationships with the derived parameters of M and RMS roughness, we perform linear regression and cross-plot the RMS roughness, M, layer 2A thickness, and spreading rate (Figure 22). The primary observations that we make from the linear regression are that: 1) the p values indicate spreading rate, M, and RMS roughness all correlate to a degree of statistical significance; 2) the coefficient of determination, R^2, is low

(<5) for all the comparisons; and, 3) layer 2A thickness does not correlate with any of the parameters.

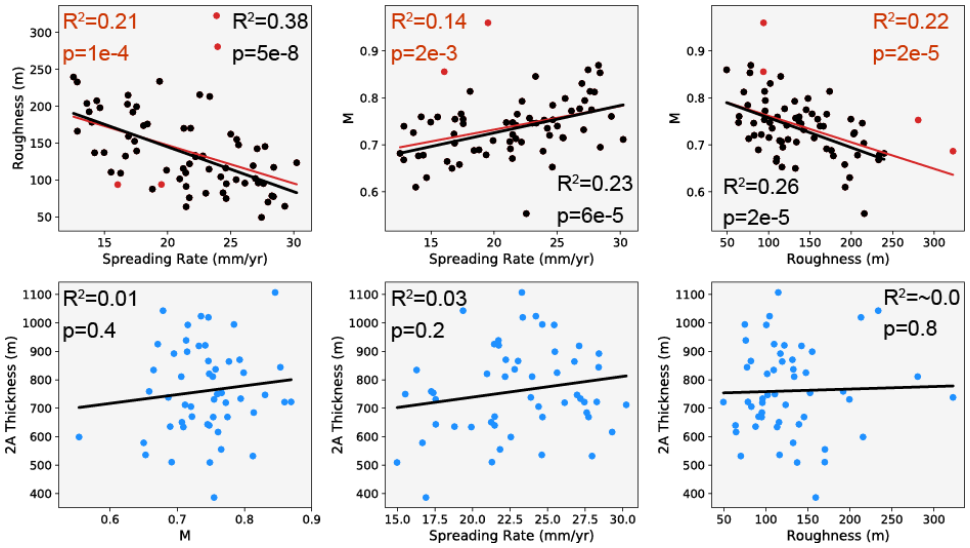

Figure 22: Correlation with linear regression trendlines of RMS roughness, M, spreading rate, and layer 2A thickness. Top: Red shaded points are from potentially atypical spreading processes. Black text and trendline is linear regression from black shaded points only. Red text and trendline is from all points.

The RMS roughness of the crust is inversely dependent on the spreading rate, with rougher crust occurring at slower spreading rates. This result is consistent with previous studies (e.g., Malinverno, 1991; Small, 1994). Linear regression of all RMS roughness data points results in a coefficient of determination of 0.21 and a p value of $1e^{-4}$. If we remove points possibly associated the locations of anomalously rough crust (Figure 23) or with potentially

atypical spreading processes near the RGR, the coefficient of determination increases to 0.38. The slope of the linear regression trendline excluding the potential anomalies is -6.1 m/(mm/yr).

The M factor is dependent on the spreading rate, increasing with increasing spreading rates. Removing the high M values from the possibly atypical crust at the margin of the RGR causes R^2 to increase from 0.14 to 0.23. We did not remove the low value of M at 40 Ma coincident with the propagator wake for the linear regression. Because the crust is heavily faulted in the area (Figure 24, Bottom) and because the other propagator wakes do not cause a similar decrease in M, we could not justify the removal of the low M, though it is an apparent outlier. The slope of the linear regression trendline excluding the potential anomalies is 0.0058/(mm/yr).

M and RMS roughness are also inversely dependent on each other. The R^2 using all data points is 0.22 with a p value of $2e^{-5}$. By excluding data points from the anomalously rough crust at 14 and 41 Ma, and from the crust on the margin of the RGR, R^2 increases to 0.26. The slope of the linear regression trendline excluding the potential anomalies is -0.001/m. The small slope values of M vs. RMS roughness and M vs. spreading rate are relevant. Because M is a fraction scale from 0 to 1, the range of roughness and spreading rate found in the study area can cause a change in M of ~0.17 and ~0.11, respectively, which is essentially the percentage of variation equal to the coefficient of determination for each.

The thickness of layer 2A does not correlate with M, RMS roughness, or spreading rate. Excluding data points from atypical locations did not create significance with any of the linear regressions. Multiple tests were run with different window lengths and no significance was found.

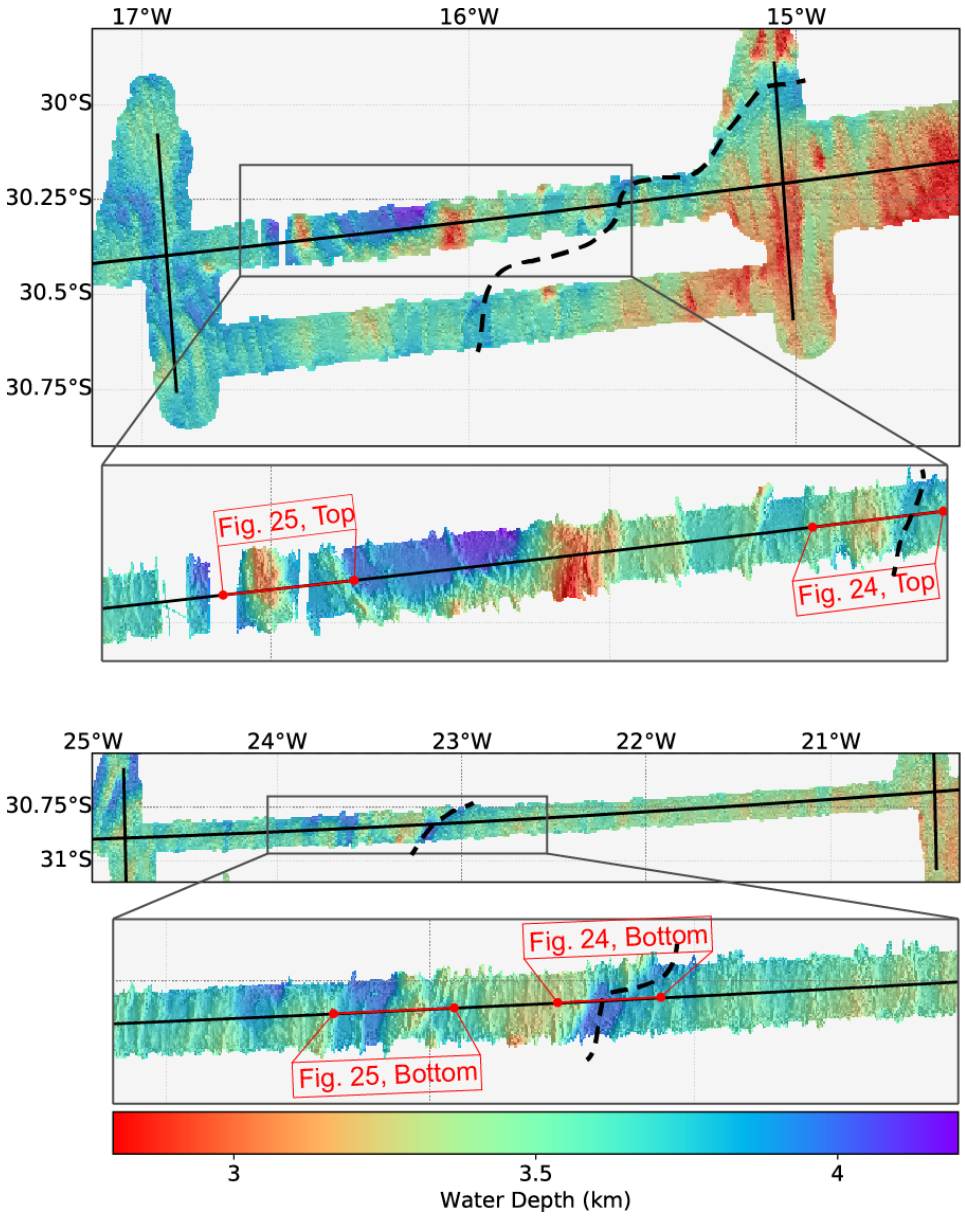

Figure 23: Multibeam bathymetry data from location of RMS roughness spikes at ~14 Ma (Top) and ~41 Ma (Bottom). Solid black lines are CREST MCS profiles. Dashed black lines are interpreted locations of propagator wakes. Red lines are locations of indicated figures.

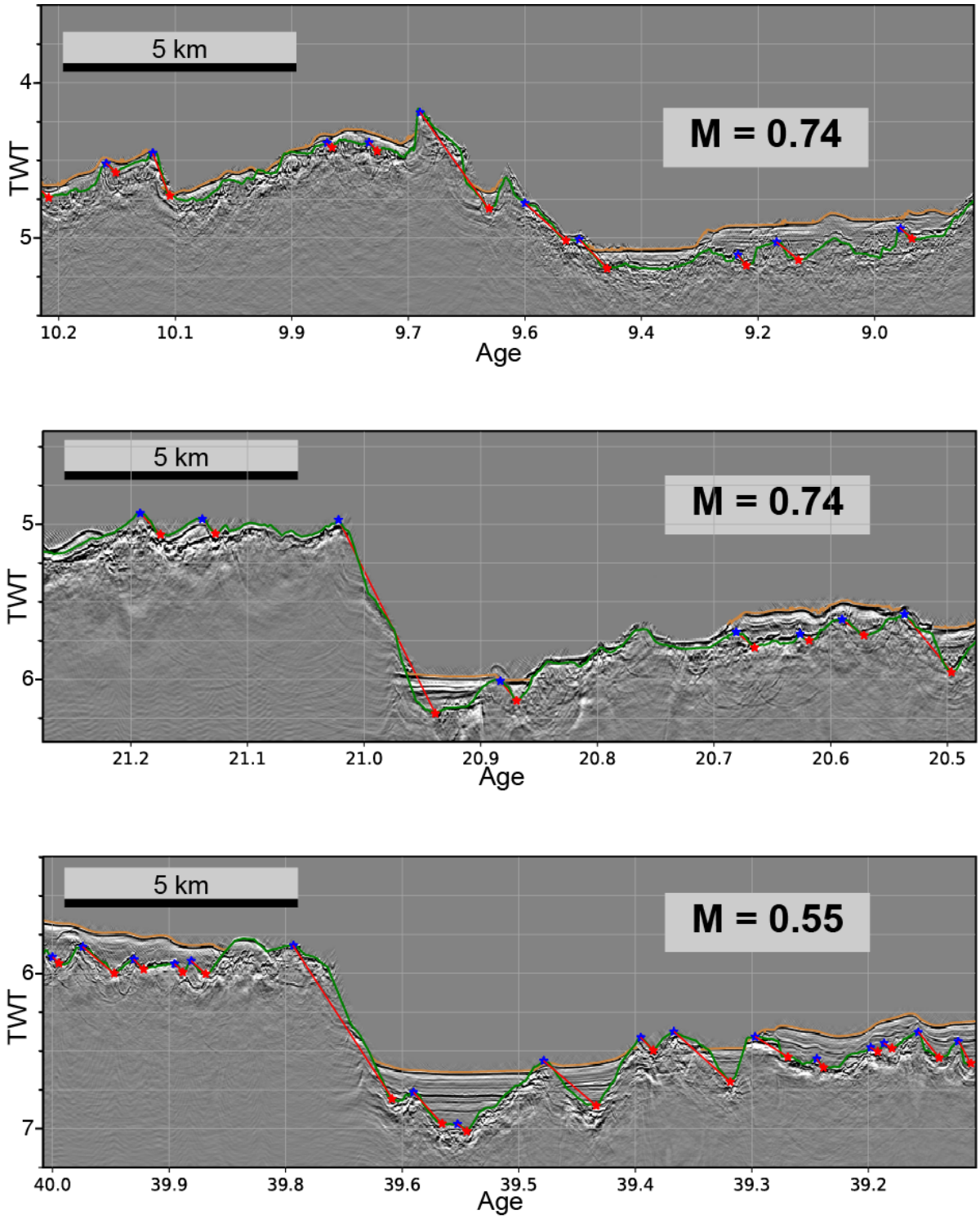

Figure 24: Propagator wakes with predicted faults at ~10 Ma (Top), ~21 Ma (Middle), and ~40 Ma (Bottom). Annotations same as Figure 20.

Discussion

Basement Roughness

Basement roughness increases linearly as spreading rate decreases in the South Atlantic, which agrees with previous results (i.e., Hayes & Kane, 1991) for the range of spreading rates recorded by the crust in our study. Malinverno (1991) found a power law relationship between seafloor roughness and spreading rate when using a range of spreading rates greater than those surveyed by the CREST data. Small (1994) and Small (1998) suggest that instead of a power law, a discontinuous relationship exists between the roughness of crust created at slow and fast spreading rates. The range of spreading rates included in our study cannot address the discontinuous relationship hypothesis; however, we do find high confidence ($p = 5e^{-8}$) in a linear relationship between RMS roughness and half-spreading rate.

The roughness values we find (Figure 21, Table 4) are higher than those of Christeson et al. (2019b) from the same area who used the CREST multibeam bathymetry data to measure abyssal hill RMS heights. Our results are of similar magnitude to the 83-212 m values from Hayes and Kane (1991), who used 2D bathymetry from a 0-62 Ma crustal flowline just to the north at 26° S. A caveat to the direct comparison of our results with the majority of previous studies of the roughness of the oceanic crust is that our method eliminates the muting effect of sediment, which likely causes our values to appear higher in comparison to studies that use only single or multibeam bathymetry. Our use of the MCS data allows us to create a 2D profile of the basement interface, even as sediment accumulation increases off-axis. Wilson et al. (2019) used this advantage of MCS data to measure crustal roughness over 6 Myrs of crust created at the

Costa Rica Rift where they found RMS roughness of 35-136 m for half-spreading rates of ~25-35 mm/yr.

The spikes we find in RMS roughness at ~14 and ~41 Ma (Figure 21) are from windows that encompass crustal topography with ~1 km of relief (Figure 25), which is anomalously high for the CREST survey. Both of these large increases in roughness occur on the older side of a propagator wake (Christeson et al., 2019b) (Figure 23), which may be evidence for the transfer of heat away from the pre-propagation crust during axis migration (Carbotte et al., 2004). If we exclude the two data points from the anomalously high roughness at ~14 and ~41 Ma (Figures 23, 25), the range of RMS roughness is 49-240 m with a mean of 137 m and a standard deviation of 49 m, which, in agreement with the findings of Christeson et al. (2019b), is lower than the means from other spreading centers with similar spreading rates (Goff et al., 1997). If we consider that our RMS values likely skew higher at older ages where sediment cover would mute more of the crustal relief in single or multibeam bathymetry data and that our results are still lower than those found in other locations with similar spreading rates, it seems the roughness of the crust surveyed by CREST at ~30° S in the South Atlantic is lower than expected for the spreading rates. Our lower than expected RMS values appear to agree with the results of Goff (2010), who predicted anomalously low RMS abyssal hill heights in the region surveyed by CREST using altimetric gravity. The roughness values we find in the South Atlantic encompass the entire range of mean RMS heights found at the intermediate-spreading South East Indian Ridge (SEIR), where Goff et al. (1997) showed that abyssal hill RMS heights can be differentiated between axial high, axial valley, and intermediate transitional axis.

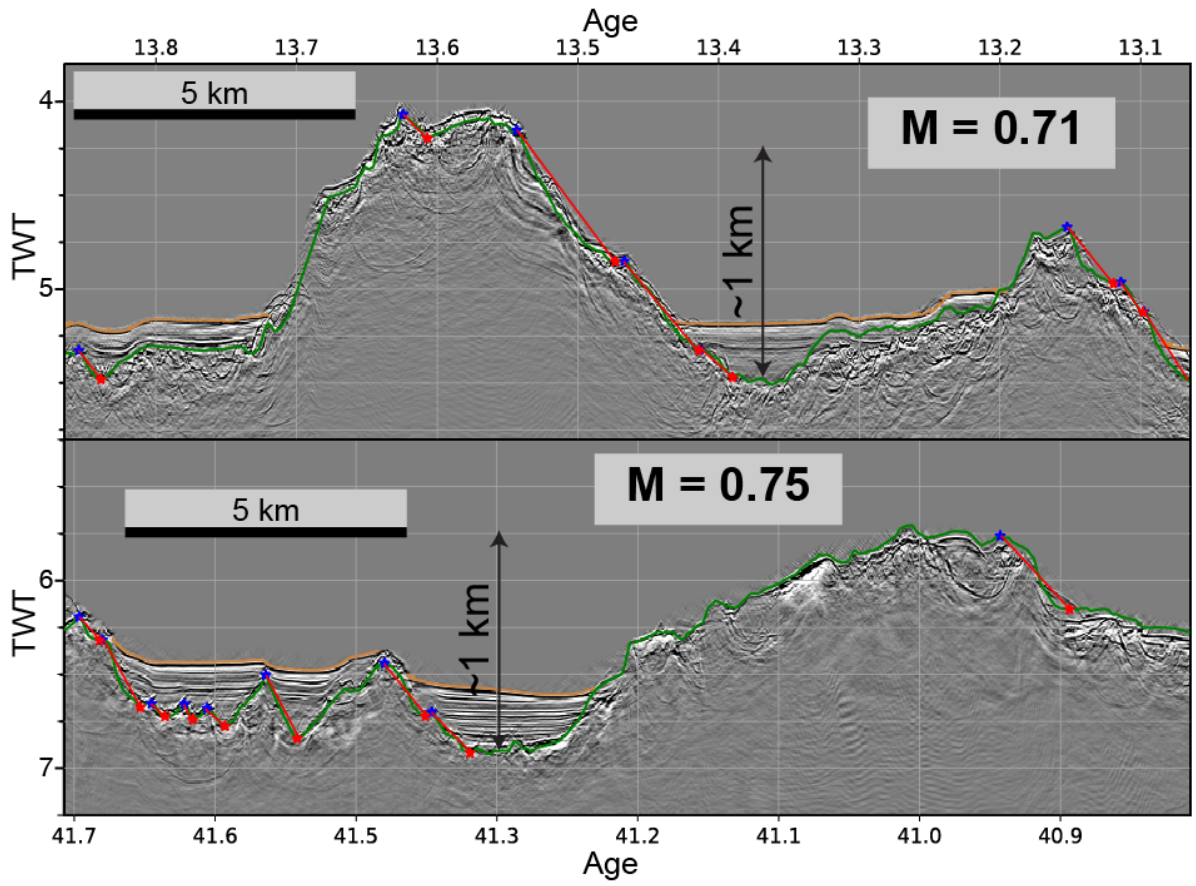

Figure 25: Anomalously rough crust that causes the spikes in roughness in Figure 21 at ~14 Ma (Top) and ~41 Ma (Bottom). Locations and multibeam bathymetry of each are shown in Figure 23. Annotations same as Figure 20.

M Factor and the Accommodation of Spreading

The mean of 0.74 for M can be thought of as, on average, 74% of the western direction of plate spreading since ~70 Ma has been accommodated by magmatic accretion. Our values of 0.55 to 0.96 are similar to those found by (Ito & Behn, 2008), who estimated M from cross-ridge bathymetric profiles at the MAR, SEIR, and the Galapagos Spreading Center and found M ranges of ~0.4-0.85.

The lowest value of M is located coincident with the ~41 Ma propagator wake (Figure 24, bottom), which, in combination with a rough crust, likely influences the result. The other two propagator wakes do not cause similar decreases in M, which suggests that the low value is not entirely due to the propagator wake. If we remove the specific fault predicted for the large change in water depth due to the migrating axis, M increases from 0.55 to 0.65 for the 20 km window, a still low value indicating substantial tectonic extension at the location. Aside from the 40 Ma value, the next lowest value of M is 0.61 in ~61 Ma crust (Figure 20, bottom). For bathymetric profiles crossing the MAR with oceanic core complexes Behn and Ito (2008) calculated M to be 0.4-0.6. Buck et al. (2005) and later Behn and Ito (2008) used numerical modeling to show that as M approaches 0.5, the long-lived detachment faults that lead oceanic core complexes can develop. While M does get close to the values associated with oceanic core complexes and the half spreading rates of the crust between ~45 Ma and 65 Ma are similar to the spreading rates at the North MAR where oceanic core complexes have been found (e.g., Blackman et al., 1998; Dick et al., 2008), based on the clarity of the observed magnetic anomalies (Kardell et al., 2019) and the lack of domed structures in the bathymetric data, Christeson et al. (2019b) concluded that no core complexes are found in the CREST survey area. It appears that, although magmatism was reduced between 65 and 40 Ma relative to the rest of the transect, it was not reduced enough to result in the formation of core complexes and remained high in comparison to the half spreading rates.

The highest value of M occurs in crust >65 Ma. M rapidly increases with crustal age where the CREST transect is close to the RGR. The RGR was created during a period of spreading when the Tristan plume had captured the MAR, resulting in additional heat and more magmatism at the axis (O'Connor & Duncan, 1990). Spreading rate also increases and roughness

decreases at the oldest ages, although neither at the same relative magnitude as M. The Tristan plume had abandoned the spreading center by 66.4 Ma, at the latest (Thoram et al., 2019), but likely would have still been proximal enough to the spreading axis to influence the thermal state of the region. We interpret the high values of M at >65 Ma to represent increased magmatic spreading due to the proximity of the Tristan plume. The rapidly declining values of M to the low at ~61 Ma indicates that the influence had likely waned quickly.

If we remove the high values of M influenced by the RGR and correct the low value of M at the ~41 Ma propagator wake, the range of M becomes 0.61 to 0.87 over a range of half spreading rates from 12 to 31 mm/yr. While we find high confidence that M and spreading rate are linearly dependent, using the slope and intercept found in our linear regression, our results predict M will never reach 0.5 in the crust in our study. This suggests that the relationship between half spreading rate and magmatic spreading is either not linear or is discontinuous across changes in spreading rate. Alternatively, it suggests that the proportion of magmatism has been high relative to the spreading rates for the spreading segment surveyed by the CREST data (Christeson et al., 2019b), and the linear trend we find does not necessarily have the same slope at other spreading centers. This explains the absence of oceanic core complexes even when spreading rates approach those where oceanic core complexes are found in the North Atlantic.

Past Axial Morphology and Crustal Thickness

The crust created between roughly 25 and 35 Ma has the highest percentage of magmatic accretion, the lowest RMS roughness, and the highest spreading rates (Figure 21). This region contains crust that is exceptionally smooth (roughness < 100 m), and unfaulted for distances up to 10 km (Figures 20, 26, top). It is difficult to imagine such smooth lengths of crust being rafted out of an axial valley intact and unfaulted. The mean RMS roughness values for crust created at

spreading centers with axial highs are 56-97 m (Goff et al., 1997), which are similar to the roughness values we find between 25 and 35 Ma. In their analysis of M vs. axial topography across multiple modern spreading centers, Ito and Behn (2008) found that for M > ~0.8 nearly all spreading centers exhibited an axial high. Between 25 and 35 Ma, we find M ranges from 0.71 to 0.87 with a mean of 0.8. The intermediate spreading Galapagos Spreading Center and the SEIR exhibit variation between axial highs, transitional axes, and axial valleys over a small range of spreading rates (Cochran & Sempéré, 1997; Sinton et al., 2003). Additionally, the MAR just south of the spreading segment surveyed by CREST varies between an axial valley and a subdued axial high (Fox et al., 1991). We propose that the spreading center has alternated between an axial high and axial valley in the past, and that the sections of crust with high values of M and low RMS roughness values were created when the MAR was an axial high. We find no indication of a spreading rate tipping point between axial morphologies; instead, it is likely the model of Ito and Behn (2008) that predicts axial morphology as a function of the time spent in a magmatic spreading regime correctly predicts the axial morphology of the spreading center.

If we compare the mean crustal thickness values of Christeson et al. (2019b) and Estep et al. (2019b) (Figure 21, blue dots) to our calculated values of M, we can visually observe a similarity in trend. The thickest crust occurs at 68.3 Ma where M is highest and the thinnest crust is found at 61.2 Ma where M is lowest. The crustal thickness values near the mean are found where M is generally near its mean for the transect. The visual comparison between crustal thickness and spreading rate is not as strong as that of M, although M and spreading rate do correlate positively, and compilations of crustal thickness have shown very little-to-no correlation between crustal thickness and spreading rate, aside from ultraslow spreading (Christeson et al., 2019a; White et al., 1992).

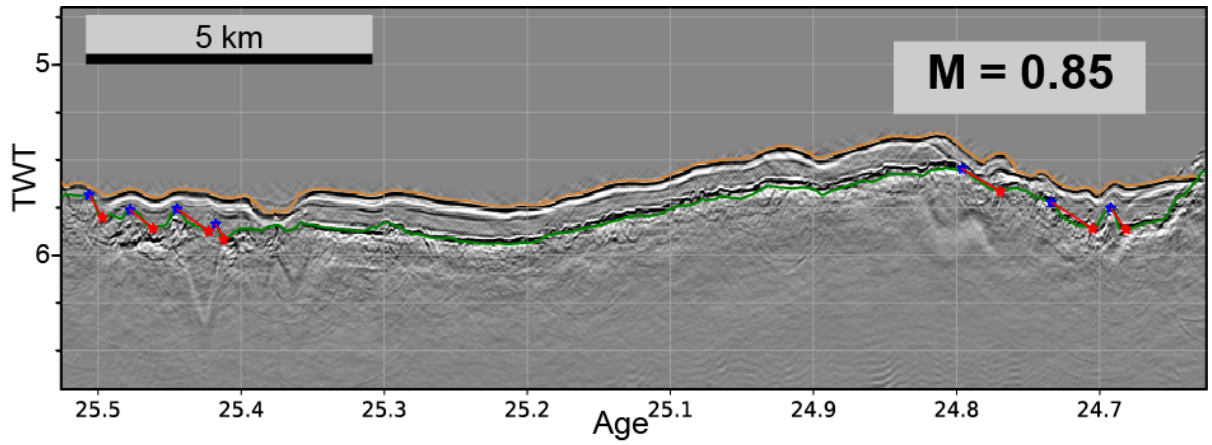

Figure 26: Smooth crust created at intermediate spreading rates. Annotations same as Figure 20.

Studies along spreading segments (rather than perpendicular like CREST) of active slow-intermediate spreading ridges have found crust is thickest in the center of spreading segments where melt supply is expected to be greatest and thinnest at segment ends (e.g., Hooft et al., 2000). Christeson et al. (2019b) do not find any changes in crustal thickness across the individual North-South profiles and conclude that the CREST data does not reach segment ends. However, instead of spatial changes in the melt supply across the segment, if there was temporal waxing and waning of melt supply we might expect a corresponding change in crustal thickness and M. An elevated thermal state or more efficient melt delivery would likely cause an increase in crustal thickness similar to those seen along spreading segments (e.g., Hooft et al., 2000). Increased melt would also likely increase the magmatic accommodation of spreading, M. The

correspondence between our calculation of M and the crustal thickness suggests that crustal thickness is related to the magmatism that accommodates spreading.

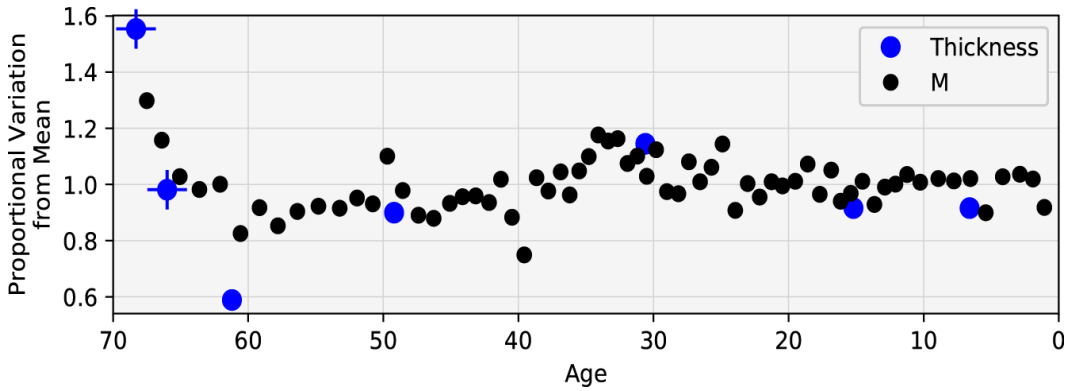

Figure 27: M (black dots) and crustal thickness (dark blue dots) normalized to their means versus age.

An alternative explanation is to think of the magmatic crustal thickness as essentially fixed and the variation in measured crustal thickness being related to the degree of faulting that thins the crust. Because 1–M is the cumulative heave along faults (Figure 19), M will be inversely proportional to the amount of crustal thinning caused by faulting, which would produce the similarity we see in M and crustal thickness. If we normalize the crustal thickness and M values to their means, we can compare the proportional variation of each parameter (Figure 27). M and crustal thickness appear to vary proportionally, except for the thickest and thinnest values of crustal thickness at 68.3 and 61.2 Ma, respectively (Figure 27). The thickest crust at 68.3 Ma is likely related to the influence of the Tristan plume, and is likely indicative of additional crustal thickness from excess melt. The thinnest crust is thinner than the proportional variation in M,

which suggests that the crust there is thin from more than the faulting inherent in the calculation of M. The remaining measurements of crustal thickness appear to correspond to a proportional change in M (Figure 27). Without more measurements of crustal thickness, we cannot say what a representative crustal thickness for normal spreading along the spreading segment surveyed by the CREST data would be, which is needed to distinguish between measured crustal thickness being primarily a product of slip along faults or changes in the melt delivery.

Layer 2A

The origin of the thickness of layer 2A remains obscure. Because velocity in the upper crust is primarily dependent on the porosity (Carlson, 2010), layer 2A thickness must be controlled by a porosity vs. depth relationship. Hydrothermal circulation relies on porous and permeable crust, so layer 2A thickness likely plays an important role in the cooling of the oceanic lithosphere, both on and off axis. If thickness is set in the axial valley for slow spreading ridges (Hussenoeder et al., 2002) and is set in the near off axis region at fast spreading ridges (Carbotte et al., 1997; Vera & Diebold, 1994), it implies the thickness of layer 2A is related to the magmatism at spreading centers. However, no correlation between layer 2A thickness and spreading rate has been found (Christeson et al., 2010; Estep et al., 2019a) and we find no correlation with the fraction of magmatism that accommodates spreading or the roughness of the crust.

Conclusions

For the first time, we have shown the temporal changes in the magmatic fraction of spreading for a large range of oceanic crust. We have also used MCS to eliminate the effect of sediment on the calculation of the roughness of the crust. We have tested these parameters against crustal age, spreading rate, and layer 2A thickness. Our main conclusions are:

1. The fraction of spreading accommodated by magmatism, the roughness of the crust, and the spreading rate are all interrelated, though the coefficient of determination for each is small (<50%). This conclusion implies that these are likely dynamic relationships that change in unison as additional parameters of spreading and crustal accretion (e.g., far-field stresses, axial thermal state) change. Furthermore, the low coefficient of determination implies that individual parameters may vary substantially without a similar magnitude change in the other two.

2. The morphology of the axis that generated the crust at ~30° S in the South Atlantic has likely alternated between an axial valley and an axial high in the past. The coincidence of high rates of M, low RMS roughness, and smooth crust is indicative of crust generated at an axial high. This implies that, similar to the SEIR and Galapagos Spreading Center, the Southern MAR can alternate between axial morphologies with relatively small changes in spreading rates. Additionally, this conclusion also suggests that it may be possible to predict past axial morphology.

3. Spreading at the ridge segment that created the crust surveyed by the CREST expedition has had a high degree of magmatic accommodation relative to the spreading rates. The slowest spreading rates surveyed are similar to those where oceanic core complexes are found in the North Atlantic; however, the magmatic fraction of spreading did not decrease enough to allow the sustained detachment faulting that produces core complexes. This further validates our conclusion that

variation in one parameter of spreading may not be accompanied by a similar magnitude variation in the others.

4. We find clear evidence of the influence of the Tristan hot spot plume on magmatic spreading at the MAR. The magmatic accommodation of spreading remained exceptionally high until ~65 Ma even after the Tristan plume had abandoned the spreading axis, likely due to proximity of the plume creating an elevated thermal state in the region. The influence of the plume waned and magmatic spreading was at its lowest by ~60 Ma. The rapid transition from relative high magmatic spreading to low magmatic spreading implies that the presence of the plume likely had little effect on spreading for the last ~60 Myrs.

5. Crustal thickness is possibly related to the magmatic fraction of spreading. We observe good visual agreement between changes in crustal thickness and the magmatic fraction. However, our measurement of crustal thickness is not robust enough to say with statistical confidence and requires a denser array of crustal thickness measurements across crustal ages.

6. Layer 2A thickness does not correlate with the magmatic fraction of spreading or the roughness of the crust in the South Atlantic. While layer 2A thickness is likely related to magmatism at the ridge, our findings indicate that the magnitude of thickness is not dependent on the ratio of magmatic accommodation within the ranges we found.

CHAPTER IV

RECENT DEFORMATION IN OLD OCEANIC CRUST

Introduction

Ocean crust undergoes well-documented deformation at both ends of its life cycle. Extensional faulting is integral to the process of creating new oceanic crust at spreading centers (e.g., Buck et al., 2005) and bend-related faulting has been found extensively where oceanic crust approaches subduction zones (e.g., Nedimović et al., 2009; Ranero et al., 2003). The deformation of oceanic crust plays a key role in a number of processes related to heat flow from the mantle (e.g., Davies, 1980) and the exchange of water and chemicals between the ocean and the crust (e.g., Johnson & Pruis, 2003). Intraplate deformation of oceanic crust that is distal from a subduction zone or spreading center has been documented in ~65-78 Ma ocean crust in the Indian Ocean, where it was attributed to the complex interplay of forces imparted on the plate from the Indian-Asian plate collision and the Sunda subduction zone (Bull, 1990; Neprochnov et al., 1988). However, additional evidence for tectonic activity in the interiors of other oceanic plates remains limited. This lack of documented intraplate deformation is possibly due to the limited amount of available data that can detect deformation within the plate interiors, which hinders our understanding of the thermal, chemical, and fluid budgets in the marine realm. Here we present evidence for, and investigate the cause of, persistent and recent intraplate deformation in the western South Atlantic Ocean. We investigate why this region has experienced intraplate deformation, and show that the relationship between the South Atlantic crust and the Tristan hotspot plume resulted in long-lived brittle strain preferentially localized by crustal thickness variations.

Background

South Atlantic and Rio Grande Rise

Due to its role in global ocean circulation and implications for plate reconstructions, the development of the South Atlantic Ocean and its paleobathymetry have been investigated multiple times using various methods and datasets (Müller et al., 2008; Pérez-Díaz & Eagles, 2017; Sclater & McKenzie, 1973; Sykes et al., 1998). The history of the Tristan Hotspot plume is of particular importance to understanding the formation of past and present bathymetry, early South Atlantic seafloor spreading, and paleocirculation patterns of the nascent South Atlantic (Pérez-Díaz & Eagles, 2017; Renne et al., 1992; Turner et al., 1994). The most prominent bathymetric feature in the western South Atlantic Ocean, the Rio Grande Rise (RGR) (Figure 27), is a relic of interaction between the Mid-Atlantic Ridge (MAR) and the Tristan plume (O'Connor & Duncan, 1990). Morphologically, the RGR is a roughly circular region of elevated seafloor ~1000 km in diameter and often described as being composed of the main western RGR and the eastern RGR (ERGR) (Camboa & Rabinowitz, 1984; Thoram et al., 2019) (Figure 27). The interactions between the MAR and Tristan plume during the formation of RGR and its conjugate in the eastern South Atlantic Ocean, the Walvis Ridge, involve one or more ridge jumps and fracture zone migrations (Barker, 1983; Thoram et al., 2019). However, there is general consensus that the RGR formed at or near the MAR during a period when the Tristan plume captured the spreading center before ~70 Ma (Barker, 1983; Morgan, 1971). Spreading and the plume had abandoned the RGR by 66.4 Ma at the latest (Thoram et al., 2019), leaving it permanently stranded on the western side (South American Plate) of the MAR.

An enigmatic event in the history of the RGR is the proposed re-eruption during the Eocene, ~20 Myrs or more after abandonment (Barker, 1983). DSDP Site 516F (Figure 27)

drilled and cored through the sediment to the igneous basement near the crest of the RGR during DSDP Leg 72 (Barker et al., 1981). The basement age was calculated at 86 ± 4 Ma from Ar^{40}/Ar^{39} dating and paleontological evidence indicates nearly the entire sedimentary section was pelagic in nature. However, within the Eocene interval, sediment contained volcanoclastic turbidite deposits and volcanic ash beds. Biotite from one of these ash beds provided a K-Ar age of 47.4 ± 0.7 Ma (Barker, 1983; Bryan & Duncan, 1983). More recently, small seamounts and guyots present on the RGR have been Ar^{40}/Ar^{39} dated at 46 ± 0.1 Ma using dredged rock samples (Rohde et al., 2013), which corresponds closely with the age of the ash beds. Barker (1983) combined the biostratigraphy from Hole 516F and the proposed thermal rejuvenation to construct a subsidence curve for the RGR that includes a partial resetting of the thermal state and an uplift of ~600 m in the Eocene.

Thermal Subsidence and Plate Cooling Models

Central to the subsidence of oceanic lithosphere are the physical properties that govern how oceanic lithosphere cools and densifies as it is transported away from the heat of the mid-ocean spreading center (Parsons & Sclater, 1977). The progressive increase in water depth with distance from the spreading center has been the subject of numerous predictive models (Grose & Afonso, 2013; Johnson & Carlson, 1992; Korenaga & Korenaga, 2008; Parsons & Sclater, 1977; Richards et al., 2018; Stein & Stein, 1992). There are predominantly two types of models that attempt to predict the depth of the seafloor: half-space cooling models (e.g., Schubert & Turcotte, 1982) and plate cooling models (e.g., Parsons & Sclater, 1977). The half-space cooling model is an elegant solution that relies on first principles of heat diffusion and the resulting predictions generally match well with the measured seafloor depth datasets for ‘normal’ crust <70 million years old. For older crust, the seafloor appears to reach an asymptotic depth that

flattens and diverges from the prediction of the half-space model. The effect of apparent seafloor flattening has caused debate regarding the cause and if the effect is even real (Korenaga & Korenaga, 2008). Plate cooling models invoke a rigid lithospheric 'plate' that produces a better fit to the apparent seafloor flattening of crust older than 70 million years by incorporating one or more plate thickness layers that simulate the lithospheric plate reaching an asymptotic thickness at old ages. Key parameters of both half-space and plate models are the thermal properties of the lithosphere that control material volume and heat loss.

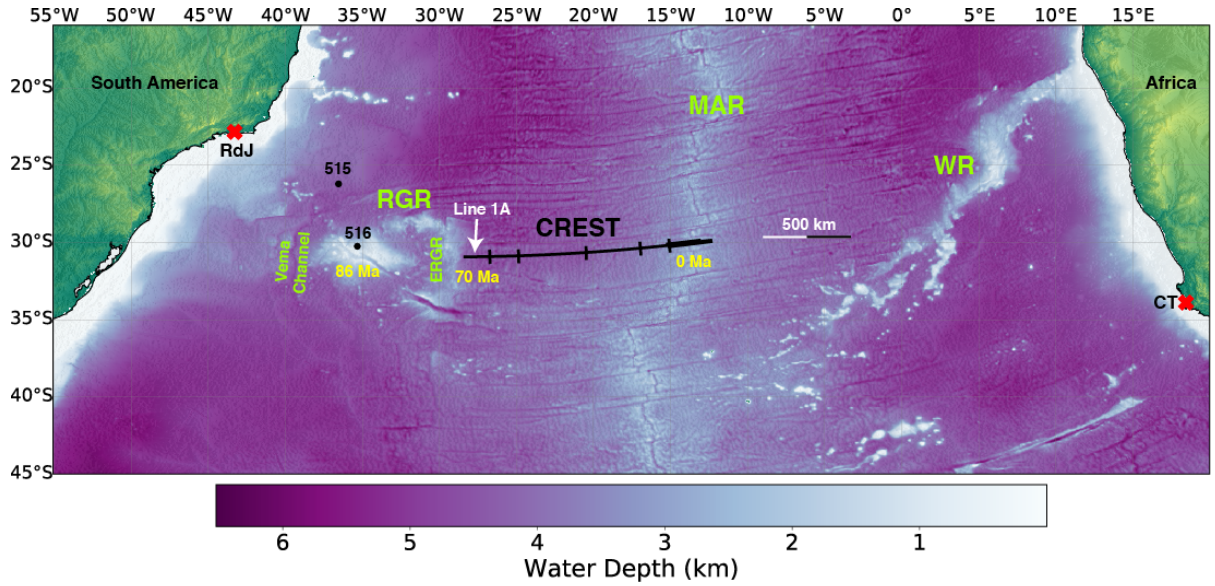

Figure 28: South Atlantic area map with prominent and pertinent features annotated. CREST survey data and seismic profiles (black lines) are described in Kardell et al. (2019). Line 1A indicates CREST MCS Line 1A from which data is shown in Figures 28, 30-32. Drill sites 515 and 516 described in text are shown with black circles. CT = Cape Town, South Africa. ERGR = East Rio Grande Rise, MAR = Mid-Atlantic Ridge, RdJ = Rio de Janeiro, Brazil, RGR = Rio Grande Rise, WR = Walvis Ridge.

Study Area

Our study uses multichannel seismic (MCS) data collected during the 2016 CREST (Crustal Reflectivity Experiment Southern Transect) expedition (Figure 27). The MCS data collection is described in detail by Estep et al. (2019a) and Kardell et al. (2019). The CREST MCS data image ocean crust at 31° S in the South Atlantic Ocean with continuous coverage from 0 Ma crust at the MAR to ~70 Ma crust on the margin of the Eastern RGR. The CREST dataset spans oceanic crust formed at a single spreading segment of the MAR at spreading half-rates of 12 – 31 mm/yr (Kardell et al., 2019; Pérez-Díaz & Eagles, 2017). CREST MCS Line 1A, ~150 km in length, is located at the westernmost end of the survey (Figure 27). The Line 1A seismic profile crosses the oldest crust of the transect; Kardell et al. (2019) used shipboard magnetic data to estimate the oldest age surveyed as 69.6 Ma; the age grids of Müller et al. (2008) and Pérez-Díaz and Eagles (2017) place the age at 69.8 Ma and 69.2 Ma, respectively. All three datasets rely on westward extrapolation from where the transect crosses magnetic chron C32r (68.737 Ma) to the western terminus of Line 1A. For the purpose of facilitating continuity in age comparison at high resolution with other locations in the South Atlantic, we use the age grid of Pérez-Díaz and Eagles (2017) for assigning ages.

Kardell et al. (2019) examined the velocity structure of the upper igneous crust across the CREST transect and showed that velocities anomalously decreased with crustal age from 5.5 km/s to 4 km/s at the western end of Line 1A. The authors attribute the decrease in velocities to crustal faulting with recent movement that corresponds with zones of low velocity. In this study,

we further explore the apparent faulting present in Line 1A. For our analysis of the CREST MCS data, we use the processed and prestack time-migrated reflection sections of Estep et al. (2019a).

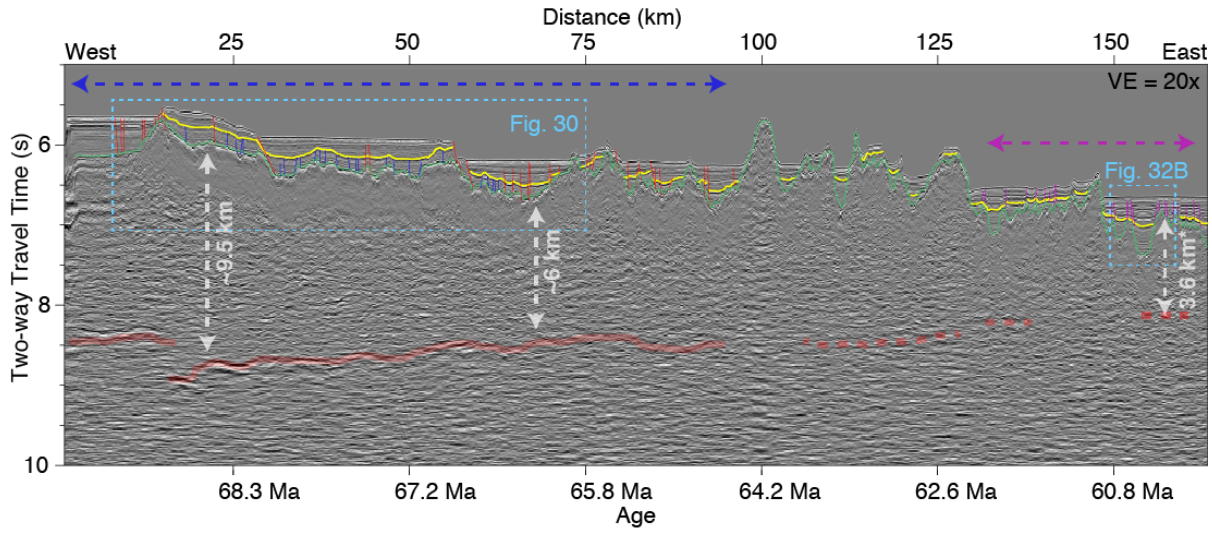

Figure 29: CREST MCS Line 1A. Red line is interpreted Moho; solid = clear Moho, dashed = faint or absent. Green line is interpreted top of igneous basement. Yellow line is interpreted regional unconformity. Blue, red, and pink lines are fault Groups 1, 2, and 3, respectively, described in text. Ages calculated from Pérez-Díaz and Eagles (2017). Blue dashed arrow is extent of blue and red faults described in text Pink dashed arrow is extent of pink faults described in text. Distortion in image quality on left is due to the reduction in fold at the edge of data collection.

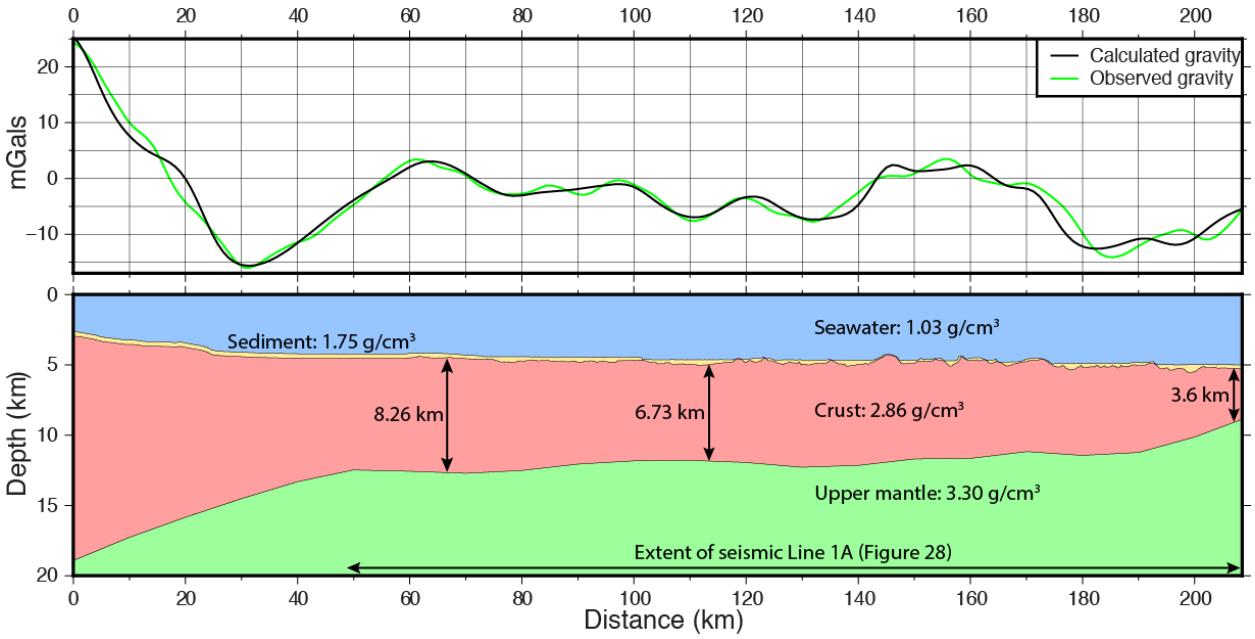

Figure 30: Crustal thickness estimation from gravity modeling using the Talwani Gravity Modeling Program (http://cybershare-portal.utep.edu/talwani). Top: calculated vs. observed gravity. Bottom: model layer thicknesses and densities. Horizontal black arrow is extent of MCS Line 1A. Vertical black arrows are same locations as thickness arrows in Figure 28.

Results and Interpretation

Crustal Thickening

We use the travel times between the basement and Moho discontinuity, where present, to estimate crustal thickness using a mean crustal velocity of 6.0 km/s for depth conversion (i.e., Christeson et al., 2019a). The Moho discontinuity is clearly imaged in the seismic reflection data at the western end of Line 1A, but becomes faint and eventually absent east of crustal age 64.2 (Figure 28). At the eastern end of Line 1A, we instead use the results of velocity modeling from ocean bottom seismometers to constrain the base of the crust and determine crustal thickness

(Christeson et al., 2019b). We find that the crust is thickening across Line 1A from 3.6 km in the east to a maximum of 9.5 km in the west, which is a ~6 km increase in the thickness of crust over a distance of ~150 km and ~8 Myrs of crustal age. The increase in crustal thickness corresponds with an overall ~800 m decrease in water depth to the west across Line 1A, from ~5000 m in the east to ~4200 m in the west.

The estimates from the MCS data are supported by similar results derived from modeling global gravity data (Sandwell et al., 2014) (Figure 29). We model crustal thickness by constraining water depth from the CREST multibeam bathymetry and sediment thickness from MCS two-way travel times of the sediment depth-converted using velocities from Kardell et al. (2019). The westward extent of the gravity model is limited to the extent of shipboard multibeam bathymetry data. Because the bathymetry extends farther west than the MCS data, we used the observed average sediment thickness in Line 1A of 315 m west of the MCS data extent. We used densities of 1.03 g/cm^3 for seawater and 3.30 g/cm^3 for the upper mantle (Schubert & Turcotte, 1982), 1.75 g/cm^3 for deep sea sediment (Hamilton, 1976), and 2.86 g/cm^3 for oceanic crust (Carlson & Herrick, 1990). A background density of 2.6 g/cm^3 was obtained by determining the average density of the model. The discrepancies in thickness between the gravity model and the MCS estimation are likely due to the difference in resolution of the data types and the simplifying assumptions made with respect to the internal density and seismic velocity structure and their lateral variation.

Regional Unconformity

Along much of CREST Line 1A we interpret an unconformity situated slightly less than halfway up through the sediment package (Figures 30, 31). The unconformity is characterized by a laterally continuous reflector of relatively high amplitude that generally mimics the basement

topography and marks a change in the character of reflectors above and below (Figure 31). In many places, reflectors below the unconformity lie parallel to the topography of the basement interface, while reflectors overlying the unconformity are flat-lying and often onlapping the unconformity. The unconformity is most readily identifiable in the western end of Line 1A where sediment is more continuous. To the east in Line 1A, the basement interface becomes progressively more rugose, with basement just to the east of Line 1A (ages ~50 – 60 Ma) having the roughest topography of the CREST transect (Estep et al., 2019a). Because of the basement roughness, the sediment is not continuous in the east and we rely on the character, frequency, and polarity of the reflectors to determine the eastern extent of the unconformity. We interpret the unconformity extends for >150 km, from the western end to at least the eastern end of Line 1A (Figure 28). We cannot identify the unconformity at the extreme western end of Line 1A due to the declining fold associated with MCS profile taper (Figure 28). This makes it difficult to determine whether the unconformity continues west of Line 1A and the CREST survey area.

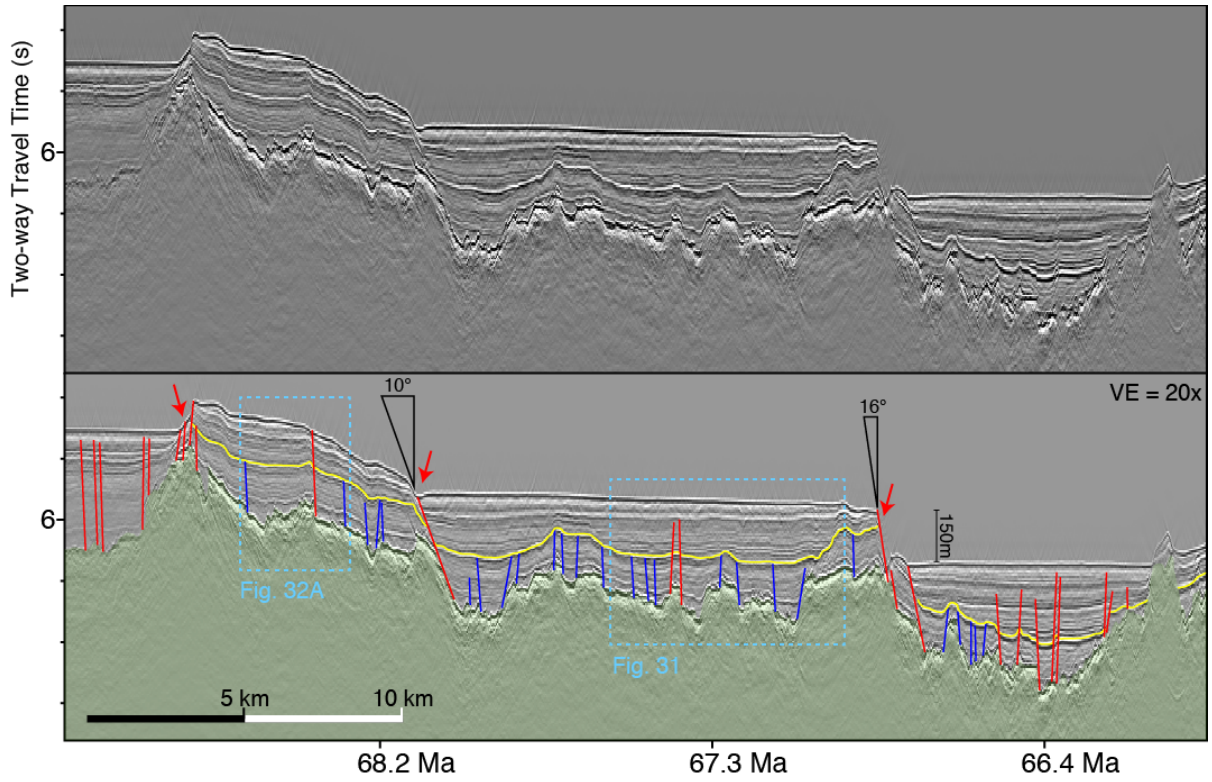

Figure 31: Zoom of Line 1A west (see Figure 28 for location). Top = uninterpreted. Bottom = interpreted. Unconformity in yellow. Blue and red faults from the text shown in respective colors. Igneous basement shaded green. Angle diagrams are corrected for vertical exaggeration. Red arrow indicated faults visible in Figure 33.

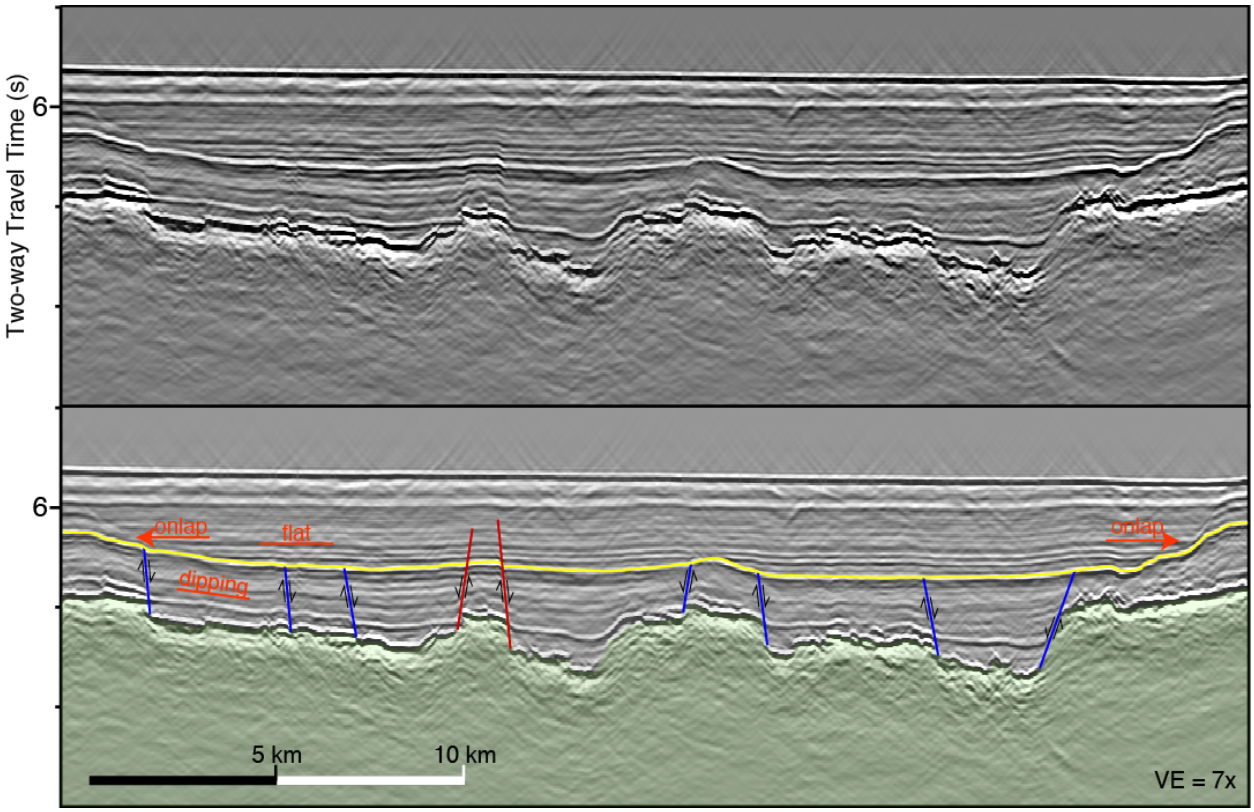

Figure 32: Zoom in to show relationship of sediment with interpreted unconformity. Top = uninterpreted. Bottom = interpreted.

Faulting and Fault Groups

We interpret numerous faults mostly concentrated in the western half of Line 1A offsetting some or all of the sedimentary package (Figures 28, 30). Because we do not image any reflectivity from fault planes beneath the basement horizon, we use observations in the sedimentary package to define fault type. All faults we interpret are normal in sense and there is no dominant vergence direction. We classify faults into three population groups represented by the colors blue, red, and pink, respectively. Blue and red faults are located only in the western half of Line 1A and pink faults are located only at the eastern end (Figure 28).

Group 1 = Blue. This fault population offsets sedimentary horizons below the regional unconformity only, and nearly all appear to terminate at the unconformity (Figure 32A). These faults are related to offsets in the basement interface horizon, suggesting movement of the basement is associated with these faults. The apparent dip of the blue faults has a mean of 50.9° and a median of 52.2°. Throw on blue faults averages ~10-15 m when calculated from the offset in the sedimentary reflectors, which is near the limit of resolution of the CREST seismic data. No packages of growth strata are apparent on the blue faults.

Group 2 = Red. The 2nd group of faults offsets sedimentary horizons below and above the regional unconformity (Figure 32A). Some of these faults clearly offset the seafloor (Figures 28, 30, & 33), which indicates recent movement. The apparent dip of the red faults has a mean of 48.2° and a median of 53.9°. The prominent faults that offset the seafloor appear to have a shallower dip of <20° (Figure 30). Similar to the blue faults, red faults are also associated with offset in the basement and throw is generally ~10-15 m. However, two of the red faults that offset the seafloor have a throw of up to 150 m (Figure 30). As with blue faults, no growth strata are distinguishable on red faults.

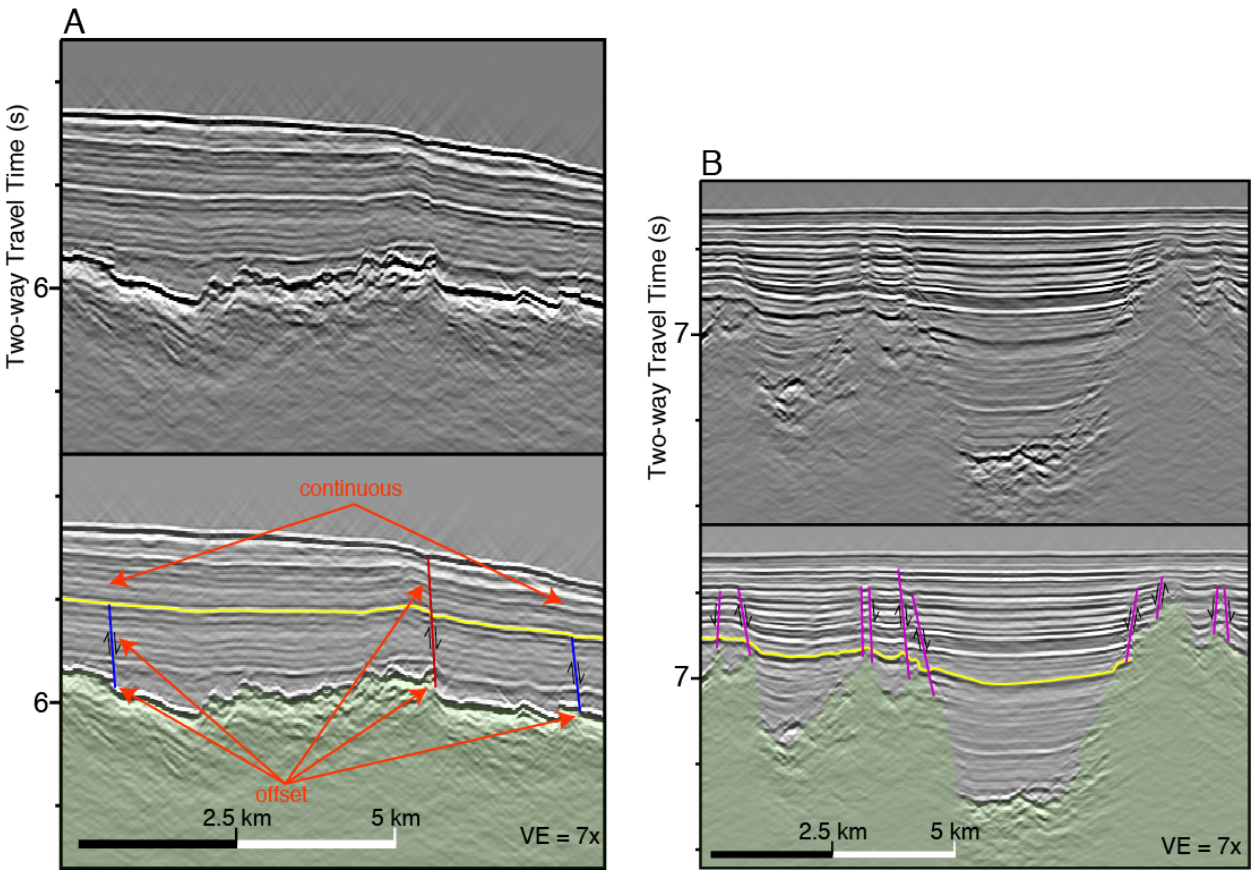

Figure 33: Zoom of fault group interpretation. Top = uninterpreted. Bottom = interpreted. A = red and blue faults in western Line 1A. B = pink faults in eastern Line 1A.

Group 3 = Pink. These faults are found extending from structural highs in the rugose basement that compartmentalize thick sedimentary depocenters at the eastern end of Line 1A (Figure 32B). The roughness of the basement scatters energy (Peirce et al., 2007) where pink faults are found, resulting in poor imaging of the crust/sediment interface (Figure 32B). This leads to pink faults not being easily associated with any basement offset. However, unlike blue and red faults, pink faults are consistently located at transitions between regions of thin and thick sediment. Found with these faults are sedimentary horizons draping the rugose basement

topography (Figures 28, 32B). At the resolution of the CREST seismic data, we cannot observe any pink faults offsetting the seafloor and the throw on the pink faults is near the limit of seismic resolution. The apparent fault dip has a mean of 60.5° and a median of 61.3°, and, similar to the blue and red faults, no sequences of growth are interpreted with the pink faults.

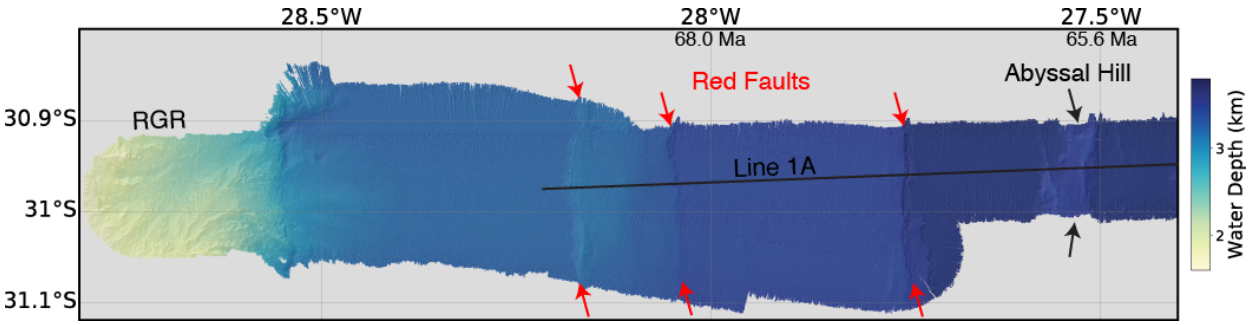

Figure 34: CREST multibeam bathymetry data around the western end of line 1A. Red arrows same as Figure 30 and indicate linear features associated with the faults that offset the seafloor. Black arrows indicate abyssal hill crustal fabric. RGR indicates dramatic decrease in water depth associated with the eastern Rio Grande Rise

Discussion

Fault Timing and Distribution

Given the association with clear offsets in the basement (Figures 32A), we contend that the blue and red faults result from tectonic movement in the igneous oceanic crust. Because the majority of blue faults terminate at, or are truncated by, the regional unconformity, we suggest that the blue faults were active before the event that caused the unconformity occurred. We have no timing constraint for the unconformity, but, if we assume relatively constant sedimentation

rates and minor erosion at the unconformity, its vertical position slightly less than halfway up through the sediment package leads us to generalize that it likely formed at or before 35 Ma. Conversely, red faults offset the unconformity, indicating movement after the event. Furthermore, some red faults offset the seafloor, which indicates that activity has occurred recently enough to not be buried by sediment. Considered together, the blue and red faults seem indicative of long-lived extensional stress, both before and after the formation of the unconformity in the western South Atlantic.

The apparent dip angles of the blue and red faults are not significantly different (p value = 0.52); together the mean is 49.2° and median is 52.5°. These angles are within the range of observed and predicted dips for faults associated with crustal accretion (Behn & Ito, 2008; Reston et al., 2004), which may indicate that preexisting faults were reactivated. The red faults that offset the seafloor can be observed in CREST shipboard multibeam bathymetry data forming linear features similar to the extensional crustal fabric created at the spreading center (Figure 33). Faults formed near slow-spreading ridge axes, which is the estimated spreading rate at the western end of line 1A (Kardell et al., 2019), typically dip toward the ridge (Carbotte & Macdonald, 1990). However, the majority of the blue and red faults do not dip toward the ridge and are associated with small offsets at the top of basement; hence, most of these faults are not easily associated with the crustal fabric that would be expected for faults developed at the ridge during crustal accretion. Perhaps some of the strain exploited preexisting weakness by reactivating old faults (faults offsetting seafloor) while some did not and developed new faults.

The pink faults are likely the result of differential consolidation of different thicknesses of sediment (e.g., Nedimović et al., 2009). They are consistently located at the transition between thin and thick sediment and are not obviously associated with any basement movement. The

mean and median apparent dip angle of the pink faults, 60.5° and 61.3° respectively, is statistically different (p value = 0.01) from that of the combined red and blue fault populations. Additionally, the location of the pink faults in eastern Line 1A compared to the blue and red faults in western Line 1A (Figure 28) further indicates a difference in origin. We suggest that the pink faults result from different thicknesses of sediment consolidating at different rates/magnitudes and they are not related to any tectonic movement in the igneous oceanic crust.

We find both blue and red faults only in the western ~100 km of Line 1A where the crust is thickening (Figure 28). To the east in the remaining ~1400 km of the CREST transect, we do not find deformation similar to that of the blue and red faults. Blue faults were active before the unconformity formed and concentrate in crust of ages between 66.5 and 68.5 Ma (Figure 30). While red faults do occur in the same location as the concentration of blue faults, including those with the most offset, the majority occur to the east and west of where the blue faults are concentrated (Figure 30). Because blue and red faults likely represent different temporal periods of deformation, the distribution of the blue and red faults in western Line 1A possibly indicates differences in where strain was accommodated through time. Unfortunately, we do not have data to the west of Line 1A and the possibility of a spatial relationship between blue and red faults remains unclear.

Differential Subsidence, the Unconformity, and the Cause of Deformation

A primary question of our study is why faulting has been occurring in the western South Atlantic. The western end of Line 1A is ~1500 km from the MAR and extensional faulting is generally only active within 30 km of the axis (Alexander & Macdonald, 1996), which suggests a more proximal source of strain. The RGR was thickened during its formation instead of later (e.g., Hawaiian-Emperor Seamount Chain), which seems to preclude the deformation being

caused by a later isostatic adjustment. Also, sediment thickness is not great enough for loading-related faulting, which would be expected in a major sedimentary basin. We suggest that the coincident occurrence of westward crustal thickening across Line 1A (Figure 28) and the presence of post-accretionary faults, some that offset the seafloor, (Figures 30, 33) are likely related.

Simple plate models (e.g., Parsons & Sclater, 1977) predict a slower seafloor subsidence with a thicker lithospheric plate. It seems intuitive that a greater plate thickness is accompanied by a greater volume of material with more heat to diffuse, and, unless the increase in plate thickness is accompanied by a proportional increase in the ability of the material to diffuse heat, a thicker plate will remain hotter longer. Recent work on both a modified half-space cooling model (Korenaga & Korenaga, 2016) and comprehensive plate models (Richards et al., 2018) shows that the addition of a crustal layer with low thermal diffusivity works to insulate the lithosphere and slow cooling, leading to a slower subsidence rate. It would seem that an increase in the thickness of the insulative oceanic crust, as in the case of the RGR, would slow its subsidence rate regardless of whether a plate model or the half-space cooling model were applied to predict it. The decrease in water depth and the crustal thickening present in Line 1A is indicative that the western edge of the CREST dataset has reached the eastern margin of the RGR. The crust of the ERGR is likely not as thick as the main body of the RGR, which is up to 30 km thick (Constantino et al., 2017). However, it is still thicker than the oceanic crust adjacent to the east (Christeson et al., 2019b); our gravity model does not cover the entire ERGR, but indicates crust >15 km thick (Figure 29). If the thickened RGR has cooled at a slower rate through time compared to the adjacent oceanic crust, it would be subsiding at a slower rate and could lead to extensional strain across the transition between the two.

An additional source of potential strain is related to the ~47 Ma Eocene thermal rejuvenation event, to which Barker (1983) attributed the volcanoclastic turbidite and ash beds sampled by DSDP 516F. More recently, Rohde et al. (2013) dated samples dredged from guyots on the RGR to similar ages adding additional evidence for an Eocene eruption. Thermal uplift and subsequent resumption of subsidence would produce a substantially different history for the RGR vs. the normal crust of the CREST transect. The difference in subsidence history could result in strain across the transition between the two, similar to our proposal of different subsidence rates from differences in thickness but with more complexity. We argue that the difference in subsidence rates between the thickened RGR (including the ERGR) and the normal oceanic crust of the CREST transect could result in the faulting and that a more complicated RGR history of subsidence-uplift-subsidence would only exaggerate the strain between the thickened and normal crust.

The discovery of a >150 km-long regional unconformity may be related to the ~47 Ma thermal rejuvenation event. The RGR substantially influenced ocean circulation in the early South Atlantic (Pérez-Díaz & Eagles, 2017) and an uplift of the RGR could have caused a perturbation in sedimentation patterns. Thus, a possible connection exists between the Eocene-aged uplift of the RGR and the regional unconformity we find in the sedimentary section to the east. However, based on MCS data near the crest and to the west of the RGR, Barker (1983) suggested that uplift was likely limited to the drill site area. Additionally, based on drilling to the west of the RGR, Johnson (1983) proposed that the thermal event at ~47 Ma did not affect paleocirculation for more than 200 km from the crest of the RGR. Another possible explanation for the unconformity is the arrival of Antarctic Bottom Water circulation (Johnson, 1983). DSDP Site 515 in the Brazil Basin to the northwest of the RGR found an unconformity representing the

absence of 22 Myrs of sediment that could be mapped in MCS data south to the Vema Channel (Figure 27) (Gamboa et al., 1983). Johnson (1983) attributed this feature to the onset of thermohaline flow in the Southwest Atlantic near the Eocene/Oligocene boundary, resulting in erosion and non-deposition from ~52 – 30 Ma at Site 515.

DSDP Site 516 is ~700 km to the west of the western end of Line 1A and Site 515 is even farther at ~1000 km. Line 1A reaches the margin of the ERGR, of which little about the history is known, including whether it experienced an Eocene thermal rejuvenation and uplift. The planned IODP Expeditions 390 and 393 will drill ocean crust along the CREST transect, including at the eastern end of Line 1A where we have interpreted the unconformity to be present. The drilling results will provide age constraint and further illuminate the origin of the unconformity.

Conclusions and Implications

The key findings of our study include:

1. The extensional strain that caused the faulting is likely the result of different subsidence histories for the RGR and normal oceanic crust. The thickened RGR would have subsided slower than the adjacent crust due to a greater amount of heat, which created strain across the transition between the two. This difference in subsidence histories may have been exacerbated by an Eocene-age thermal rejuvenation and uplift of the RGR.

2. Deformation of ~65-70-million-year-old crust along the eastern margin of the RGR has been long-lived. We find faulting that occurred both before and after the development of an unconformity less than halfway up the sedimentary package with

some activity recently enough to presently offset the seafloor. We do not, however, find growth strata or other evidence that activity on individual faults was sustained.

3. The presence and extent of the unconformity indicates a regional change in paleocirculation and sedimentation patterns in the young South Atlantic, and is possibly additional evidence for the Eocene thermal rejuvenation, uplift, and eruption of the RGR.

Implications of the faulting can be related to the upper crustal water reservoir. Faulting can provide exchange pathways between the crustal reservoir and the ocean for fluid, heat, and dissolved chemicals (Fisher & Becker, 2000), and faulting caused by the differential subsidence has likely not been considered before as a discharge or recharge site for the crustal reservoir. Given that the differential subsidence faulting is associated with the igneous crust, it is also likely that the faulting modifies the crustal reservoir properties. Kardell et al. (2019) showed a decrease in seismic velocities coincident with the faulting in CREST Line 1A, implying a change in the effective porosity of the upper crust likely caused by faulting.

Our proposed mechanism for the faulting present on the margin of the RGR suggests a fundamental process. A significant amount of crust in the oceans has been termed ‘anomalous’ due to thicknesses outside a ‘normal’ range (Korenaga & Korenaga, 2008). Thickened crust, whether thickened during accretion (e.g., RGR) or during later emplacement (e.g., Hawaiian-Emperor seamounts) will have a different subsidence history than normal oceanic crust. Why extensional faulting due to differences in subsidence rate has not been previously reported may be due to the uniqueness of the RGR history, but it is also possible that similar extensional

faulting is present on the margins of other regions of thickened crust and has simply not been observed due to a paucity of data that can capture it.

CHAPTER V

SUMMARY

The work performed for this dissertation advances our understanding of the processes that govern and influence the evolution of oceanic crust. The CREST dataset is unique in that it allowed us to study oceanic crust created at a single spreading segment over a 0–70 Myr age range and 12–31 mm/yr spreading rate.

Chapter II shows the evolution of the thickness of layer 2A in the South Atlantic versus age and spreading rate, and provides evidence for the continued hydrothermal alteration of the upper crust for at least ~48 Myrs. These findings imply that the thickness of layer 2A is not related to spreading rate, does not systematically thin with crustal age, and in the crust where basement outcrops remain exposed, circulation in the upper crust is never a fully closed system and alteration of the rock and pore space can continue into older ages.

In Chapter III, we show evidence for the interrelation of the spreading rate, the roughness of the crust, and the magmatic accommodation of spreading. We find that the crust surveyed by the CREST expedition was predominantly created with high proportions of magmatic accommodation relative to spreading rate and that the spreading center has likely alternated between an axial valley and an axial high in the past. We also show that crustal thickness trends with the relative accommodation of magmatic spreading. These findings imply that with estimates of both crustal roughness and the magmatic fraction of spreading, it is possible to predict past first-order axial morphology (e.g., axial valley or high).

Lastly, in Chapter IV, we show how a difference in crustal thickness can lead to deformation as thermal subsidence takes place at different rates. Extension between the thickened Rio Grande Rise and the adjacent normal crust lead to normal faulting across the

transition between the two and was possibly exacerbated by a thermal uplift event at ~47 Ma. This implies that crust can be deformed along the margins of thickened crust, which composes a significant portion of the global ocean basins.

REFERENCES

Alexander, R. T., & MacDonald, K. C. (1996). Sea Beam, SeaMARC II and ALVIN-based studies of faulting on the East Pacific Rise 9 degrees 20' N 9 degrees 50' N. *Marine Geophysical Researches, 18*(5), 557-587. doi:10.1007/Bf00310069

Alt, J. C., Honnorez, J., Laverne, C., & Emmermann, R. (1986). Hydrothermal Alteration of a 1-Km Section through the Upper Oceanic-Crust, Deep-Sea Drilling Project Hole 504b - Mineralogy, Chemistry, and Evolution of Seawater-Basalt Interactions. *Journal of Geophysical Research-Solid Earth and Planets, 91*(B10), 309-335. doi:10.1029/JB091iB10p10309

Arnulf, A. F., Harding, A. J., Singh, S. C., Kent, G. M., & Crawford, W. C. (2014). Nature of upper crust beneath the Lucky Strike volcano using elastic full waveform inversion of streamer data. *Geophysical Journal International, 196*(3), 1471-1491. doi:10.1093/gji/ggt461

Arnulf, A. F., Singh, S. C., Harding, A. J., Kent, G. M., & Crawford, W. (2011). Strong seismic heterogeneity in layer 2A near hydrothermal vents at the Mid-Atlantic Ridge. *Geophysical Research Letters, 38*, L13320. doi:10.1029/2011gl047753

Baker, E. T., Chen, Y. J., & Morgan, J. P. (1996). The relationship between near-axis hydrothermal cooling and the spreading rate of mid-ocean ridges. *Earth and Planetary Science Letters, 142*(1-2), 137-145. doi:10.1016/0012-821x(96)00097-0

Baran, J. M., Carbotte, S. M., Cochran, J. R., & Nedimović, M. R. (2010). Upper crustal seismic structure along the Southeast Indian Ridge: Evolution from 0 to 550 ka and variation with axial morphology. *Geochemistry Geophysics Geosystems, 11*, Q02001. doi:10.1029/2009GC002629

Baran, J. M., Cochran, J. R., Carbotte, S. M., & Nedimović, M. R. (2005). Variations in upper crustal structure due to variable mantle temperature along the Southeast Indian Ridge. *Geochemistry Geophysics Geosystems, 6*, Q11002. doi:10.1029/2005GC000943

Barker, P. F. (1983). Tectonic Evolution and Subsidence History of the Rio-Grande Rise. *Initial Reports of the Deep Sea Drilling Project, 72*(Dec), 953-976.

Barker, P. F., Carlson, R. L., Johnson, D. A., Cepek, P., Coulbourn, W., Gamboa, L. A., . . . Weiss, W. (1981). Deep-Sea Drilling Project Leg-72 - Southwest Atlantic Paleocirculation and Rio-Grande Rise Tectonics. *Geological Society of America Bulletin, 92*(5), 294-309. doi:10.1130/0016-7606(1981)92<294:Dsdpls>2.0.Co;2

Behn, M. D., & Ito, G. (2008). Magmatic and tectonic extension at mid‐ocean ridges: 1. Controls on fault characteristics. *Geochemistry, Geophysics, Geosystems, 9*(8).

Blacic, T. M., Ito, G., Canales, J. P., Detrick, R. S., & Sinton, J. (2004). Constructing the crust along the Galapagos Spreading Center 91.3°-95.5°W: Correlation of seismic layer 2A

with axial magma lens and topographic characteristics. *Journal of Geophysical Research, 109*. doi:10.1029/2004JB003066

Blackman, D. K., Cann, J. R., Janssen, B., & Smith, D. K. (1998). Origin of extensional core complexes: Evidence from the Mid‐Atlantic Ridge at Atlantis fracture zone. *Journal of Geophysical Research: Solid Earth, 103*(B9), 21315-21333.

Boudier, F., & Nicolas, A. (1995). Nature of the Moho Transition Zone in the Oman Ophiolite. *Journal of Petrology, 36*(3), 777-796. doi:10.1093/petrology/36.3.777

Bown, J. W., & White, R. S. (1994). Variation with spreading rate of oceanic crustal thickness and geochemistry. *Earth and Planetary Science Letters, 121*, 435-449.

Bryan, W. B., & Duncan, R. A. (1983). Age and Provenance of Clastic Horizons from Hole-516f. *Initial Reports of the Deep Sea Drilling Project, 72*(Dec), 475-477.

Buck, W. R., Lavier, L. L., & Poliakov, A. N. B. (2005). Modes of faulting at mid-ocean ridges. *Nature, 434*(7034), 719-723. doi:10.1038/nature03358

Buck, W. R., & Poliakov, A. N. B. (1998). Abyssal hills formed by stretching oceanic lithosphere. *Nature, 392*(6673), 272-275. doi:10.1038/32636

Bull, J. M. (1990). Structural style of intra-plate deformation, Central Indian Ocean Basin: evidence for the role of fracture zones. *Tectonophysics, 184*(2), 213-228.

Camboa, L. A. P., & Rabinowitz, P. D. (1984). The Evolution of the Rio-Grande Rise in the Southwest Atlantic-Ocean. *Marine Geology, 58*(1-2), 35-58. doi:10.1016/0025-3227(84)90115-4

Canales, J. P., Detrick, R. S., Carbotte, S. M., Kent, G. M., Diebold, J., Harding, A. J., . . . van Ark, E. (2005). Upper crustal structure and axial topography at intermediate spreading ridges: Seismic constraints from the southern Juan de Fuca Ridge. *Journal of Geophysical Research, 110*, B12104. doi:10.1029/2005JB003630

Carbotte, S., & Macdonald, K. C. (1994). Comparison of seafloor tectonic fabric at intermediate, fast, and super fast spreading ridges: Influence of spreading rate, plate motions, and ridge segmentation on fault patterns. *Journal of Geophysical Research, 99*, 13609-13631.

Carbotte, S. M., & Macdonald, K. C. (1990). Causes of Variation in Fault-Facing Direction on the Ocean-Floor. *Geology, 18*(8), 749-752. doi:10.1130/0091-7613(1990)018<0749:Coviff>2.3.Co;2

Carbotte, S. M., Mutter, J. C., & Xu, L. Q. (1997). Contribution of volcanism and tectonism to axial and flank morphology of the southern East Pacific Rise, 17 degrees 10'-17 degrees 40'S, from a study of layer 2A geometry. *Journal of Geophysical Research-Solid Earth, 102*(B5), 10165-10184. doi:10.1029/96jb03910

Carbotte, S. M., Small, C., & Donnelly, K. (2004). The influence of ridge migration on the magmatic segmentation of mid-ocean ridges. *Nature, 429*(6993), 743-746. doi:10.1038/nature02652

Carlson, R. L. (1998). Seismic velocities in the uppermost oceanic crust: Age dependence and the fate of layer 2A. *Journal of Geophysical Research-Solid Earth, 103*(B4), 7069-7077. doi:10.1029/97jb03577

Carlson, R. L. (2010). How crack porosity and shape control seismic velocities in the upper oceanic crust: Modeling downhole logs from Holes 504B and 1256D. *Geochemistry Geophysics Geosystems, 11*, Q04007. doi:10.1029/2009GC002955

Carlson, R. L. (2011). The effect of hydrothermal alteration on the seismic structure of the upper oceanic crust: Evidence from Holes 504B and 1256D. *Geochemistry Geophysics Geosystems, 12*, Q09013. doi:10.1029/2011gc003624

Carlson, R. L. (2014a). The effects of alteration and porosity on seismic velocities in oceanic basalts and diabases. *Geochemistry Geophysics Geosystems, 15*(12), 4589-4598. doi:10.1002/2014gc005537

Carlson, R. L. (2014b). The influence of porosity and crack morphology on seismic velocity and permeability in the upper oceanic crust. *Geochemistry Geophysics Geosystems, 15*(1), 10-27. doi:10.1002/2013gc004965

Carlson, R. L., & Herrick, C. N. (1990). Densities and Porosities in the Oceanic-Crust and Their Variations with Depth and Age. *Journal of Geophysical Research-Solid Earth and Planets, 95*(B6), 9153-9170. doi:10.1029/JB095iB06p09153

Carlson, R. L., & Jacobson, R. S. (1994). Comment on "Upper crustal structure as a function of plate age" by Robert Houtz and John Ewing. *Journal of Geophysical Research, 99*, 3135-3138.

Chen, Y. J. (1992). Oceanic Crustal Thickness Versus Spreading Rate. *Geophysical Research Letters, 19*(8), 753-756. doi:10.1029/92gl00161

Christeson, G. L., Goff, J. A., & Reece, R. S. (2019a). Synthesis of Oceanic Crustal Structure From Two‐Dimensional Seismic Profiles. *Reviews of Geophysics, 57*(2), 504-529. doi:10.1029/2019rg000641

Christeson, G. L., Karson, J. A., & McIntosh, K. D. (2010). Mapping of seismic layer 2A/2B boundary above the sheeted dike unit at intermediate-spreading crust exposed near the Blanco Transform. *Geochemistry Geophysics Geosystems, 11*, Q03015. doi:10.1029/2009GC002864

Christeson, G. L., McIntosh, K. D., & Karson, J. A. (2007). Inconsistent correlation of seismic layer 2a and lava layer thickness in oceanic crust. *Nature, 445*(7126), 418-421. doi:10.1038/nature05517

Christeson, G. L., Purdy, G. M., & Fryer, G. J. (1992). Structure of young upper crust at the East Pacific Rise near 9°30'N. *Geophysical Research Letters, 19*, 1045-1048.

Christeson, G. L., Purdy, G. M., & Fryer, G. J. (1994). Seismic Constraints on Shallow Crustal Emplacement Processes at the Fast Spreading East Pacific Rise. *Journal of Geophysical Research-Solid Earth, 99*(B9), 17957-17973. doi:10.1029/94jb01252

Christeson, G. L., Reece, R. S., & Carlson, R. L. (2018). *Variations in crustal structure and thickness for South Atlantic Oceanic crust.* Paper presented at the American Geophysical Union Fall Meeting, Washington, D.C.

Christeson, G. L., Reece, R. S., Estep, J., Kardell, D. A., & Carlson, R. L. (2019b). *South Atlantic Transect Site Survey Data in Support of IODP Expeditions 390 and 393*. Paper presented at the 2019 AGU Fall Meeting, San Francisco, CA.

Cochran, J. R., & Sempere, J. C. (1997). The southeast Indian ridge between 88 degrees E and 118 degrees E: Gravity anomalies and crustal accretion at intermediate spreading rates. *Journal of Geophysical Research-Solid Earth, 102*(B7), 15463-15487. doi:10.1029/97jb00511

Constantino, R. R., Hackspacher, P. C., de Souza, I. A., & Costa, I. S. L. (2017). Basement structures over Rio Grande Rise from gravity inversion. *Journal of South American Earth Sciences, 75*, 85-91. doi:10.1016/j.jsames.2017.02.005

Davies, G. F. (1980). Review of Oceanic and Global Heat-Flow Estimates. *Reviews of Geophysics, 18*(3), 718-722. doi:10.1029/RG018i003p00718

Detrick, R., Sinton, J., Ito, G., Canales, J., Behn, M., Blacic, T., . . . Mahoney, J. (2002). Correlated geophysical, geochemical, and volcanological manifestations of plume‐ridge interaction along the Galápagos Spreading Center. *Geochemistry, Geophysics, Geosystems, 3*(10), 1-14.

Dick, H. J., Lin, J., & Schouten, H. (2003). An ultraslow-spreading class of ocean ridge. *Nature, 426*(6965), 405-412. doi:10.1038/nature02128

Dick, H. J., Tivey, M. A., & Tucholke, B. E. (2008). Plutonic foundation of a slow‐spreading ridge segment: Oceanic core complex at Kane Megamullion, 23 30′ N, 45 20′ W. *Geochemistry, Geophysics, Geosystems, 9*(5).

Doin, M. P., & Fleitout, L. (1996). Thermal evolution of the oceanic lithosphere: An alternative view. *Earth and Planetary Science Letters, 142*(1-2), 121-136. doi:10.1016/0012-821x(96)00082-9

Elsasser, W. M. (1971). Sea-Floor Spreading as Thermal Convection. *Journal of Geophysical Research, 76*(5), 1101-&. doi:10.1029/JB076i005p01101

Escartin, J., Cowie, P., Searle, R., Allerton, S., Mitchell, N., MacLeod, C., & Slootweg, A. (1999). Quantifying tectonic strain and magmatic accretion at a slow spreading ridge segment, Mid‐Atlantic Ridge, 29° N. *Journal of Geophysical Research: Solid Earth, 104*(B5), 10421-10437.

Estep, J., Reece, R., Kardell, D. A., Christeson, G. L., & Carlson, R. L. (2019a). Seismic Layer 2A: Evolution and Thickness From 0-to 70-Ma Crust in the Slow-Intermediate Spreading South Atlantic. *Journal of Geophysical Research-Solid Earth, 124*(8), 7633-7651. doi:10.1029/2019jb017302

Estep, J., Reece, R., Kardell, D. A., Christeson, G. L., & Carlson, R. L. (2019b). *Recent Deformation in Old Ocean Crust*. Paper presented at the 2019 AGU Fall Meeting, San Francisco, CA.

Fisher, A. T., & Becker, K. (1995). Correlation between seafloor heat flow and basement relief: Observational and numerical examples and implications for upper crustal permeability. *Journal of Geophysical Research, 100*, 12641-12657.

Fisher, A. T., & Becker, K. (2000). Channelized fluid flow in oceanic crust reconciles heat-flow and permeability data. *Nature, 403*(6765), 71-74. doi:10.1038/47463

Fox, P. J., Grindlay, N. R., & Macdonald, K. C. (1991). The Mid-Atlantic Ridge (31-Degrees-S-34-Degrees-30's) - Temporal and Spatial Variations of Accretionary Processes. *Marine Geophysical Researches, 13*(1), 1-20. doi:10.1007/Bf02428193

Gamboa, L. A., Buffler, R. T., & Barker, P. F. (1983). Seismic Stratigraphy and Geologic History of the Rio-Grande Gap and Southern Brazil Basin. *Initial Reports of the Deep Sea Drilling Project, 72*(Dec), 481-497.

Goff, J. A. (1991). A Global and Regional Stochastic-Analysis of near-Ridge Abyssal Hill Morphology. *Journal of Geophysical Research-Solid Earth, 96*(B13), 21713-21737. doi:10.1029/91jb02275

Goff, J. A. (2010). Global prediction of abyssal hill root‐mean‐square heights from small‐scale altimetric gravity variability. *Journal of Geophysical Research: Solid Earth, 115*(B12).

Goff, J. A., & Jordan, T. H. (1988). Stochastic modeling of seafloor morphology: Inversion of sea beam data for second‐order statistics. *Journal of Geophysical Research: Solid Earth, 93*(B11), 13589-13608.

Goff, J. A., Jordan, T. H., Edwards, M. H., & Fornari, D. J. (1991). Comparison of a stochastic seafloor model with SeaMARC II bathymetry and Sea Beam data near the East Pacific Rise 13°-15°N. *Journal of Geophysical Research, 96*, 3867-3885.

Goff, J. A., Ma, Y., Shah, A., Cochran, J. R., & Sempere, J. C. (1997). Stochastic analysis of seafloor morphology on the flank of the southeast Indian ridge: The influence of ridge

morphology on the formation of abyssal hills. *Journal of Geophysical Research-Solid Earth, 102*(B7), 15521-15534. doi:10.1029/97jb00781

Grevemeyer, I., Kaul, N., Villinger, H., & Weigel, W. (1999). Hydrothermal activity and the evolution of the seismic properties of upper oceanic crust. *Journal of Geophysical Research-Solid Earth, 104*(B3), 5069-5079. doi:10.1029/1998jb900096

Grevemeyer, I., & Weigel, W. (1996). Seismic velocities of the uppermost igneous crust versus age. *Geophysical Journal International, 124*(2), 631-635. doi:10.1111/j.1365-246X.1996.tb07041.x

Grevemeyer, I., & Weigel, W. (1997). Increase of seismic velocities in upper oceanic crust: The "superfast" spreading East Pacific Rise at 14 degrees 14'S. *Geophysical Research Letters, 24*(3), 217-220. doi:10.1029/96gl04005

Grose, C. J., & Afonso, J. C. (2013). Comprehensive plate models for the thermal evolution of oceanic lithosphere. *Geochemistry Geophysics Geosystems, 14*(9), 3751-3778. doi:10.1002/ggge.20232

Hamilton, E. L. (1976). Variations of Density and Porosity with Depth in Deep-Sea Sediments. *Journal of Sedimentary Petrology, 46*(2), 280-300. doi:10.1306/212f6f3c-2b24-11d7-8648000102c1865d

Harding, A. J., Kent, G. M., & Orcutt, J. A. (1993). A Multichannel Seismic Investigation of Upper Crustal Structure at 9-Degrees-N on the East Pacific Rise - Implications for Crustal Accretion. *Journal of Geophysical Research-Solid Earth, 98*(B8), 13925-13944. doi:10.1029/93jb00886

Hayes, D. E., & Kane, K. A. (1991). The dependence of seafloor roughness on spreading rate. *Geophysical Research Letters, 18*(8), 1425-1428.

Hooft, E. E. E., Detrick, R. S., Toomey, D. R., Collins, J. A., & Lin, J. (2000). Crustal thickness and structure along three contrasting spreading segments of the Mid-Atlantic Ridge, 33.5 degrees-35 degrees N. *Journal of Geophysical Research-Solid Earth, 105*(B4), 8205-8226. doi:10.1029/1999jb900442

Hooft, E. E. E., Schouten, H., & Detrick, R. S. (1996). Constraining crustal emplacement processes from the variation in seismic layer 2A thickness at the East Pacific Rise. *Earth and Planetary Science Letters, 142*(3-4), 289-309. doi:10.1016/0012-821x(96)00101-X

Houtz, R., & Ewing, J. (1976). Upper Crustal Structure as a Function of Plate Age. *Journal of Geophysical Research, 81*(14), 2490-2498. doi:10.1029/JB081i014p02490

Hussenoeder, S. A., Kent, G. M., & Detrick, R. S. (2002). Upper crustal seismic structure of the slow spreading Mid-Atlantic Ridge, 35 degrees N: Constraints on volcanic emplacement processes. *Journal of Geophysical Research-Solid Earth, 107*(B8). doi:2156 10.1029/2001jb001691

Hyndman, R. D., & Drury, M. J. (1976). The physical properties of oceanic basement rocks from deep drilling on the Mid-Atlantic Ridge. *Journal of Geophysical Research, 81*, 4042-4052.

Ito, G., & Behn, M. D. (2008). Magmatic and tectonic extension at mid-ocean ridges: 2. Origin of axial morphology. *Geochemistry Geophysics Geosystems, 9*, Q09O12. doi:10.1029/2008GC001970

Jacobson, R. S. (1992). Impact of Crustal Evolution on Changes of the Seismic Properties of the Uppermost Ocean Crust. *Reviews of Geophysics, 30*(1), 23-42. doi:10.1029/91rg02811

Johnson, D. A. (1983). Paleocirculation of the Southwestern Atlantic. *Initial Reports of the Deep Sea Drilling Project, 72*(Dec), 977-994.

Johnson, H. P., & Carlson, R. L. (1992). Variation of Sea-Floor Depth with Age - a Test of Models Based on Drilling Results. *Geophysical Research Letters, 19*(19), 1971-1974. doi:10.1029/92gl01946

Johnson, H. P., & Pruis, M. J. (2003). Fluxes of fluid and heat from the oceanic crustal reservoir. *Earth and Planetary Science Letters, 216*(4), 565-574. doi:10.1016/S0012-821x(03)00545-4

Kardell, D. A., Christeson, G. L., Estep, J. D., Reece, R. S., & Carlson, R. L. (2019). Long‐Lasting Evolution of Layer 2A in the Western South Atlantic: Evidence for Low‐Temperature Hydrothermal Circulation in Old Oceanic Crust. *Journal of Geophysical Research: Solid Earth, 124*(3), 2252-2273. doi:10.1029/2018jb016925

Karson, F. A. (2002). Geologic structure of the uppermost oceanic crust created at fast-to intermediate-rate spreading centers. *Annual Review of Earth and Planetary Sciences, 30*, 347-384. doi:10.1146/annurev.earth.30.091201.141132

Kent, G. M., Harding, A. J., Orcutt, J. A., Detrick, R. S., Mutter, J. C., & Buhl, P. (1994). Uniform Accretion of Oceanic-Crust South of the Garrett Transform at 14-Degrees-15's on the East Pacific Rise. *Journal of Geophysical Research-Solid Earth, 99*(B5), 9097-9116. doi:10.1029/93jb02872

Korenaga, T., & Korenaga, J. (2008). Subsidence of normal oceanic lithosphere, apparent thermal expansivity, and seafloor flattening. *Earth and Planetary Science Letters, 268*, 41-51. doi:10.1016/j.epsl.2007.12.022

Korenaga, T., & Korenaga, J. (2016). Evolution of young oceanic lithosphere and the meaning of seafloor subsidence rate. *Journal of Geophysical Research-Solid Earth, 121*(9), 6315-6332. doi:10.1002/2016jb013395

Lavier, L. L., & Buck, W. R. (2002). Half graben versus large‐offset low‐angle normal fault: Importance of keeping cool during normal faulting. *Journal of Geophysical Research: Solid Earth, 107*(B6), ETG 8-1-ETG 8-13.

Macdonald, K. C., Fox, P. J., Alexander, R. T., Pockalny, R., & Gente, P. (1996). Volcanic growth faults and the origin of Pacific abyssal hills. *Nature, 380*(6570), 125-129. doi:10.1038/380125a0

Macdonald, K. C., Scheirer, D. S., & Carbotte, S. M. (1991). Mid-ocean ridges: discontinuities, segments and giant cracks. *Science, 253*(5023), 986-994. doi:10.1126/science.253.5023.986

Malinverno, A. (1991). Inverse Square-Root Dependence of Mid-Ocean-Ridge Flank Roughness on Spreading Rate. *Nature, 352*(6330), 58-60. doi:10.1038/352058a0

Maxwell, A. E., Von Herzon, R. P., Andrews, J. E., Boyce, R. E., Milow, E. D., Hsu, K. J., . . . Saito, T. (1970). *Initial Reports of the Deep Sea Drilling Project, Volume III*. Washington: U.S. Government Printing Office.

Mcclain, J. S., Orcutt, J. A., & Burnett, M. (1985). The East Pacific Rise in Cross-Section - a Seismic Model. *Journal of Geophysical Research-Solid Earth and Planets, 90*(Nb10), 8627-8639. doi:10.1029/JB090iB10p08627

Menard, H. W. (1964). *Marine geology of the Pacific*. New York: McGraw-Hill Book Company.

Morgan, J. P., & Chen, Y. J. (1993). Dependence of Ridge-Axis Morphology on Magma Supply and Spreading Rate. *Nature, 364*(6439), 706-708. doi:10.1038/364706a0

Morgan, W. J. (1971). Convection plumes in the lower mantle. *Nature, 230*(5288), 42-43.

Müller, R. D., Sdrolias, M., Gaina, C., & Roest, W. R. (2008). Age, spreading rates, and spreading asymmetry of the world's ocean crust. *Geochemistry Geophysics Geosystems, 9*, Q04006. doi:10.1029/2007GC001743

Müller, R. D., Sdrolias, M., Gaina, C., & Roest, W. R. (2008). Age, spreading rates, and spreading asymmetry of the world's ocean crust. *Geochemistry, Geophysics, Geosystems, 9*(4), n/a-n/a. doi:10.1029/2007gc001743

Mutter, J. C., & Karson, J. A. (1992). Structural Processes at Slow-Spreading Ridges. *Science, 257*(5070), 627-634. doi:10.1126/science.257.5070.627

Nedimović, M. R., Bohnenstiehl, D. R., Carbotte, S. M., Canales, J. P., & Dziak, R. P. (2009). Faulting and hydration of the Juan de Fuca plate system. *Earth and Planetary Science Letters, 284*(1-2), 94-102.

Nedimović, M. R., Carbotte, S. M., Diebold, J. B., Harding, A. J., Canales, J. P., & Kent, G. M. (2008). Upper crustal evolution across the Juan de Fuca ridge flanks. *Geochemistry Geophysics Geosystems, 9*, Q09006. doi:10.1029/2008GC002085

Neprochnov, Y. P., Levchenko, O. V., Merklin, L. R., & Sedov, V. V. (1988). The Structure and Tectonics of the Intraplate Deformation Area in the Indian-Ocean. *Tectonophysics, 156*(1-2), 89-106. doi:10.1016/0040-1951(88)90285-5

O'Connor, J., & Duncan, R. (1990). Evolution of the Walvis Ridge-Rio Grande Rise hot spot system: Implications for African and South American plate motions over plumes. *Journal of Geophysical Research, 95*(B11), 17475-17502.

O'Connor, J., & le Roex, A. P. (1992). South Atlantic hot spot-plume systems: 1. Distribution of volcanism in time and space. *Earth and Planetary Science Letters, 113*(3), 343-364.

Parsons, B., & Sclater, J. G. (1977). An analysis of the variation of ocean floor bathymetry and heat flow with age. *Journal of Geophysical Research, 82*, 803-827.

Peirce, C., Sinha, M., Topping, S., & Gill, C. (2007). Morphology and genesis of slow-spreading ridges - seabed scattering and seismic imaging within the oceanic crust. *Geophysical Journal International, 168*(1), 59-89. doi:10.1111/j.1365-246X.2006.03223.x

Pérez-Díaz, L., & Eagles, G. (2017). South Atlantic paleobathymetry since early Cretaceous. *Scientific reports, 7*(1), 11819.

Pérez‐Díaz, L., & Eagles, G. (2017). A new high‐resolution seafloor age grid for the South Atlantic. *Geochemistry, Geophysics, Geosystems, 18*(1), 457-470.

Perfit, M. R., & Chadwick, W. W., Jr.,. (1998). Magmatism at mid-ocean ridges: Constraints from volcanological and geochemical investigations. In W. R. Buck, P. T. Delaney, J. A. Karson, & Y. Lagabrielle (Eds.), *Faulting and Magmatism at Mid-Ocean Ridges* (pp. 59-115). Washington, D.C.: American Geophysical Union.

Purdy, G. M. (1987). New Observations of the Shallow Seismic Structure of Young Oceanic-Crust. *Journal of Geophysical Research-Solid Earth and Planets, 92*(B9), 9351-9362. doi:10.1029/JB092iB09p09351

Raitt, R. W. (1963). The crustal rocks. In M. N. Hill (Ed.), *The Sea* (Vol. 3, pp. 85-100). New York: Interscience.

Ranero, C. R., Morgan, J. P., McIntosh, K., & Reichert, C. (2003). Bending-related faulting and mantle serpentinization at the Middle America trench. *Nature, 425*(6956), 367-373. doi:10.1038/nature01961

Renne, P. R., Ernesto, M., Pacca, I. G., Coe, R. S., Glen, J. M., Prevot, M., & Perrin, M. (1992). The age of parana flood volcanism, rifting of gondwanaland, and the jurassic-cretaceous boundary. *Science, 258*(5084), 975-979. doi:10.1126/science.258.5084.975

Reston, T. J., Ranero, C. R., Ruoff, O., Perez-Gussinye, M., & Danobeitia, J. J. (2004). Geometry of extensional faults developed at slow-spreading centres from pre-stack depth migration of seismic reflection data in the Central Atlantic (Canary Basin). *Geophysical Journal International, 159*(2), 591-606. doi:10.1111/j.1365-246X.2004.02444.x

Rice, J. A. (2006). *Mathematical statistics and data analysis*: Cengage Learning.

Richards, F. D., Hoggard, M. J., Cowton, L. R., & White, N. J. (2018). Reassessing the Thermal Structure of Oceanic Lithosphere With Revised Global Inventories of Basement Depths and Heat Flow Measurements. *Journal of Geophysical Research-Solid Earth, 123*(10), 9136-9161. doi:10.1029/2018jb015998

Rohde, J. K., van den Bogaard, P., Hoernle, K., Hauff, F., & Werner, R. (2013). Evidence for an age progression along the Tristan-Gough volcanic track from new 40Ar/39Ar ages on phenocryst phases. *Tectonophysics, 604*, 60-71.

Rohr, K. M. M. (1994). Increase of Seismic Velocities in Upper Oceanic-Crust and Hydrothermal Circulation in the Juan-De-Fuca Plate. *Geophysical Research Letters, 21*(19), 2163-2166. doi:10.1029/94gl01913

Ryan, W. B. F., Carbotte, S. M., Coplan, J. O., O'Hara, S., Melkonian, A., Arko, R., . . . Zemsky, R. (2009). Global Multi-Resolution Topography synthesis. *Geochemistry Geophysics Geosystems, 10*(3). doi:10.1029/2008gc002332

Sandwell, D. T., Muller, R. D., Smith, W. H., Garcia, E., & Francis, R. (2014). Marine geophysics. New global marine gravity model from CryoSat-2 and Jason-1 reveals buried tectonic structure. *Science, 346*(6205), 65-67. doi:10.1126/science.1258213

Schouten, H., Smith, D. K., Cann, J. R., & Escartin, J. (2010). Tectonic versus magmatic extension in the presence of core complexes at slow-spreading ridges from a visualization of faulted seafloor topography. *Geology, 38*(7), 615-618. doi:10.1130/G30803.1

Schreiber, E., & Fox, P. J. (1976). Compressional wave velocities and mineralogy of fresh basalts from the Famous area and the Oceanographer fracture zone and the texture of layer 2A of the oceanic crust. *Journal of Geophysical Research, 81*, 4071-4076.

Schubert, G., & Turcotte, D. (1982). Geodynamics applications of continuum physics to geological problems: John Wiley & Sons Verlag.

Sclater, J. G., & McKenzie, D. P. (1973). Paleobathymetry of the South Atlantic. *Geological Society of America Bulletin, 84*(10), 3203-3216.

Scotese, C. R., Gahagan, L. M., & Larson, R. L. (1988). Plate Tectonic Reconstructions of the Cretaceous and Cenozoic Ocean Basins. *Tectonophysics, 155*(1-4), 27-48. doi:10.1016/0040-1951(88)90259-4

Searle, R. (1984). GLORIA survey of the East Pacific Rise near 3.5 S: Tectonic and volcanic characteristics of a fast spreading mid-ocean rise. *Tectonophysics, 101*(3-4), 319-344.

Seher, T., Crawford, W. C., Singh, S. C., & Cannat, M. (2010). Seismic layer 2A variations in the Lucky Strike segment at the Mid-Atlantic Ridge from reflection measurements. *Journal of Geophysical Research, 115*, B07107. doi:10.1029/2009jb006783

Shillington, D. J., Becel, A., Nedimovic, M. R., Kuehn, H., Webb, S. C., Abers, G. A., . . . Mattei-Salicrup, G. A. (2015). Link between plate fabric, hydration and subduction zone seismicity in Alaska. *Nature Geoscience, 8*(12), 961-U998. doi:10.1038/Ngeo2586

Sinton, J., Detrick, R., Canales, J. P., Ito, G., & Behn, M. (2003). Morphology and segmentation of the western Galápagos Spreading Center, 90.5°–98° W: Plume‐ridge interaction at an intermediate spreading ridge. *Geochemistry, Geophysics, Geosystems, 4*(12).

Sinton, J. M., & Detrick, R. S. (1992). Mid-ocean ridge magma chambers. *Journal of Geophysical Research, 97*, 197-216.

Small, C. (1994). A global analysis of mid-ocean ridge axial topography. *Geophysical Journal International, 116*, 64-84.

Small, C. (1998). Global systematics of mid-ocean ridge morphology. *Washington DC American Geophysical Union Geophysical Monograph Series, 106*, 1-25.

Stein, C. A., & Stein, S. (1992). A Model for the Global Variation in Oceanic Depth and Heat-Flow with Lithospheric Age. *Nature, 359*(6391), 123-129. doi:10.1038/359123a0

Stein, C. A., & Stein, S. (1994). Constraints on Hydrothermal Heat-Flux through the Oceanic Lithosphere from Global Heat-Flow. *Journal of Geophysical Research-Solid Earth, 99*(B2), 3081-3095. doi:10.1029/93jb02222

Swift, S., Reichow, M., Tikku, A., Tominaga, M., & Gilbert, L. (2008). Velocity structure of upper ocean crust at Ocean Drilling Program Site 1256. *Geochemistry Geophysics Geosystems, 9*, Q10O13. doi:10.1029/2008GC002188

Sykes, T., Royer, J.-Y., Ramsay, A., & Kidd, R. (1998). Southern hemisphere palaeobathymetry. *Geological Society, London, Special Publications, 131*(1), 1-42.

Thoram, S., Sager, W. W., & Jokat, W. (2019). Implications of Updated Magnetic Anomalies for the Late Cretaceous Tectonic Evolution of Walvis Ridge. *Geophysical Research Letters, 46*(16), 9474-9482. doi:10.1029/2019gl083467

Toomey, D. R., Purdy, G. M., Solomon, S. C., & Wilcock, W. S. D. (1990). The three-dimensional seismic velocity structure of the East Pacific Rise near latitude 9°30'N. *Nature, 347*, 639-645.

Turner, S., Regelous, M., Kelley, S., Hawkesworth, C., & Mantovani, M. (1994). Magmatism and continental break-up in the South Atlantic: high precision40Ar-39Ar geochronology. *Earth and Planetary Science Letters, 121*(3-4), 333-348.

Vera, E. E., & Diebold, J. B. (1994). Seismic imaging of oceanic layer 2A between 9°30'N and 10°N on the East Pacific Rise from two-ship wide-aperture profiles. *Journal of Geophysical Research, 99*, 3031-3041.

Vera, E. E., Mutter, J. C., Buhl, P., Orcutt, J. A., Harding, A. J., Kappus, M. E., . . . Brocher, T. M. (1990). The structure of 0- to 0.2-m.y.-old oceanic crust at 9°N on the East Pacific Rise from expanded spread profiles. *Journal of Geophysical Research, 95*, 15,529-515,556.

White, R. S., Mckenzie, D., & Onions, R. K. (1992). Oceanic Crustal Thickness from Seismic Measurements and Rare-Earth Element Inversions. *Journal of Geophysical Research-Solid Earth, 97*(B13), 19683-19715. doi:10.1029/92jb01749

Wilkens, R. H., Fryer, G. J., & Karsten, J. (1991). Evolution of Porosity and Seismic Structure of Upper Oceanic-Crust - Importance of Aspect Ratios. *Journal of Geophysical Research-Solid Earth, 96*(B11), 17981-17995. doi:10.1029/91jb01454

Wilson, D., Robinson, A., Hobbs, R., Peirce, C., & Funnell, M. (2019). Does intermediate spreading-rate oceanic crust result from episodic transition between magmatic and magma-dominated, faulting-enhanced spreading?—The Costa Rica Rift example. *Geophysical Journal International, 218*(3), 1617-1641.